UNIVERZA NA PRIMORSKEM
FAKULTETA ZA MATEMATIKO, NARAVOSLOVJE IN
INFORMACIJSKE TEHNOLOGIJE

MASTER'S THESIS
(MAGISTRSKO DELO)

SIMULATION OF WIND DRIVEN RAIN EFFECT ON AESTHETICAL PERFORMANCE OF WOODEN FACADE
(SIMULACIJA DEŽEVNEGA UČINKA NA ESTETIČNO DELOVANJE LESENE FASADE)

RICHARD ACQUAH

2021
MASTER'S THESIS
RICHARD ACQUAH

UNIVERZA NA PRIMORSKEM
FAKULTETA ZA MATEMATIKO, NARAVOSLOVJE IN INFORMACIJSKE TEHNOLOGIJE

Master's thesis

(Magistrsko delo)

Simulation of wind driven rain effect on aesthetical performance of wooden facade

(Simulacija deževnega učinka na estetično delovanje lesene fasade)

Ime in priimek: Richard Acquah
Študijski program: Trajnostno grajeno okolje, 2. stopnja
Mentor: doc. dr. Jakub Michal Sandak

Koper, avgust 2021

Ključna dokumentacijska informacija

Ime in PRIIMEK: Richard ACQUAH

Naslov magistrskega dela: Simulacija deževnega učinka na estetično delovanje lesene fasade

Kraj: Koper

Leto: 2021

Število listov: 83 Število slik: 26 Število tabel: 1

Število prilog: 8 Št. strani prilog: 19

Število referenc: 45

Mentor: doc. dr. Jakub Michal Sandak

UDK: 692.232(043.2)

Ključne besede: horizontalni dež (WDR), računska dinamika fluidov (CFD), informacijsko modeliranje gradenj (BIM), laminarni tok in sledenje delcev, simulacija.

Povzetek: Inženirji, oblikovalci ter lastniki stavb že v zgodnjih fazah gradbenih projektov hočejo vedeti, kako bo lesena fasada izgledala skozi leta izpostavljenosti zunajnim dejavnikom. Tehnologije, kot so računska dinamika fluidov (CFD) in informacijsko modeliranje gradenj (BIM), ki vse bolj pridobivajo na priljubljenosti, nudijo pomoč pri reševanju tega problema. V tej raziskavi je predstavljena uporaba računske dinamike fluida (CFD) in informacijsko modeliranje gradenj (BIM) za predvidevanje videza lesene fasade po izpostavljenosti zunanjim faktorjem za določeno obdobje. Potek dela je bil razdeljen v štiri faze. V prvi fazi se je uporabilo orodje BIM za načrtovanje gradbene geometrije. V drugi fazi so se določili vzorci vlaženja stavbne fasade. Tretja faza je vključevala obdelalo podatkov in v zadnji, četrti, fazi se je rezultate predstavilo vizualno s pomočjo orodja BIM. Analiza v tej raziskavi je vključevala osem samostojnih deževji. Simulaciji laminarnega toka in sledenja delcev sta bili uspešni, kot tudi določitev vzorcev vlaženja in odmerkov vlage. Na podlagi mape vzorcev je bila opravljena simulacija teksture lesa ter videza smreke. Vizualizacija končnega videza lesa se je uspešno izvedla s pomočjo orodja Revit. V tej študiji smo ugotovili, da je predlagani potek dela učinkovit in prinaša ustrezne rezultate. Namen raziskave je, da lahko služi tudi kot podlaga za prihodnje znanstvene razprave o uporabi orodja BIM ter ostale računalniške tehnologije za simulacije predvidevanja videza lesenih fasad, pri izpostavljanju lesa zunanjim klimatskim pogojem.

Key document information

Name and SURNAME: Richard ACQUAH

Title of the thesis: Simulation of wind driven rain effect on aesthetical performance of wooden facade

Place: Koper

Year: 2021

Number of pages: 83 Number of figures: 26 Number of tables: 1

Number of appendix: 8 Number of appendix pages: 19

Number of references: 45

Mentor: Assist. Prof. Jakub Michal Sandak, PhD

UDC: 692.232(043.2)

Keywords: Wind-Driven Rain, Computational Fluid Dynamics, Building Information Modelling, Laminar Flow and Particle Tracing, Simulations.

Abstract: Engineers, designers as well as building owners at early design stages of construction projects are concerned about how the wooden facade will look like over years of exposure to climatic conditions. Novel technologies including Computational Fluid Dynamics and Building Information Modelling possess a great potential in helping solve this problem. This research proposes a workflow that integrates Computational Fluid Dynamics and Building Information Modelling to predict the aesthetical performance of wooden facade when exposed to external climatic conditions over a pre-defined period of time. The proposed workflow in this research is classified into four stages. The first stage involved using Building Information Modelling tool to prepare the building geometry. The second step was to compute for the wetting patterns on the building facade. The third step was determination of the building response to the given dose of weathering. The fourth step involves the visualization of the results in BIM. The demonstration of the simulation approach was performed on the basis of the typical climate in Ljubljana. Eight wind driven rain scenarios most frequently occurring were used. The laminar flow and particle tracing simulations performed were successful. The dose maps of the wetting patterns were successfully computed for all wall of the model building. Textures that are dependent on the dose map computed for and aesthetical appearance of spruce wood were generated successfully. Also, the final aesthetical appearance of the wood based on the wetting patterns were successfully visualized in Revit. In this study, it was found that the proposed workflow was effective. This study serves as a conversation opener for research discussions on the integration of BIM and computational simulation techniques to quantify the aesthetical appearance of wood exposed to external climatic conditions.

LIST OF CONTENTS

LIST OF TABLES

LIST OF FIGURES

LIST OF APPENDICES

LIST OF ABBREVATIONS

CFD	Computational Fluid Dynamics
BIM	Building Information Modelling
WDR	Wind Driven Rain
RANS	Reynolds Averaged Navier-Stokes
LES	Large Eddy Simulation
BPS	Building Performance Simulation

ACKNOWLEDGEMENTS

I would like to thank AD FUTURA and the Ghana Scholarship Secretariat, for their financial support during my master studies.

I would also like to express my deepest gratitude to Assist. Prof. Jakub Sandak, my research supervisor, for his patient guidance, enthusiastic encouragement and useful critiques of this research work. To my program coordinators Assist. Prof. Matthew Schwarzkopf and Prof. Andreja Kutnar for their enormous assistance throughout my master studies. And to all my professors for the knowledge they shared.

I would also want to acknowledge the entire CLICKdesign Project Team for making it possible for me to work on this research and for making available to me their resources. And to Innorenew CoE for giving me the opportunity to work on some of its projects.

My grateful thanks are also extended to Urban Kavka and Cvetanka Petrova for helping in the translation of relevant sections of this research into Slovenian and also for helping make my stay in Slovenia memorable.

A special thanks to Hanka Remešová, Giovanni Allesi, all my colleagues and friends in Slovenia for helping to make my stay in Slovenia exceptional.

And finally, to my family for the support.

1 INTRODUCTION

Wood as a bio-based material has widely been used as a construction material for centuries. With the growing concerns about the worsening effect of carbon dioxide emissions, global climate change as well as creating sustainable living environment, there is an increasing interest towards the use of bio-based materials (largely wood) in the construction industry. This is because, it is estimated that bio-based materials will play a significant role in making the construction industry more sustainable than alternative building solutions. In addition, low lifecycle cost of using wood, relatively ease of processing and easy accessibility makes the use of wood within the construction space a better choice [1]. Furthermore, Plesser et al, [2] as cited by Rüther and Time [1] found that the use of wood as facade is favourable in terms of greenhouse gas emissions and lifecycle environmental impact, when compared to cement-based materials, or brick and metals. They have also demonstrated that the use of wood as facade is even more sustainable in terms of reducing greenhouse emissions and environmental impact when the wood is untreated. This is a significant finding since contemporary architectural developments are moving towards reducing surface treatments of construction materials. However, wood when used untreated undergo changes from its natural colour when it is exposed to the external climatic conditions.

As the design of wooden facade continue to evolve, engineers and designers continue to research into ways of assessing and improving its performance. The performance requirements for the facade can be classified into technical performance and aesthetical performance. Technical performance is related to the ability of the facade to perform its function of protecting the building from the effect of the external climatic conditions. The aesthetical performance on the other hand is related to the ability of the facade to meet the requirement of being visually appealing. Building Performance Simulation (BPS) relays on the replicating the performance of the whole building (or its part) by utilizing computer-based models relaying on the fundamental physics and engineering principles. BPS has introduced a whole new dimension into the assessment of the building performance and become over the years popular solution for the assessment of the building performance. Technical performance of wooden facade has gained a lot of attention over the years within the research context of BPS. However, the aesthetical performance of the wooden facade which has not gained as much attention in research till now, is considered as a highly relevant aspect of the building service life.

Engineers, designers as well as the building owners desire to know how the facade will look like over years of climatic exposure. The change of the visual appeal of the building facade is a very complex process. Consequently, it is hard to predict the appearance with a high level of accuracy at the time of design. However, with recent developments in technologies including Computational Fluid Dynamis (CFD) as well as Building Information Modelling

(BIM), both gaining popularity in the modern construction industry, has a great potential to solve this problem.

1.1 AIM AND OBJECTIVES

The aim of this study is to propose and test a workflow that integrates Computational Fluid Dynamics (CFD) and Building Information Modelling (BIM) to predict the aesthetical appearance changes of the wooden facade when exposed to external climatic conditions over a certain period of time. Three specific objectives were defined in other to achieve this goal. They include

- Quantify Wind Driven Rain (WDR) loads on the wooden facade of a building using BIM and CFD.
- Estimate WDR doses on the wooden facade.
- Visualise the change in appearance of the wooden facade over time based on the estimated dose.

1.2 BACKGROUND AND SIGNIFICANCE

For the past two decades, there is an increasing concern for the use of renewable materials in the Architectural, Engineering and Construction (AEC) sector. This is because the AEC sector contributes massively to the worldwide environmental crises including global warming. The use of renewable material such as wood has the potential to help the AEC sector to cut down on the adverse impact towards the global environmental crises. The increasing use of wood in construction comes with its use under external climatic conditions, particularly as building facades.

When the wood is exposed to the external climatic conditions in its use as facade, it is subjected to the complex process of wood weathering.

Wood as a biodegradable material undergoes physical and chemical changes when subjected to a combination of external factors such as light, moisture, or heat as well as diverse mechanical forces. Natural weathering affects the surface layer of wood the most and this is easily manifested by a change in appearance and colour of the wooden element. This process will be referred in this study as an "aesthetical change in wood".

The understanding of the mechanisms as well as kinetics of changes that wood as a construction material undergo are very important to engineers and architects. Architects and clients are particularly interested in the aesthetical performance of wood when it undergoes changes due to weathering. This is because, the ability to predict the aesthetical appearance may help architects to optimize the facade design options and to make relevant design changes to the facade at the earliest stage of the designing process. It will also give clients the opportunity to make informed choices about the building facade material. Considering

all these benefits, it is still difficult to predict the aesthetical performance at the early stages of building conceptualization. However, the rapid development of the Computational Fluid Dynamics within the AEC industry, combined with the increasing use of Building Information modelling for structure design and management makes the prediction of the aesthetical performance of wooden facade possible.

Temperature, wind driven rain as well as solar radiation are the key climatic factors that influence the aesthetical performance of wooden facade [3]. These climatic factors are all important in the wood weathering process. However, only the simulation of the influence of wind driven rain on the aesthetical performance of wooden facade has been considered in this research. To the best knowledge of the author of this study, there is no research study that simulates the effect of wind driven rain on the aesthetical performance of wooden facade by integrating BIM and CFD. This makes this study, the first to propose an original workflow to simulate the influence of wind driven rain on the aesthetical performance of wooden facade significant.

1.3 SCOPE AND ORGANIZATION OF STUDY

This thesis is an integral part of the CLICKdesign project led by the UK company Building Research Establishment (BRE). CLICKdesign is a multi-institutional project that seeks to deliver fingertip knowledge to enable service life performance specification of wood. The study presented falls under the Work Package 3, that is focused on the aesthetic performance of buildings.

In this research, a simulation protocol that assesses the aesthetical appearance changes of the wooden facade subjected to the external climatic conditions is developed. A workflow that integrates BIM and CFD is used. Among the various climatic factors influencing the aesthetical performance of the wooden facade, the simulation and quantification of the wind driven rain dose was selected as a case study. This Master Thesis is organized in four chapters:

- *Chapter one* is an introduction to the study. The aim and objectives are presented, the background for this study as well as the significance of the study is defined. In addition, the scope of the study and a general overview is provided. As part of chapter 1, the Key terminologies and principles related to this study are defined. Also in chapter 1, a background on the chemical composition of wood and its role in determining the appearance (colour) of wood is discussed. Key principles that are related to the process of wood weathering as well as the factors that influence wood weathering are explained. In addition, a brief description of terminologies used in this study, including Building Information Modelling, Computational Fluid Dynamics, Wind Driven Rain is presented. It also details the related conditions that are required for the performance of CFD simulation of the wind driven rain. In addition, a brief review of relevant literature is presented.

- In *chapter two*, descriptions of the materials, methods and proposed workflow used in the study are outlined. The chapter explains all the processes proposed for an effective prediction of the aesthetical changes in wooden facade when exposed to the climatic conditions.
- *Chapter three* is a presentation and discussion of the results obtained in this study. The statistically relevant wind driven rain scenarios are presented and analysed. Results obtained for the wind flow simulation as well as determination of the raindrop trajectories and wetting patterns are presented and discussed. Finally, the resulting weathering dose map combined with the computer-generated textures of the wooden boards are used for demonstration and visualization of the aesthetical changes.
- *Chapter four* presents the conclusions, limitations, and future research considerations.

1.4 CHEMICAL COMPOSITION OF WOOD AND WOOD COLOUR

The chemical composition of wood varies based on several factors, including the type of wood, the part of the tree from which the wood was obtained and the geographical location as well as the climatic condition in which the tree grew, among others [4]. This makes it difficult to determine the specific content of constitutive wood polymers for a certain species or even for a given tree.

The core chemical components of the wood cell wall include three types of organic substances: carbohydrates (cellulose and hemicellulose), lignin and extractives. Cellulose, hemicellulose, and lignin together represents more than 90% of the content and are considered as the main structural components of wood [5]. Conversely, extractives even if representing only a small proportion of the wood mass, highly determine several of its critical properties. It should be mentioned that cellulose, hemicellulose, lignin as well as extractives are differently responding to the degrading factors when exposed to natural climatic conditions.

1.4.1 Carbohydrates

The carbohydrate portion of wood consists of cellulose and hemicelluloses. Cellulose and hemicellulose are polymers of sugar that makes up about 55% to 65% of wood mass [5]. Cellulose as well as hemicellulose make up the main structural composition in wood [6]. Cellulose is insoluble in most solvents including strong alkali as well as water. Hemicellulose, on the other hand, is soluble in alkali while insoluble in water [4]. Cellulose and hemicellulose absorb very little visible and ultraviolet light. They therefore do not significantly contribute to the photodegradation by ultraviolent radiation emitted by the Sun [7]. However, both are highly hygroscopic resulting in absorption/desorption of the moisture from the surrounding air or rain/wetting events.

1.4.2 Lignin

Lignin corresponds to approximately 20% to 30% of the wood mass. Due to the rigid structure, it contributes to the structural strength of wood. Unlike cellulose and hemicellulose, lignin is a good light absorber [7] resulting in the higher susceptibility to photodegradation [8]. Lignin is not easily dissolved by water and less hygroscopic than carbohydrates.

1.4.3 Extractives

Extractives are the non-structural chemical components of wood that corresponds to 4% - 10% of the wood dry mass. Extractives are present outside the cell wall and do not contribute therefore to the cell wall structure. However, extractives help the preserve wood from fungal and/or bug attacks. Most extractives in wood are soluble to diverse solvents such us acetone, alcohol as well as water [5]. Extractives in wood are usually sensitive to UV light and heat [6], leading to the pronounced photodegradation and photo-discoloration. The quantity of extractives differs between wood species but is also influenced by factors such as growing conditions and the amount of heartwood. Extractive content in wood comprises of a diverse range of organic compounds in relatively small amounts. Wood extractives contain compounds including sterols, fatty acids, phenolic compounds such as quinones, flavonoids, tannins, sugars, gums, starches, and colouring matter [6]. These phenolic compounds in wood extractives have been found to have a close relation to the wood discolouration. Nzokou and Kamdem [7] reported that the discolouration that occurs in wood during exposure to weathering depends on the type and content of wood extractives.
In addition, it has been found that wood cellulose, hemicellulose and lignin does not exhibit any distinctive colour [3], [8]. As a result, the colour of the natural wood is attributed to the amount and chemical nature of the dominant-coloured extractives [7]. It was confirmed in the work of William [3] and Chang et al [9] who stated that extractives are key chemical components determining wood colour.

1.4.4 Colour of Wood

Colour is a key aesthetical performance attribute of building materials that influences building design decisions and the perception of building owners. Colour is recognized by humans when light-sensitive receptors called cones and rods in the retina absorbs visible light rays (wavelength from 380 to 780 nm) that enter the eye. When visible light hits the surface of a material, all the light or some of the light is absorbed or reflected. An object is perceived as white because it reflects all the light without any absorbance. Conversely, an object perceived as black when absorbs all the light. The reflected light, particularly its spectral composition and intensity at each wavelength is perceived by the human eye as the

colour. The chemical composition and physical properties of every material, such as density, determine the way how the light is absorbed/reflected from the surface, resulting in the differences in the colour perception. Thus, the colour of wood as we perceive is a result of the composition and amount of light that is reflected from the wood surface. The colour of wood varies according to the wood species and its morphology. Wood colour may range from almost white in the case of the softwood sapwood to almost black in the heartwood of some exotic broadleaf species [10]. As mentioned earlier, extractive components are the major compounds determining the wood colour [9], [3]. The yellow shades in wood are governed by wood lignin photochemistry [11] while the extractives are correlated to the red and hue colour tones [12]. Nzokou and Kamdem [7] found that the total discolouration rate of wood due to weathering is significantly affected by the water extractable compounds in wood.

Generally, wood colour changes during weathering are affected by the chemical deterioration of lignin and extractives [3]. The yellowing or browning of wood is observed after several months of exposure to external climatic conditions. Extractives are first components to be bleached, even before the change of wood surface colour becomes apparent. Usually, the dark wood turns to become light, while light wood becomes darker, especially at the early phases of the natural weathering process.

1.5 WEATHERING OF WOOD

Wood exposed to external outdoor environment deteriorates due to several processes including weathering, decay, biodegradation, or oxidation [13]. These processes cause wood to lose its original appearance. In this study, the influence of weathering was the focus.

“Weathering” is a general term that is used to describe the slow degradation of materials that are exposed to the weather conditions. “Natural wood weathering”, on the other hand, is a term used to describe the natural degradation process occurring in the unprotected wood that is exposed to the external climatic conditions. The intensity of the wood weathering is highly dependent on the local micro climatic conditions as well as the type of wood and its species. Wood weathering influences the mechanical, chemical, and biological properties of wood, as well as its aesthetical appearance. Nevertheless, the most evident effect of the wood weathering is the aesthetical (colour and texture) change from its natural colour to dark grey. The discoloration process is followed by the loosening of wood fibres and the gradual erosion of the surface [3]. Most of the aesthetical changes undergoing on the wooden facade are superficial. Sandak et al [13], stated that apparent colour changes are visible already after three months of the exposure to natural weathering. They also found that the longer wood is exposed to natural weathering, the darker it becomes.

Weathering of wood occurs as a result of a complex combinations of mechanical (abrasion effect by wind-blown materials), chemical, biological and climatic phenomena. The latest

factor is related to the cyclical wetting (rain, dew, snow, and high air humidity), temperature changes or solar radiation (sunlight). These factors are briefly described below.

1.5.1 Sunlight

Sunlight is the primary factor influencing wood weathering. Although visible light can contribute to wood deterioration due to weathering, the ultraviolet radiation has the greatest influence. UV usually initiates deterioration and causes photo-oxidation or photochemical degradation of the surface of wood. Wood degradation starts as soon as the wood is exposed to sunlight [3]. Although the UV spectrum represents only 5% of the sunlight energy, its photodegradation effect on wood is most pronounced. UV radiation degrades mainly the lignin and extractive components [14]. Decomposed lignin (as well as extractives) is then leached from the surface of wood. The wood fibres become loosen and only barely attached to the surface. These are usually removed from the wood surface during first rain event or even by the wind action. The intensity of losing fibres is different in the late and early woods that leads to the uneven surface erosion.

1.5.2 Precipitation (Moisture)

Frequent exposure to rapid moisture changes is a significant factor that boost weathering of wood. In that case, the wood may be exposed to the moisture from diverse sources such as rain, snow, dew or airborne humidity. When the unprotected wood surface is wetted, the moisture is quickly absorbed by the surface layer through capillary action. This is followed by the absorption of the moisture within the cell wall of the wood. This may lead to the mechanical damages such as splits, cracks and other deformations. These severe deterioration actions are accelerated by the photodegradation processes of wood caused by the UV light irradiation. Rainwater leaches soluble extractives as well as hydrophobic lignin that are decomposed by ultraviolet light. It results in sever chemical changes and discoloration of the surface layer of wood. Rainwater abrades the surface of wood and washes away degraded components. The colour of woods weathered solely by sunlight irradiation become red brown [8]. Conversely, the weathered wood surface colour with a presence of moisture become grey [14].

1.5.3 Temperature

The influence of temperature changes in wood are not as essential as the influence of ultraviolet light or moisture in the wood weathering process. However, the rate of photochemical degradation or oxidative reactions in wood increases at elevated temperatures [11]. Although hardwoods generally discolour at lower temperatures than softwood, it is

generally known that the rate of colour change due to weathering increases as temperature increases.

1.6 BUILDING INFORMATION MODELING (BIM)

BIM is a collaborative design process that permits all project stakeholders of diverse disciplines to collaboratively design, build and manage construction projects. It has developed rapidly in the Architectural, Engineering and Construction industry in the past two decades and has emerged as a key modelling technology in the field of architecture [15]. The BIM model is meant to contain information including the building geometry, site characteristics, characteristics of the building components as well as other operational parameters of the building in a digital model.

The data contained in the BIM model can be explored in several applications. It is used to manage and control the entire design and construction processes as well as computational simulations. Building Energy Simulations (BES) or Computational Fluid Dynamics (CFD) requires 3D models of buildings. BIM has proven to help increase consistency and speed up the computational simulation processes since the 3D model as well as the data stored in BIM model is used to set conditions required in the simulation process. With focus on simulating the facade of the building, a 3D model containing basic elements including wall, roof, floor, windows, and door as well as their relevant mechanical properties can be easily created by implementing BIM-compatible software tools.

1.7 WIND AND WIND DRIVEN RAIN

Wind is defined as the movement of an air from regions of higher pressure to regions of lower pressure in the earth’s atmosphere [16]. When the weather is calm and windless, raindrops fall vertically. On the other hand, when the events of wind and rain happen at the same time, there is a deviation to the trajectory of raindrops from the vertical fall in mid-air. This results in the development of an oblique trajectory component of raindrops known as wind driven rain.

Wind driven rain is an event that is important in several research fields including meteorological sciences as well as building science and design [17]. In building design, wind driven rain is a principal moisture source that directly affects the durability, hygrothermal and aesthetical performance of facades. Wind driven rain influence on buildings include both, droplet runoff and splashes. The destructiveness of the wind driven rain happens in several forms including accumulation of moisture, discoloration, structural cracking as well as rapid thermal and moisture changes. Building facades, which are mostly exposed to the external climatic conditions are one of the major building components that are severely

affected by the wind driven rain. As a result, it is important to accurately quantify the wind driven rain loads on building facades.

1.8 NUMERICAL SIMULATION OF THE WIND DRIVEN RAIN

Quantification methods used to estimate the wind driven rain loads include experimental methods, semi-empirical methods, and numerical methods. Each possess peculiar set of disadvantages and advantages.

Experimental measurements involve full scale in-situ measurement with a dedicated equipment, such as wind driven rain gauges. These sensors are similar to the classical rainfall gauges. The difference is that rainfall gauges have horizontal aperture to measure rainfall. Wind driven rain gauges, however, are equipped with a vertical aperture to collect the amount of wind driven rain [17]. The experimental methods of quantifying wind driven rain are considered as the primary tool used in majority of applications. Though, experimental methods are time consuming, expensive and may suffer from large measurement errors [18]. Since wind driven rain is not a standard meteorologically measured weather parameter, researchers tend to use alternative solutions that allow to quantify wind driven rain. It is usually done by establishing a relationship between the quantity of wind driven rain and measured climatic variables including wind velocity, wind direction and horizontal rainfall intensity. This technique is considered as a semi-empirical and has solid theoretical bases as well as a reliance on estimated parameters. Semi-empirical methods are easy to use [19] and allow for a quick estimation of the wind driven rain on buildings. Although estimates from semi-empirical methods may be sufficient in some situations, they are not efficient to provide thorough information such as the complete wind driven rain distribution on the building facade. Therefore, there is the need to resort numerical methods in more demanding and reliable applications [17]. The result of numerical simulation to quantify wind driven rain is more accurate, faster and provide less limited results than the use of alternative semi-empirical methods [20]. Especially nowadays, the progress in numerical simulation methods of quantifying wind driven rain provides a new impulse in the wind driven rain research space. An approach of coupling wind flow simulation with particle tracing for fluid flow simulation is most frequently implemented solution.

In this study, the numerical method of quantifying wind driven rain was adopted. There have been similar attempts to quantify wind driven rain through numerical simulations since the early 1990s. Computational models solving equations of the motion for droplets were implemented as pioneer solutions [21]. Since then, several researchers have contributed significantly to the development and application of alternative techniques to quantify wind driven rain [16], [22] - [23] . Especially Computational Fluid Dynamics (CFD) algorithms achieved significant advancement. They are capable of delivering precise spatial distribution of wind driven rain even on complex building geometries

Karagiozis et al [22] studied the pattern of wind driven rain falling on the exterior facade of two buildings (with one being twice the size of the other) using three dimensional CFD approach for solving airflow around the building and particle tracking of raindrops around both buildings. It was reported that the amount of wind driven rain that is hitting the facade of the building increase from the bottom to the top. They also found that, the rainfall intensity did not have any significant influence on the wetting pattern. However, the higher wind velocity significantly increased the amount of wind driven rain that the building facade receives. This explains the reason why high-rise buildings do not significantly receive more wind driven rain than low-rise buildings [23]. Mohaddes et al [24] studied the effect of overhangs on the wind driven rain wetting patterns using numerical simulation methods. They found that wind speed and wind direction (when compared to rainfall intensity) have a greater influence on the performance of overhangs, as well as wind driven rain loads. Rychtáriková and Vargová [25] studied the behaviour of the wind driven rainwater on the surfaces of windows and explored the self-protecting effect of buildings. They used the numerical simulation method of CFD as well as the semi-empirical method. It was found that the areas that are immediately underneath the overhangs are shielded from the wind driven rainwater. It confirmed an observation that overhangs have a significant influence on the wetting patterns by wind driven rain. Nore et al [26] measured wind driven wetting on the low-rise test building in Norway. It was found that wetting patterns are highly influenced by the wind direction. Karagiozis et al [27] researched an influence of the wind driven rain on the hygrothermal performance of buildings. They found that wind driven rain is strongly dependent on the orientation of the building. Similar research was performed by Pérez-Bella et al [28] for assessing wind driven rain influence on buildings in Spain.

Several other researchers performed significant studies using experimental and semi-empirical techniques for describing wind driven rain phenomenon. These studies serve as a foundation for the principles that are recently used in the quantification of wind driven rain by numerical simulation. Wolf and Griffith [29] stated that the intensity of the wind driven rain differs significantly depending on the building location and elevation. Ge et al [30] used the experimental method to estimate the spatial distribution of the wind driven rain on the facades as “wall factor” and “catch ratio”. They found that, the spatial distribution of wind driven rain on the surface of the facade was influenced significantly by the building geometry. Particularly the details of the facade and the conditions of the surrounding of the building were identified as highly influential factors.

Advancement in the computer’s performance allowed intensive development of the wind driven rain numerical simulations. However, implementation of numerical solutions for buildings requires a large amount of time necessary to produce geometrical models and define the required model parameters. Complex geometries result in the necessity for using high performing computers and elongation of the calculation times. However, these

challenges can be properly addressed when combining numerical simulations with Building Information Modelling software.

It can be summarized from the reviewed literature that the extent at which wind driven rain affects facades is dependent on diverse parameters including: the nature of the building geometry, the orientation of the building and the facade, the topology of the building's location, wind direction, wind speed, rainfall intensity, raindrop size and distribution, the frequency as well as duration of rain events [17]. It is also necessary to consider additional factors, such as water splashes and/or runoffs on the surface of the facade to achieve most reliable simulation results. Nevertheless, all these factors make numerical simulations of wind driven rain a highly complex problem. A usual protocol for estimation of the wind driven rain consists of two basic steps. The first step is related to simulation of the airflow, typically considered as a laminar flow problem. Modelling of the raindrops trajectories is performed in the second step by implementing particle tracing for fluid flow theorem

1.9 COMPUTATIONAL FLUID DYNAMICS (CFD)

The interactive effect of environmental conditions (thermal, wind, rain) on the buildings is an essential phenomenon that helps to improve the ability of structure to meet the expectations for which it was designed. The capacity to estimate diverse effects of environmental conditions on buildings is of a great help for designers and engineers to optimise the project at its early design stages. However, it is not an easy task to properly understand the interaction of buildings with the environment. A special focus on the development and use of new applications and powerful simulation tools to analyse the environment and building interaction was directed over the past few decades. One of such tools that gained particular attention within the AEC industry is CFD, used primarily as a Building Performance Simulation (BPS) tool.

CFD is a branch of fluid mechanics that analyses fluid flow, heat transfer and related phenomena using numerical methods and algorithms. CFD comprises the combination of physics, mechanics, flow technology, mathematics, and computer applications [31]. The basis of most CDF problems is associated with the Reynolds-averaged Navier-strokes (RANS) equations or simply the Navier-strokes equations. RANS simulations have been used to gain understanding of different wind flow problems, especially for solving stationary CFD questions. Large Eddy Simulation (LES) on the other hand is used when handling non-stationary studies that are associated with turbulent flow processes [32].

CFD has proved, over years of application and development, to be a suitable tool that can be useful during the design stage. It simplifies the designing procedures and makes it faster to make informed modifications of projected building geometry already at the earliest stages. CFD was originally developed as a cost effective and efficient way to experimentally test aircraft components before building prototypes [33]. Although CFD is nowadays largely

used in the aerospace and automobile industries, its use in the architectural and construction industries is rapidly growing. CFD techniques have improved over the years and become more adjusted to the specific needs of architects and construction engineers. CFD is used as a building physics tool to predict heat transfer characteristics, humidity levels as well as wind and airflow paths within and around the building. It helps architects and engineers to predict the future performance of the structure, understand the impact of design changes and help evaluate, compare or optimize different design options. CFD like other simulation techniques is a tool useful in complementing or entirely replacing already existing analytical techniques. It is especially useful in situations where variety of initial design variations must be analysed and compared. Simulation is highly useful when physical testing is prohibited/restricted by cost, scale, accessibility and/or the environmental hazard, health, and safety factors [31].

There are several tools used to compute CFD problems, including OpenFOAM, COMSOL Multiphysics, ANSYS, SimScale and Autodesk CFD. COMSOL Multiphysics was used in this study due to the license availability and high convenience for implementing architecture-related problems. An important advantage of this software is a possibility to directly import BIM models including building geometries.

Typical CFD simulations can be divided into three main processes: pre-processing, processing (solver), and post processing.

1.10 PRE-PROCESSING

Pre-processing is the first step of the CFD simulation process. Pre-processing includes creating and detailing the reference building geometry, the computational grid (mesh) generation, defining the material properties and setting of the boundary conditions.

1.10.1 Building Geometry

The first step in any CFD simulation involves creation of the computational domain as well as the object/building geometry. The greatest challenge of using CFD tools within the construction industry is the difficulty to import complex building geometries with high detail representation. The best way to overcome this problem is a direct software integration of CFD with BIM. Such an approach was implemented for the needs of this research.

1.10.2 Computational Mesh (Grids)

The second step of the pre-processing phase involves mesh creation. A proper mesh generation is a critical to assure reliable results obtained after reasonable computational time. The spatial resolution of the simulation results highly depends on the mesh characteristics.

Optimal mesh helps to simplify the calculations and makes CFD simulation analysis more accurate. In addition, the mesh setup significantly influences the hardware requirements, especially RAM memory and number of CPU cores. Computation of mesh involves dividing the geometry and the computational domain into finite number of grids [15]. The numerical solution is computed individually for each grid. The most accurate analysis require finer meshes. However, its further refining results in elongation of the simulation time.
Meshes can be classified into structured (mapped or regular) and unstructured (free) meshes. Structured/mapped meshes can be cartesian or curvilinear, creating a consistent and uniform pattern [42]. Gridlines are arranged parallel to the coordinate axis for cartesian structured meshes. Conversely, the gridlines are curved to fit properly with the boundaries of the geometry or computational domain in the case of curvilinear meshes.
Unstructured meshing creates typically a ″free″ type of shapes and patterns for the given geometrical element. Even if unstructured meshes are considered as less accurate, they are most preferred for describing more complicated geometries and domains [43]. This makes unstructured meshes most widely used for the CFD simulations. The individual grids of unstructured meshes are usually triangular shaped for two dimensional geometries and domains. Conversely, tetrahedral shaped elements are usually implemented for three dimensional geometries and domains.

1.10.3 Boundary Conditions

The definition of boundary conditions is required after completing the pre-processing step. In CFD simulation, boundary conditions should be defined for each of the surfaces on the computational domain. The boundary conditions set in the simulation model define inputs of the simulation. It also allows the simulation model “interact” with its virtual surroundings. The simulation cannot be complete without the properly selected boundary conditions and in most instances the simulation cannot even proceed. Some of the most common boundary conditions used in CFD simulations includes wall, inlet, outlet, and symmetry.

1.10.3.1 Wall Boundary Condition

Wall is the most common boundary condition that is encountered in in confined fluid flow problems. For Laminar fluid flow interface, the boundary options include Slip, No Slip and leaking.
The fluid will have a zero-velocity relative to the boundary when the surface of a stationary wall boundary is set as no slip. It implicates that there is no relative movement between the fluid particle and the boundary [34]. This set condition ensures that particles (rain drops) that falls parallel to the surface are brought to the rest when they meet at the surface. For the stationary wall, this is expressed by setting the velocities of the wall boundary to 0 m/s.

On the other hand, a slip boundary condition is applied when a no-slip condition is not desired. In this case, the velocity of the fluid at the boundary is not zero. There is no clinging effect at the wall boundary when the slip boundary option is used. The slip boundary option specifies that there will be no penetration at the boundary layer at which it is set. A slip option is a reasonable approximation if the purpose of the wall is to prevent fluid from leaving the computational domain [35].

Unlike slip and non-slip boundary conditions, a leaking boundary option is set to simulate a wall where the leaks into or leaves the computational domain. It is required to specify the fluid velocity on the leaking wall.

For particle tracing interface, some boundary options for wall include bounce, freeze, stick, disappear, pass though, diffuse scattering, isotropic scattering, general reflection, and mixed diffuse and specular reflection.

The wall bounce boundary option makes the particles reflected from the wall. The wall freeze boundary option causes the particle to no longer change position and velocity after contacting the wall. The velocity of the particle remains the same as when the particle hits the wall. The disappear boundary option when used implies that the particles should not be displayed when they touch the wall. The pass-through boundary option implies that the particles are allowed to cross the wall boundary without any resistance and is similar to the disappear boundary alternative. The stick boundary fixes the particle position when it hits the wall boundary.

1.10.3.2 Inlet Boundary Condition

The inlet is a key boundary condition for fluid flow problem definition and determines a net flow into the computational domain [35]. Inlets are usually indispensable for any CFD simulation in a forced convection situation. It specifies the flow variables such as the inlet fluid velocity. It is advised to consider setting an outlet boundary condition in addition to the inlet to assure a well-defined mathematically problem. The options for inlet boundary conditions include velocity and pressure.

The inlet boundary condition is applied in the particle tracing module to the boundary from which the particles (for example rain drops) will be released into the computational domain.

1.10.3.3 Outlet Boundary Condition

Outlet boundary conditions are set on the boundary where the flow is directed out of the domain. It defines the fluid departure. Typically, a specified relative pressure is imposed [36]. In analogy to the inlet boundary condition, the outlet condition has velocity and pressure as the available boundary options [35]. For a numerically sound problem definition, the pressure may be specified as the outlet boundary condition when the fluid velocity is

defined as the inlet boundary condition. Conversely, velocity at the outlet should defined when pressure at the inlet is used. This is necessary to avoid the occurrence of any convergence difficulties.
The outlet boundary for the particle tracing module defines what happens to the particles when these exit the computational domain. Freeze and disappear of the particle are usually used as the options for the outlet boundary condition. Both, the particle position and its velocity get still (frozen) when “freeze” is selected. “Disappear” option results in elimination of the particles once these hit the selected outlet boundary selection.

1.10.3.4 Symmetry Boundary Condition

The symmetry boundary condition is used in CFD simulations when the physical geometry and the expected pattern of fluid flow have a mirror symmetry. By setting symmetry boundary conditions in a model, its size is reduced by a half or even more [35]. This makes symmetry boundary condition a highly useful tool when solving complex problems.

1.10.3.5 Drag force Boundary Condition

The drag force boundary condition is set to exert a drag force on the particles in a fluid flow problem. The drag force is usually required in all the computational domains.

1.10.3.6 Gravity force Boundary Condition

The gravity force is used to define the gravity vector and density. When gravity force is applied, it causes particles with a suitably high mass and density to move in the same orientation as the gravity vector.

1.11 PROCESSING (SOLVER)

Numerical solution of the problem can be determined only after the geometry, computational domain, mesh and all the boundary conditions are correctly defined. All the calculations are performed in the solver process based on the equations and boundary conditions set during the pre-processing stage. The laminar flow module was coupled in this research with the particle tracing module to analyse the phenomena of the wind driven rain. First, the fluid flow field was computed with the laminar flow module. The results obtained were used as the basis for the follow-up computation of the particle (raindrops) motion.

1.12 POST PROCESSING

The final step in the CFD process sequence is post-processing. It is performed directly after getting the results from the solver and involves deriving information from the raw results. The post-processor software allows visualisation of the simulation outcomes. The results obtained in this step are graphically represented with different graphical tools including vector plots, contour plots and/or customized reports.

1.13 BIM-CFD INTEGRATION

The application of CFD in building performance simulation (such as wind around buildings, heat transfer at building exteriors and wind driven rain on building facades) requires importing of the building geometries. Since majority of the CFD software are not specifically designed to model complex building geometries, an integration of BIM into the CDF makes the simulation process faster and more efficient.

Even if BIM and CFD are distinct tools with different primary application fields, they both have the potential to complement each other in several ways. For instance, results generated by CFD tools are not easily interpreted by non-professionals since these usually contains waste numerical data which are difficult to relate to the modelled object in 3D space [37]. Though, BIM has a great potential to easily visualise the simulation results generated from the CFD simulation. Integrating BIM with the CFD software makes the simulation process smarter by taking advantage of the information already stored within the BIM model database. This provides a simplified approach as compared to the traditional CFD simulation process and widens the usability of CFD in the Architectural, Engineering and Construction industry. Amidst all these advantages, the integration of BIM and CFD has not reached yet enough attention and further research is indispensable to mature this technology.

Revit software offered by Autodesk was used in this study as the BIM platform. The CFD simulation was performed with the help of the COMSOL Multiphysics package. There are several alternative approaches for the integration of both, Revit and COMSOL Multiphysics software tools. They include the use of the Import Module of COMSOL Multiphysics which allows the import of industry standard CAD system and formats such as AutoCAD (*.dwg and *.dfx), STEP, IGES, Inventor, ACIS, Parasolid and SOLIDWORKS. Another alternative is to export/import BIM models utilizing Industry Foundation Classes (IFC) format recently introduced as an open-source interoperability solution. Nevertheless, the Live Link feature of the COMSOL was finally selected in this research for a seamless integration between BIM and CFD. This was the most convenient approach as the LiveLink feature possess the ability to directly synchronise material properties stored in the Revit BIM model with COMSOL Multiphysics [35].

The results obtained after CFD simulation as well as processed metadata (such as dose maps and facade textures) were visualised in Autodesk Revit. A custom Revit dynamo script was developed here to facilitate this process and to further integrate the BIM with CFD software.

2 MATERIALS AND METHODS OF STUDY

In this chapter, the material and methods used in this study are presented. The historical climatic data used in the simulation is discussed, as well as the process of filtering the wind driven rain events. The processes required for the simulation, the test building geometry as well as all other methods related to the simulation is outlined. The proposed workflow of the data used for simulation of the aesthetical appearance changes as used in this study is also presented. Finally, the boundary conditions for the Laminar Flow (wind flow) and the Particle Tracing (raindrop trajectories) simulations are detailed.

2.1 HISTORICAL CLIMATIC DATA AND PREDICTION OF WIND DRIVEN RAIN EVENTS

The climatic boundary condition is an essential factor that influences the reliability and accuracy of the climate dependent building simulations. The historical climatic data can be classified according to the size of the weather systems, or the area included in the model domain of the simulation. Russell [33] defined synoptic scale models which covers hundreds to thousands of kilometres and mesoscale models which only covers a few hundred kilometres. Other systems, such as Hang [38], defines urban flow simulations into meso and micro scales. They define the meso scale CFD simulation domains to cover up to 10 km to 200 km in the horizontal direction. The micro scale model domains can be further limited to 0.1-2.0 km. Wind driven rain loads on the building facade highly depend on the microclimate at the proximity of the building's location. Therefore, the simulation model developed in this study can be classified as a microscale solution precisely determining so called "material climate".

The quantification of the wind driven rain distribution on buildings requires an access to the historical climatic data set including rainfall intensity, wind velocity, and wind direction. All of these are considered as indispensable input required to perform reliable CFD simulations. The horizontal rainfall intensity (mm/h) refers to the averaged amount of rainfall reaching the horizontal surface plane in the specified time period. The reference wind velocity (m/s) corresponds to the horizontal component of the wind-velocity vector. The wind direction data denote the direction from which the wind comes. The direction is expressed in degrees or cardinal direction, ranging from 0° (North) through 90° (Est), 180° (South) and 270° (West). The wind-related data were collected for the needs of this research from the Meteonorm database [39]. An average daily weather data for the period between June 2016 and June 2017 for Ljubljana (Slovenia) was chosen as a case study for all simulations.

Figure 3 and Figure 2 presents changes of the daily average rain intensity, wind velocity and wind direction, respectively. The predominant wind directions, wind velocity and rainfall intensity in Ljubljana is summarized in Table 1. It can be noticed that the wind direction for the wind driven rain scenarios had three dominating directions including 112.5°, 157.5° and 202.5° clockwise from North.

It should be mentioned that COMSOL Multiphysics allows a direct access to the historical weather data provided by the American Society of Heating, Refrigeration, and Air-Conditioning Engineers (ASHRAE). ASHRAE has a dedicated weather database for more than 6000 weather stations around the World. It includes diverse climate descriptors such as temperature, humidity, solar radiation, and wind velocity. Unfortunately, this historical data set (as available in COMSOL software) was not directly used in this study. This is because, surprisingly, the available database does not include wind direction record. For that reason, the historical climatic data was sampled from an alternative source, namely Meteonorm database. A custom script was developed in LabVIEW for the needs of CLICKdesign project to identify the most relevant wind driven rain scenarios. The weather data processing algorithm is presented in APPENDIX D. The filtering process include:

- filtering out all time periods when no rain was detected
- create rain events histogram
- filtering out minor rain scenarios

Eight relevant wind driven rain scenarios were identified for Ljubljana location throughout the specified period. Each scenario included quantifiers describing the wind velocity, wind direction and summarized rainfall intensity, as presented in Table 1. Both, *U(x)* and *V(y)* vector velocity components corresponding to the model domain coordinate system were calculated for each wind scenario. The calculation was based on the formular below,

$$U(x) = \mathrm{wv} * \cos(\theta)$$

$$V(y) = \mathrm{wv} * \sin(\theta)$$

where, *wv* - corresponds to the wind velocity and θ is wind direction expressed in degrees. The *U(x)* and *V(y)* velocity components are relevant in the laminar flow (wind flow) simulation determining the inlet boundary conditions.

Table 1: Wind direction, Wind Velocity and Rainfall Intensity of Scenarios

WDR Scenarios	Wind Velocity (m/s)	Wind Velocity (x- Component) (m/s)	Wind Velocity (y- Component) (m/s)	Rainfall Intensity (mm/h)	Wind Direction (Deg.)	Direction
1	11.25	-4.31	10.39	100.27	112.5	ESE
2	11.25	-10.39	4.31	114.22	157.5	SSE
3	13.75	-12.7	5.26	91.35	157.5	SSE
4	18.75	-17.32	7.18	111.09	157.5	SSE
5	11.25	-10.39	-4.31	63.38	202.5	SSW
6	13.75	-12.7	-5.26	126.91	202.5	SSW
7	18.75	-17.32	-7.18	163.71	202.5	SSW
8	21.75	-20.09	-8.32	61.21	202.5	SSW

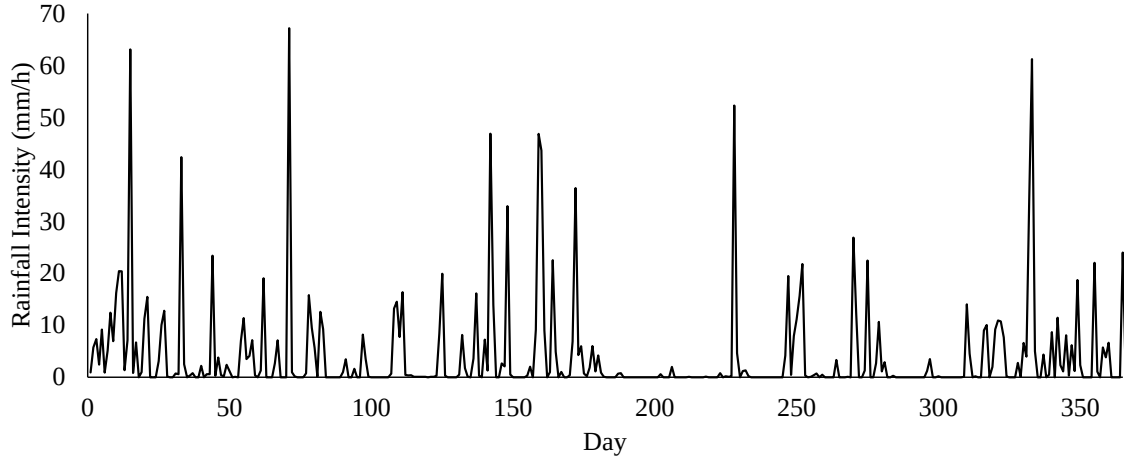

Figure 1: Daily Average Rainfall Intensity Graph (June, 2016-2017, Ljubljana)

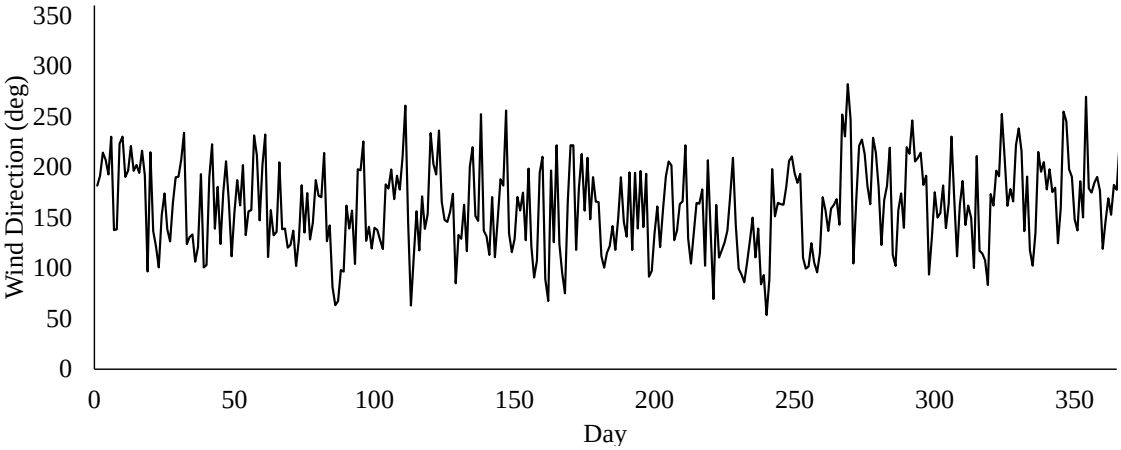

Figure 2: Daily Average Wind Direction Graph (June, 2016-2017, Ljubljana)

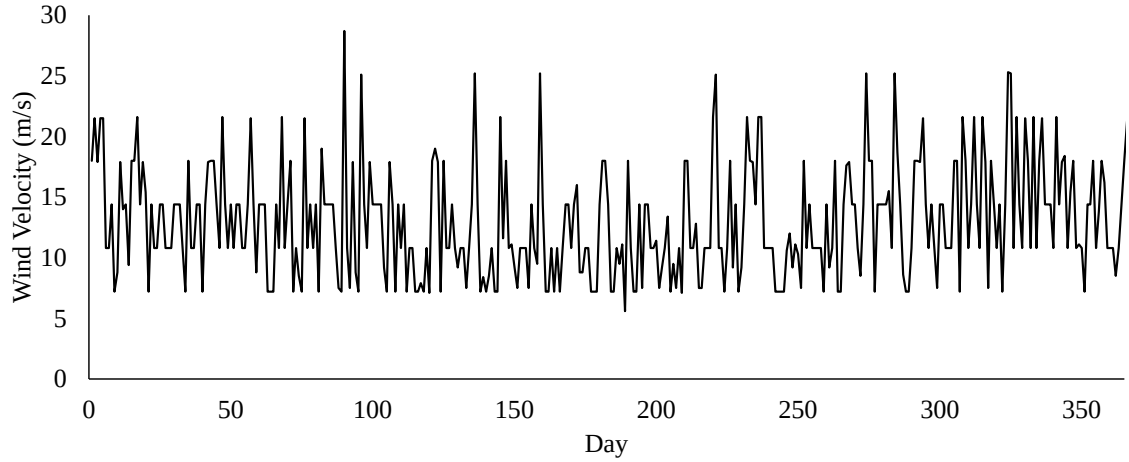

Figure 3: Daily Average Wind Velocity Graph (June, 2016-2017, Ljubljana)

2.2 COMPUTATIONAL FLUID DYNAMICS STAGES

2.2.1 Pre-Processing

2.2.1.1 Building Geometry

In this study, the building geometry was modelled in Autodesk Revit as explained in section 1.6. The model was imported for the CFD simulation using the LiveLink feature in COMSOL. The building has a simple rectangular geometry with dimensions 8.2 m x 6.2 m and a pitched roof with 0.6 mm roof overhang. The building model included two windows and a single door. The door is oriented to the West direction and each of the two windows are oriented to North and South. Figure 4 represents the building geometry and location of the basic structural components.

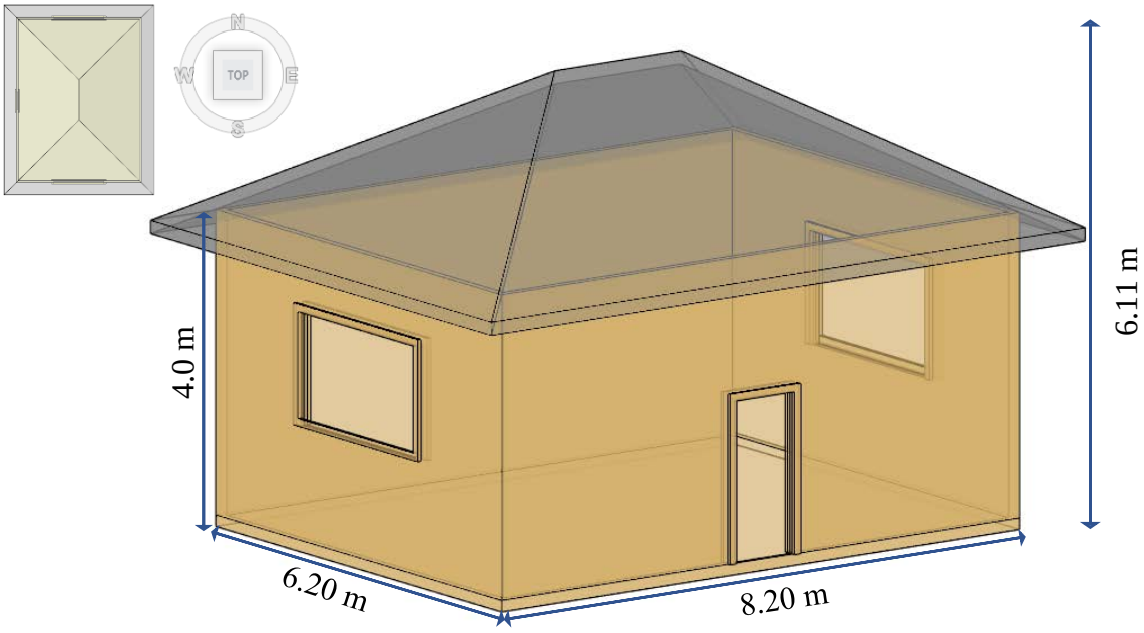

Figure 4: Building Geometry and Dimensions

2.2.1.2 Computational Domain

The computational domain within CFD simulation corresponds to the volumetric region that surrounds the building geometry. It defines the section of 3D space that bounds the area for which the governing equations are solved. It is very important to properly define the computational domain as it influences the accuracy of the simulation. A rectangular

bounding box, which serves as the fluid flow computational domain was generated around the building geometry. The computational domain has dimension L x B x H (225 m x 30 m x 17 m, respectively). The dimensions of the computational domain were set according to the guidelines set by [40], [41]. This guideline defines the recommended size of the computational domain, the minimum distances between the building model and the computational domain as well as the maximum allowed blockage ratio. The blockage ratio defines the ratio of the cross-sectional area of the building to the cross-sectional area of the domain. It is mathematically expressed as in the formula below:

$$Blockage\ Ratio = \frac{\text{Area}_{building}}{\text{Area}_{domain}}$$

Where, $Area_{building}$ is the cross-sectional area of the building geometry and $Area_{domain}$ is the cross-sectional area of the computational domain.

Franke et al [41] stated that considering an effect of the computational domain on wind load predictions of a low-rise building it is recommended to assure 3% maximum blockage ratio. It was also reported that the greater the wind blocking effect by the building, the lesser it will receive wind driven rain at its lower parts [18]. The wind blocking effect was defined there as the disturbance of wind flow pattern by the presence of the building geometry.

With the cross-sectional area of the building geometry being 50.84 m^2 (8.2 m x 6.2 m) and the cross-sectional area of the computational domain being 6,750 m^2 (225 m x 30 m), the blockage ratio calculated for this study is 0.74 % for wind directions perpendicular to the building geometry. This is sufficiently lesser than the maximum blockage as recommended in the guidelines.

It was also suggested by Lee et al [15] and Tominaga et al [40] that the size of the computation domain in the lateral direction (L) should be five times the height (H) or more. The total height of the domain H = 17 m and the lateral distance L = 225 m were defined in this simulation, what fulfils the above constrains. The configuration of the computational domain as well as the building location within it are shown in Figure 5.

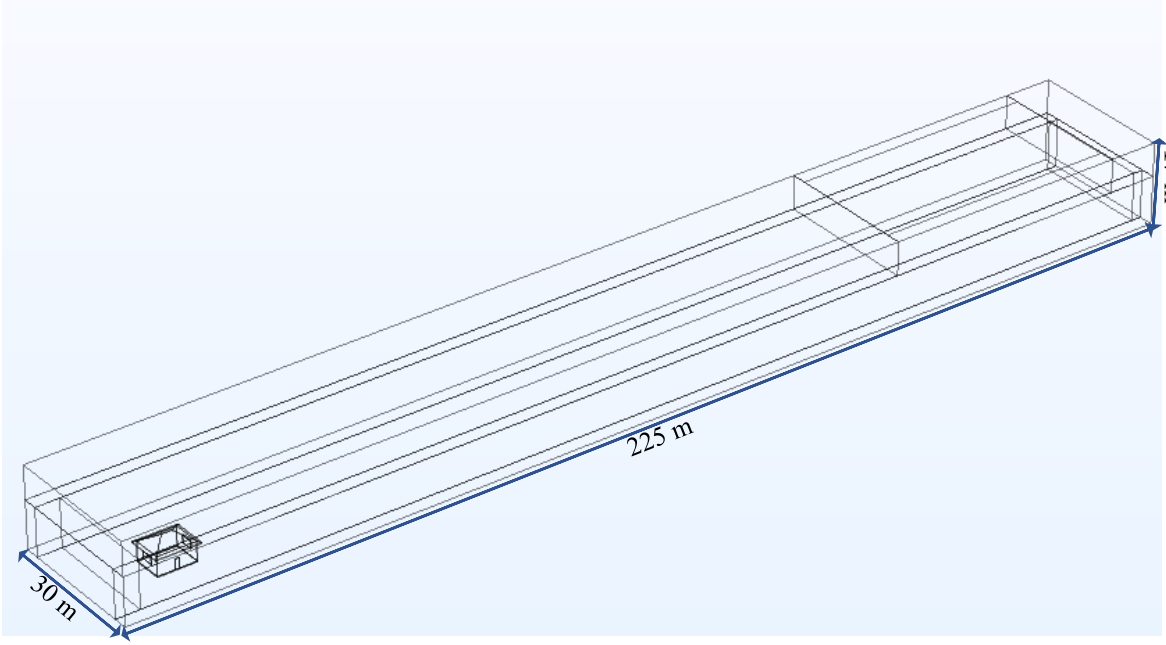

Figure 5: Dimensioned Computational Domain

2.2.1.3 Computational Mesh (Grids)

Four different mesh element types are natively available in the COMSOL Multiphysics software package. These include pyramids, triangular prisms, hexahedra and tetrahedra meshes [35]. The software allows for pre-defining of the meshing element size as well as user defined meshing element size settings. In this case, nine size options are provided for predefined element size meshing ranging from “extremely course” to “extremely fine” [44]. Unstructured (free) tetrahedral meshes were used in this study to define the building geometry and computational domain.

Figure 6 is a pictorial representation of the meshes for both the computational domain and the modelled building.

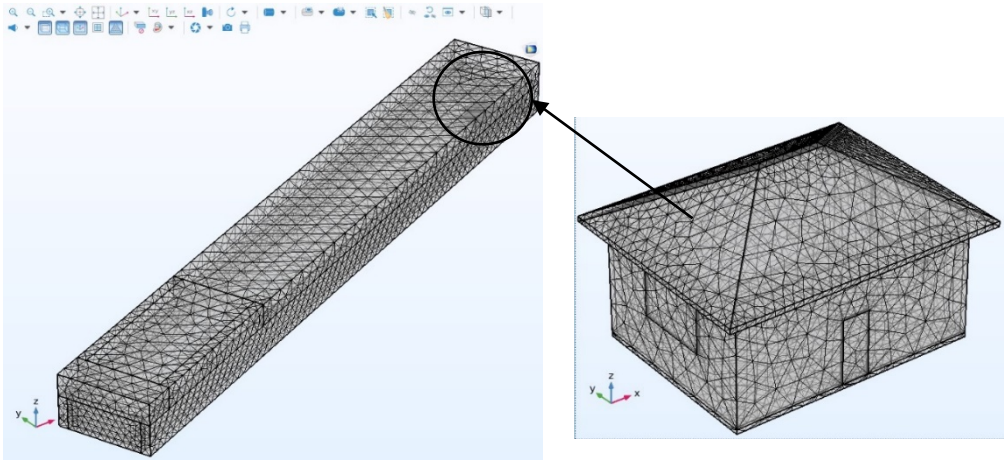

Figure 6: Meshes of Computational Domain (left) and Building Geometry (right)

2.3 COMSOL MULTIPHYSICS

COMSOL Multiphysics is a comprehensive finite element analysis, solver and Multiphysics simulation software environment. The overall functionality of this software is to mimic real-world events as close as possible revealing these in the scientific context. It can simulate different phenomena including, electromagnetic, fluid flow, heat transfer, acoustic and chemical reactions.

COMSOL Multiphysics has a CFD module that defines and computes problems that consists of solely fluid flow or fluid flow coupled with other physical phenomena. The CFD module of COMSOL Multiphysics has embedded fluid flow analysis tools (so called “physics”) including incompressible and compressible flows, laminar and turbulent flows, thin film flow, single-phase and multiphase flows, free and porous media flow as well as flow in open media [35], [44]. COMSOL Multiphysics performs both, transient (time-dependent) and steady state fluid flow problems in 2D and 3D. Steady state simulations assumes that all the parameters run for a long time without any changes or interruptions throughout the simulation. Conversely, the transient state simulations vary with time. COMSOL Multiphysics permits the implementation of multiple physics in the same software environment to compute fluid flow problems simultaneously. The wind driven rain simulation was performed for the needs of this study in three-dimensional space (3D) combining laminar flow and particle tracing for fluid flow “physic” tools.

2.4 AUTODESK REVIT AND DYNAMO

Autodesk Revit is a BIM application program that allows generation of 3D parametric building models with related information defined. Building models produced in Revit have intelligent elements (objects) that are stored within the model. Set of information regarding each element include its geometry details, constitutive materials, physical/technical properties, as well as others considering environmental impact or economical aspects. This implies that these elements are linked and can easily be altered throughout the design process. Any changes made to any element are automatically updated in relation to all other elements linked throughout the model. In addition, all information regarding the stored elements can be easily extracted and used for any other purposes within BIM model or even out of the Revit software.

Dynamo is an open-source visual programming tool that enables designers and engineers to customize their building information workflow. It allows users to have dynamic control over the model geometry and any other related information. It serves designers and engineers to solve complex model-based problems that are otherwise time consuming and difficult to solve within the basic Revit program interface.

BIM modelling software used in this research for creating the building geometry was Autodesk Revit. Revit Dynamo software was used for development of the custom tool to visualise the results of the aesthetical deterioration directly in Revit.

2.5 PROPOSED WORKFLOW

The workflow used in this study can be categorised into five main steps, including as follows:

- The workflow begins with the development of the building model in a BIM tool. The Autodesk Revit BIM software was used for the needs of this research.
- The second step involved processing of the historical climatic data as recorded for Ljubljana between June, 2016 and June, 2017. The script was used to identify all relevant wind driven rain scenarios. The LabView software printscreen as well as the algorithm implemented are illustrated in APPENDIX D.
- The third step involved performing the wind driven rain simulations by CFD tool. The CDF module within the COMSOL Multiphysics software was used here. It included both, the simulation of Laminar Flow (wind flow simulation) and Particle Tracking (raindrop trajectories and wetting patterns). These are described in detail within section 2.6 and 2.7 respectively.
- The following step was used for processing of the simulation results. Custom scripts developed in LabVIEW as part of the CLICKdesign project were used here. The data processing step were divided into two processes. First LabView script was used to process the wind driven rain (wetting patterns) data obtained after the simulation process. It was converted into the weather dose maps for each facade element of the studied building. The wind driven rain dose maps were used by the custom software (LabView) to generate colour images corresponding to the textures representing the aesthetical changes of the wooden facade. Print screens of the both LabVIEW scripts are presented APPENDIX E and APPENDIX G**.**
- The final step involves the visualization of the final result in the BIM tool. Revit was used in this study for this step. This was facilated with a script developed by the Dynamo for Revit scripting tool. The dynamo script developed in this stage is presented in APPENDIX H**.**

The overal protocol of the aesthetical appearance simulation is illustrated in Figure 7, including the flow of data (arrows) and main operations involved (rectangles). Different software development environments are identifed as different colour areas.

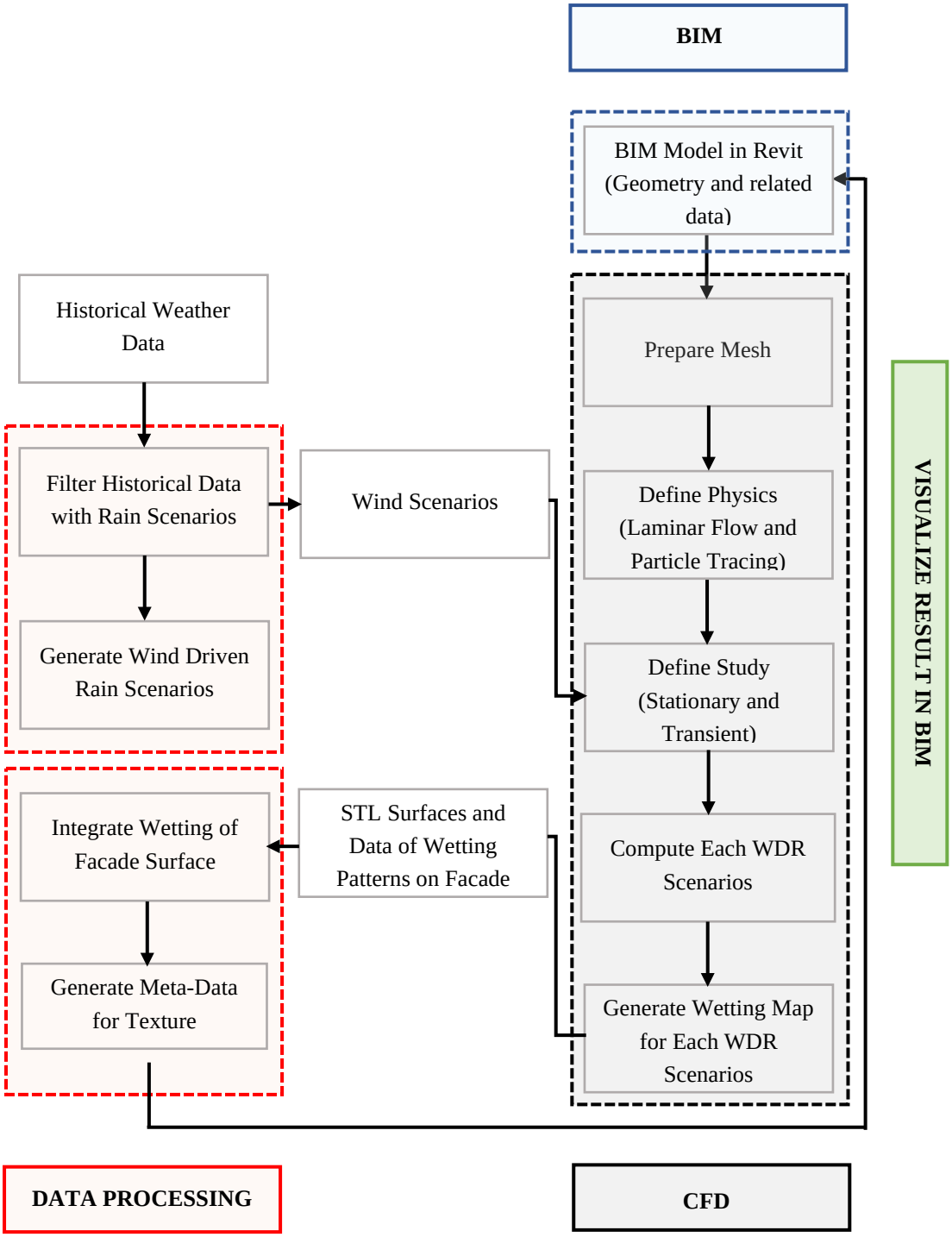

Figure 7: Proposed Study Workflow

2.6 LAMINAR FLOW SIMULATION AND GOVERNING CONDITIONS

Laminar flow and turbulent flow are subdivisions of the generalized fluid flow. Laminar flow is defined as a fluid flow where the fluid moves in one direction (parallel streamlines) without any disruptions between layers. Laminar flow is used when the Reynolds number is below a critical value of about 2000 [45], [35]. A tendency of disturbances to grow and cause a transition to turbulence is usually observed when the Raynolds number is higher than the critical value. The fluid moves irregularly in several directions in the turbulent flow circumstances with the speed of the fluid at some time continuously undergoing changes in direction and magnitude. Laminar flow supports incompressible flow, weakly compressible flow and non-Newtonian fluid flows.
In this study, an incompressible laminar flow was performed with the assumption that the temperature variation in the flow was negligable. This is a suitable approximation when the fluid is under normal conditions and have low velocities [35]. Laminar flow physics of the CFD was used in the computation of the velocity and pressure fields for the flow of a single-phase fluid in the laminar flow system following the equation below.
Equation 1: Stationary Laminar Flow

$$\rho(\mathbf{u}\cdot\nabla)\mathbf{u} = \nabla\cdot\left[-p\mathbf{I}+\mathbf{K}\right]+\mathbf{F}$$
$$\rho\nabla\cdot\mathbf{u} = 0$$

where ρ - denotes density (kg/m^3),
u - denotes the velocity vector (m/s),
p denotes pressure (Pa),
K - denotes the viscous stress tensor (Pa),
F - denotes the volume force vector (N/m^3),

A stationary study was used for the laminar flow simulation, assuming that there is no time variation with the inlet velocity.

2.6.1 Boundary Conditions

The boundary conditions set in this physics include fluid particles, initial values, wall 1 and wall 2, Inlet 1, outlet 1 symmetry 1 and symmetry 2.

2.6.1.1 Inlet and Outlet Boundary Conditions

An inlet boundary condition was set under laminar flow “physics”. The velocity option was used because the intention was to define the velocity at which fluid flows into the computational domain. A normal inflow velocity was defined as

$$u = u_o$$

where; u_o is the normal inflow speed of the fluid.

The parametric sweep feature in COMSOL Multiphysics was used to define the velocities set at the inlet boundary condition. These velocities were based on the historical climatic wind data used in this study. In addition, an outlet boundary condition was specified. The boundary option set for the outlet boundary condition was selected as pressure to avoid convergence difficulties in the simulation. A reference static pressure of 0 Pa was set at the physics interface level.

$$P_{\text{wall}} = 0$$

where; P_{wall} is pressure (Pa).

The domain boundaries at which the inlet and outlet conditions were set are presented in Figure 8.

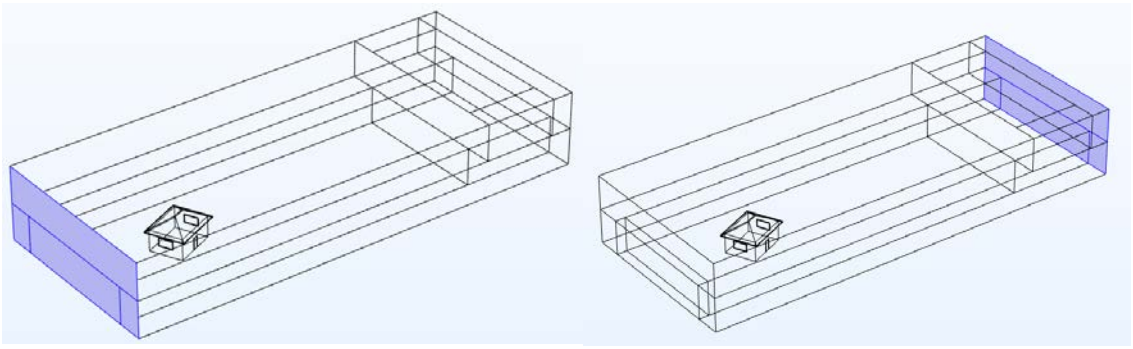

Figure 8: Inlet and Outlet Boundary selection[1]

2.6.1.2 Initial Values Boundary Condition

In addition, initial conditions were assigned to the laminar flow model. The initial values for the velocity field were set as 0 m/s for x, y, and z directions. The pressure field *p* was also 0 Pa. Figure 9 presents the initial values at boundary selection.

[1] Not to scale

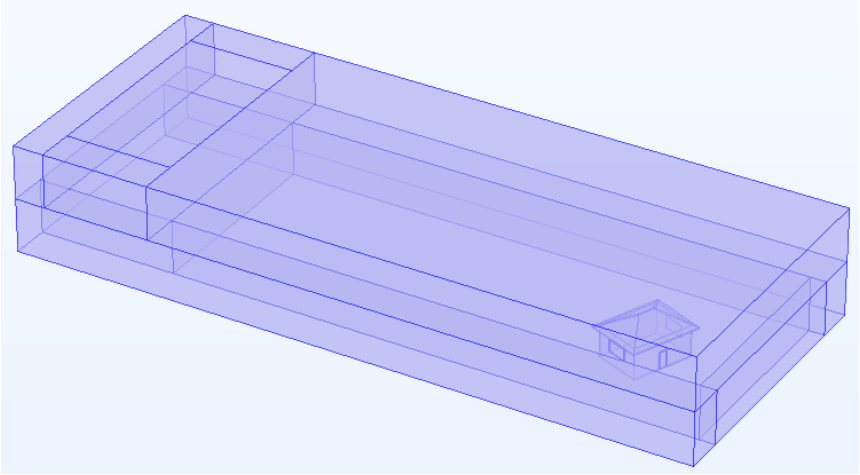

Figure 9: Initial Values

2.6.1.3 Wall 1 and Wall 2 Boundary Conditions[2]

Two wall boundary conditions were set. The intention of the first wall boundary condition was to have a zero velocity on the selected boundary. As a result, a no slip boundary option was set, as defined in equation below:

$$U_{\text{wall}} = 0$$

where; U_{wall} corresponds to the normal inflow velocity of the fluid.
A slip boundary option was selected for the second wall boundary condition. This assumes a "no penetration" condition at the selected boundary selection. Figure 10 below specifies the boundary selections for the first and second wall boundary conditions.

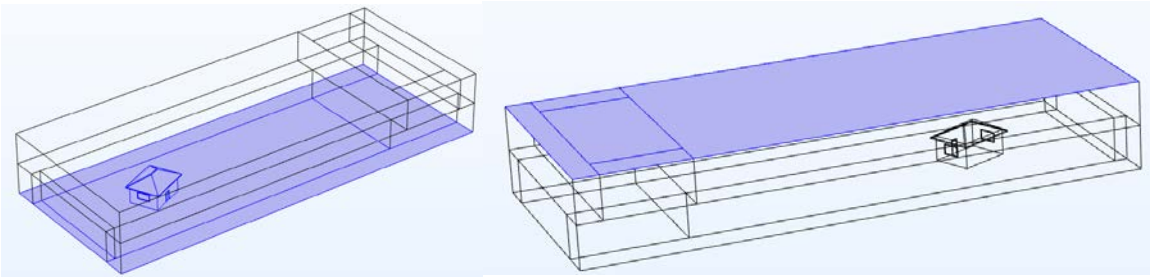

Figure 10: Wall 1 and Wall 2 Boundary Selection[2]

2.6.1.4 Symmetry 1 and Symmetry 2 Boundary Conditions

Figure 11 presents both symmetry boundary conditions assumed at the lateral sides of the computational domain. This ensures a zero normal gradient of all variables and a zero normal

[2] Not to scale

velocity at the selected boundaries. This allows for a parallel flow within the computational domain.

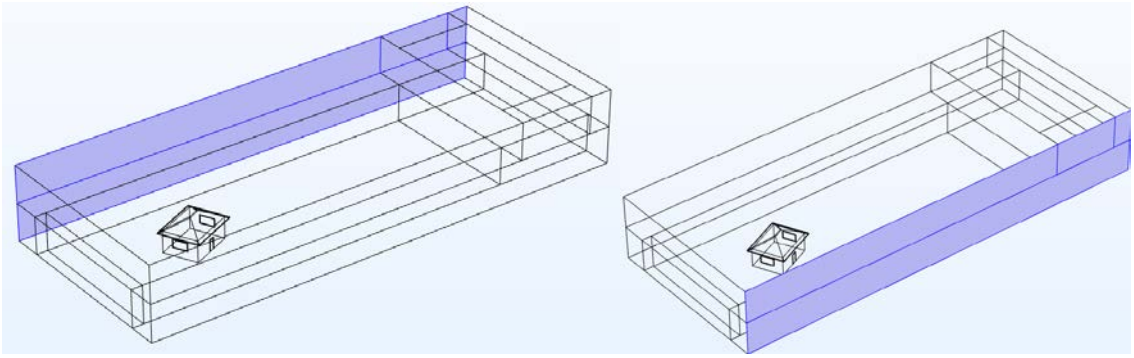

Figure 11: Symmetry 1 and 2 Boundary selection[3]

2.7 PARTICLE TRACING FOR FLUID FLOW AND GOVERNING CONDITIONS

A three-dimensional rain drops particle trajectories were determined for each of the wind flow pattern simulations identified as relevant for Ljubljana. This involved the injection of hundred thousand raindrops into the inlet boundary selection. The particle trajectory simulation was performed based on the laminar flow simulation as explained in 2.6. In this study, the computation of particle trajectories was done by using the Particle Tracing Module. It is a general tool for computing the paths of particles as they move through the computational domain and as they are subjected to various forces. Particle tracing provides a Lagrangian description of the problem. The boundary conditions defined in this physics included: wall, inlet 1, particle properties, drag force, gravity force, Outlet 1 and 2, symmetry 1 and 2, particle counter 1,2,3 and 4. The density of the water particles (raindrops) used in the simulation was 1000 kg/m^3.

2.7.1 Boundary Conditions

2.7.1.1 Inlet and Two Outlet Boundary Condition

The inlet boundary condition for particle tracing specifies the horizontal plane from which the raindrops are injected. Two outlet boundary conditions were defined for this study. The Outlet 1 and 2 boundary conditions were set.

[3] Not to scale

For outlet 1 boundary condition, the disappear wall option was used. The expectation was for the particles (raindrops) to disappear from the boundary selections for the outlet 1 boundary condition.This was chosen because the particles on these boundary selections are not needed to be rendered during results processing. The particle location for the disappear boundary option is defined mathematically as not-a-number (NaN) for all the time steps after the particles (raindrops) touches the outlet 1 boundary selections. Figure 12 presents the boundary selections for inlet 1 and outlet 1 boundary selections.

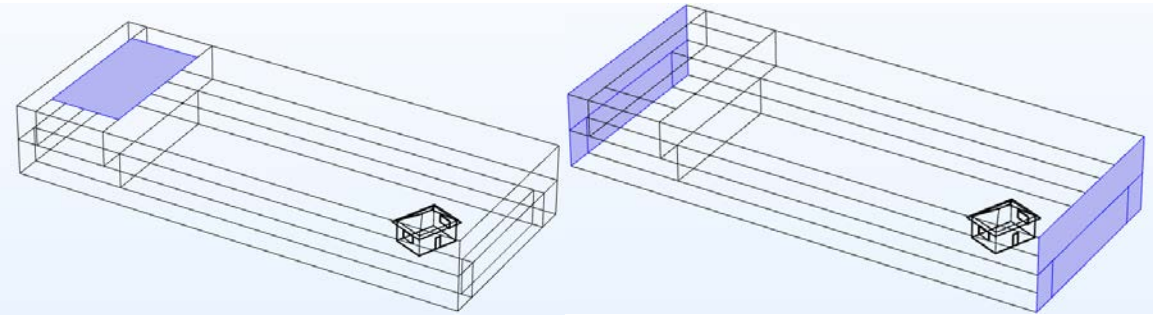

Figure 12: Inlet 1 and Outlet 1 Boundary Selection (Particle Tracing)[4]

The "freeze" boundary option was selected for the second outlet boundary. The expectation for a freeze boundary selection is to be able to recover the velocity of the particles (raindrops) when it touches the surface of the boundary selection. It was especially desired for the external wall surfaces of the building geometry. The outlet 2 selection is presented in Figure 13.

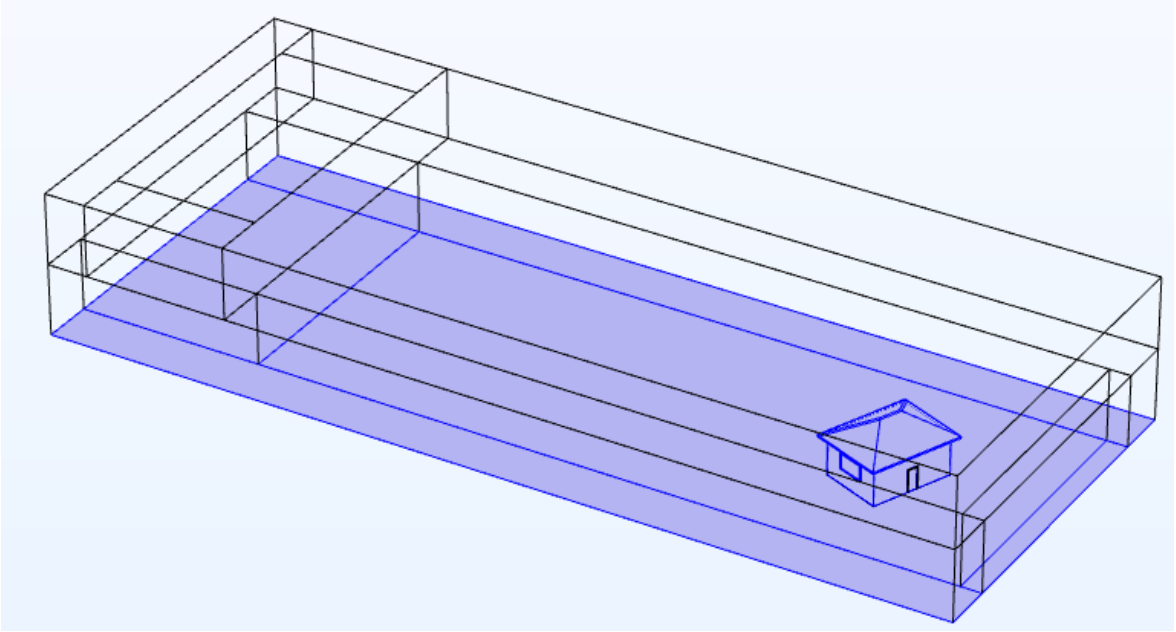

Figure 13: Outlet 2 Boundary Selection (Particle Tracing)[4]

[4] Not to scale

2.7.1.1 Wall Boundary Conditions

The wall boundary condition defines what happens when particles reach the surface of the wall. Only one wall boundary condition (Wall 1, as shown in Figure 14) was necessary to define in this part of the simulation. A disappear boundary option was set for Wall 1 to ensure that the raindrops are not displayed as soon as they contact the selected boundary selection.

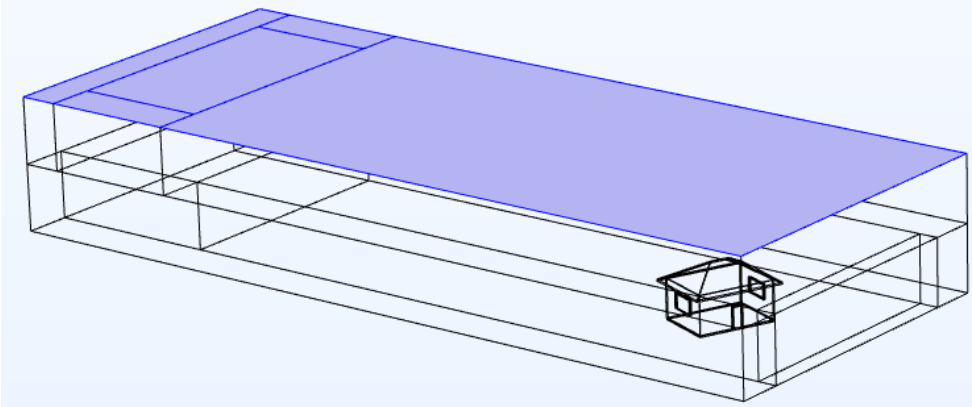

Figure 14: Wall Boundary Selection (Particle Tracing)[5]

2.7.1.2 Drag Force and Gravity Force

The drag force represents the force that a fluid exerts on the particle as a result to the difference in velocity between the particle and the fluid. The gravity force boundary condition exerts gravitational force on the particles (raindrops). Figure 15 presents the boundary selections for drag and gravity force boundary conditions.

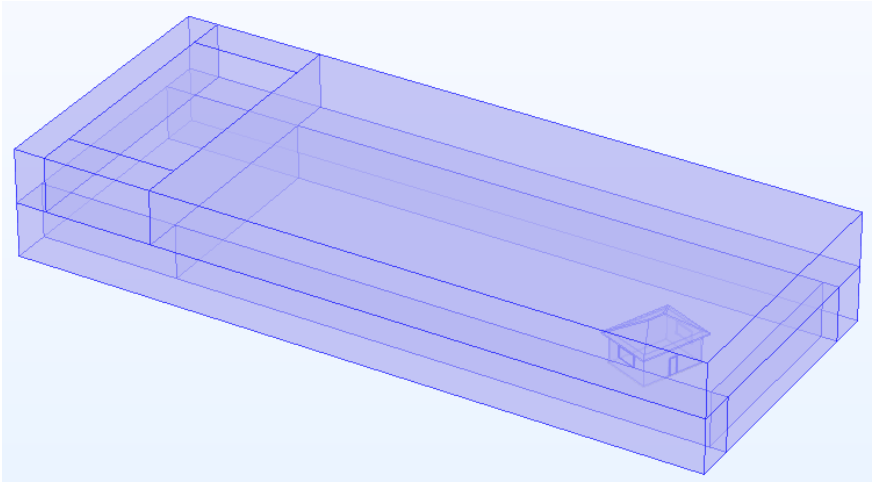

Figure 15: Drag and Gravity Force Boundary Selection[6]

[5] Not to scale

[6] Not to scale

2.7.1.3 Symmetry 1 and 2 Boundary Condition

For particle tracing simulation performed in thus study, symmetry boundary conditions were set on the opposite longitudinal lengths of the computational domain. Figure 16 represents the boundary selections of the two symmetry boundary conditions.

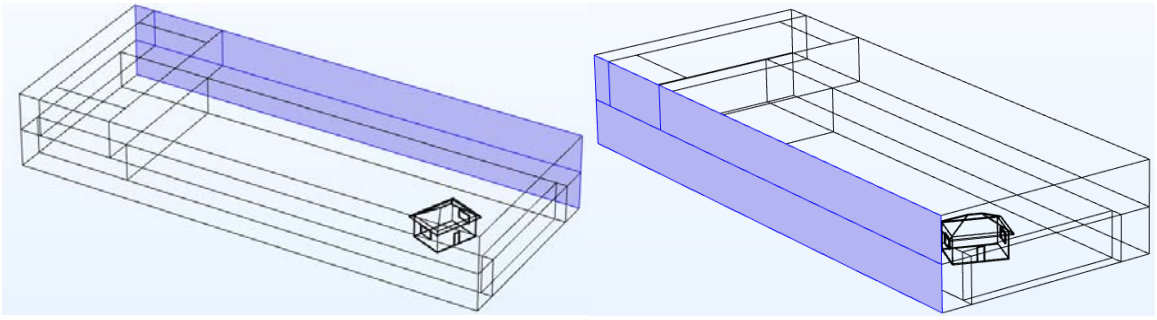

Figure 16: Symmetry 1 and 2 Boundary Selection (Particle Tracing)[6]

2.7.1.4 Particle Tracing Boundary Condition

A particle counter boundary feature available in the particle tracing "physics" in COMSOL provides information regarding the particles that arrives on the selected domains. Four wall surfaces of the building geometry as shown in Figure 17 were selected and assigned as particle counter surfaces.

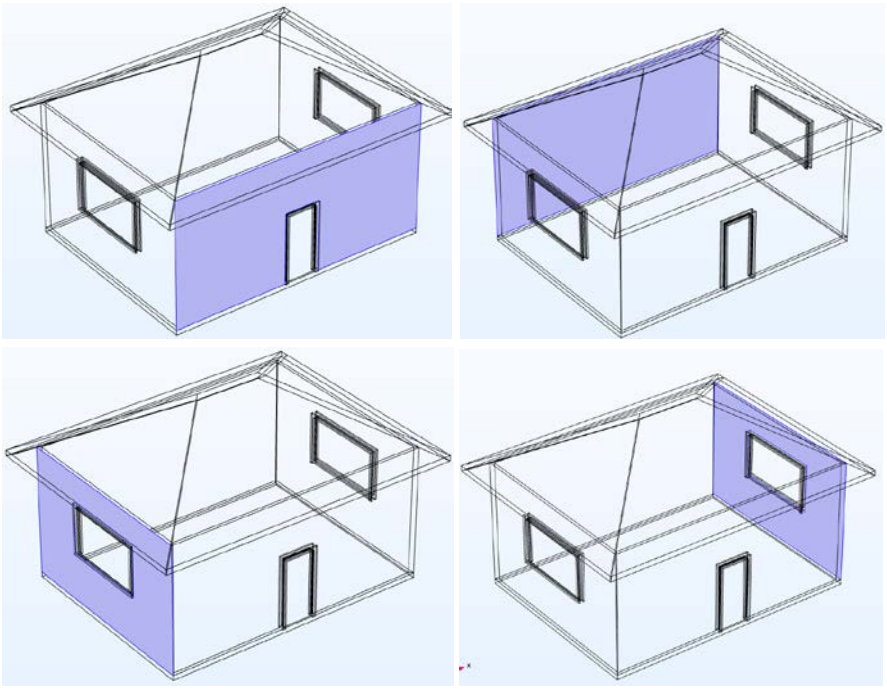

Figure 17: Particle Counters Boundary Selection (Particle Tracing)[7]

[7] Not to scale

The parametric sweep feature was used to automate the simulation process within COMSOL Multiphysics. The parametric sweep feature is used to compute solution to a sequence of time-dependent or stationary problems which requires the use of varying parameters. This feature was very handy in this study simplifying computations for the varying wind velocities and directions.

3 RESULTS AND DISCUSSIONS

In this chapter, the results obtained from the numerical simulations are presented and discussed.
A three-dimensional simulation model was set up for a simple building geometry designed in Autodesk Revit. It was imported for the simulation in the COMSOL using the LiveLink feature. A simple building geometry was intentionally chosen to make it easier to trace any errors that occurred when implementing the developed protocol. This simplified the software debugging and helped to identify causes of errors. These faults can be avoided when more complex building geometry will be analysed in the follow-up research. In addition, a simple building geometry was used to reduce the considerable simulation time necessary to perform computations. It is especially important at the pilot study phase as presented here, where several simulations must be performed till a fully reliable procedure is delivered. Figure 4 presents the modelled building as designed with the BIM tool (Revit).

3.1 CLIMATIC DATA AND WIND DRIVEN RAIN SCENARIOS

The first step under the data processing stage of the proposed workflow (Figure 7) used in this research is related to the filtering of the climatic data into wind driven rain scenarios.
Eight relevant scenarios were identified for Ljubljana as summarized in Table 1, including three prime wind directions (112.5°, 157.5° and 202.5°) and four major wind velocities (11.25, 13.75, 18.75 and 21.25 m/s).

3.2 WIND FLOW, RAINDROP TRAJECTORIES AND WETTING PATTERNS

In this section results from the laminar flow and particle tracing studies results are summarized. The wind flow patterns, and raindrop trajectories determined for eight scenarios are compared and discussed. Finally, the simulated wetting patterns are presented for four walls of the model building.
A steady state fluid (wind) flow pattern around the building geometry and the within the computational domain were performed, as explained in chapter 2 of this study. Correspondingly, a stationary study was performed for the fluid flow simulation.

APPENDIX C presents a schematic of the model settings of the Laminar flow (wind flow) simulation as implemented in this research.

Two set of results were generated after the laminar flow simulation, including the velocity and pressure plots. However, only results for the wind flow velocity magnitudes are reported here. The wind flow velocity and movement within the computational domain and around the building geometry are presented with velocity slides and arrow plots.

The raindrop trajectories were calculated based on the steady state wind flow simulations using the reference wind velocities and directions as presented in Table 1. A 3-dimensional Lagrangian particle tracing simulation was performed separately for each of the eight wind flow scenarios. The particle tracing module was used for the computation of trajectories of the particles applying a time dependent “physics” study. The schematic of the model settings is presented in APPENDIX C**.** It includes an overview of the operations and options that were required for the simulation of the model.

Rainfall trajectories were obtained by injecting raindrops in the simulated fluid (wind) flow pattern. The intensity and amount of the rainwater that falls on different sections of the building walls are determined as the result of the simulation. The particle trajectories plot was used to visualize the particle paths. The wind driven rain results are arranged into three groups according to the relevant wind directions. The first group was WDR scenario 1 which had wind direction of 112.5° from the North. The second group consist of WDR scenario 2, 3 and 4 possessing the wind direction of 157.5°. Finally, the third group consisted of WDR scenarios 5, 6, 7 and 8 covering wind direction of 202.5°. Figure 18 presents an exemplar result for the wind flow pattern observed around the modelled building. On the contrary, Figure 19 presents an example of the simulation results for WDR scenario 8. It is a representation of a typical time-step results derived from the particle tracing simulation performed in this study.

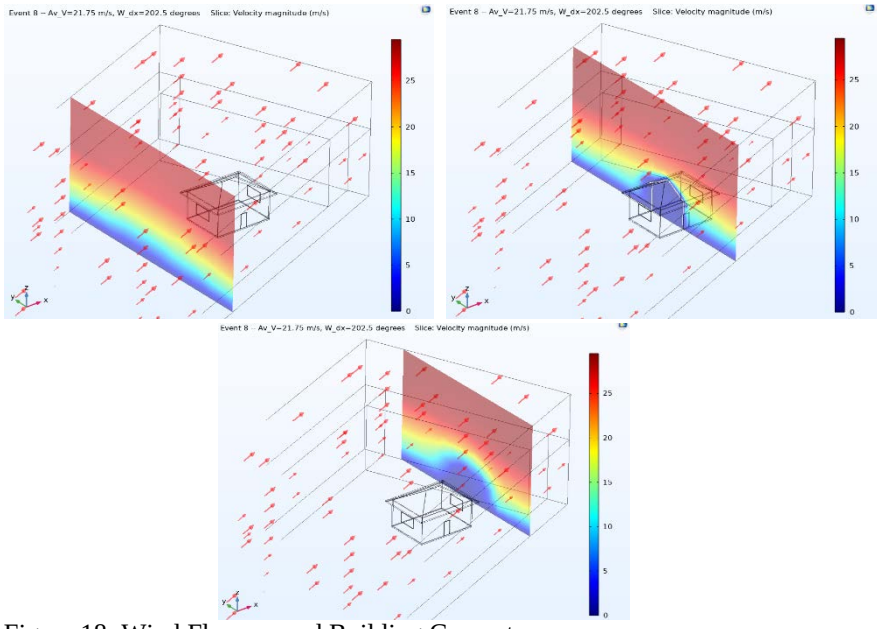

Figure 18: Wind Flow around Building Geometry

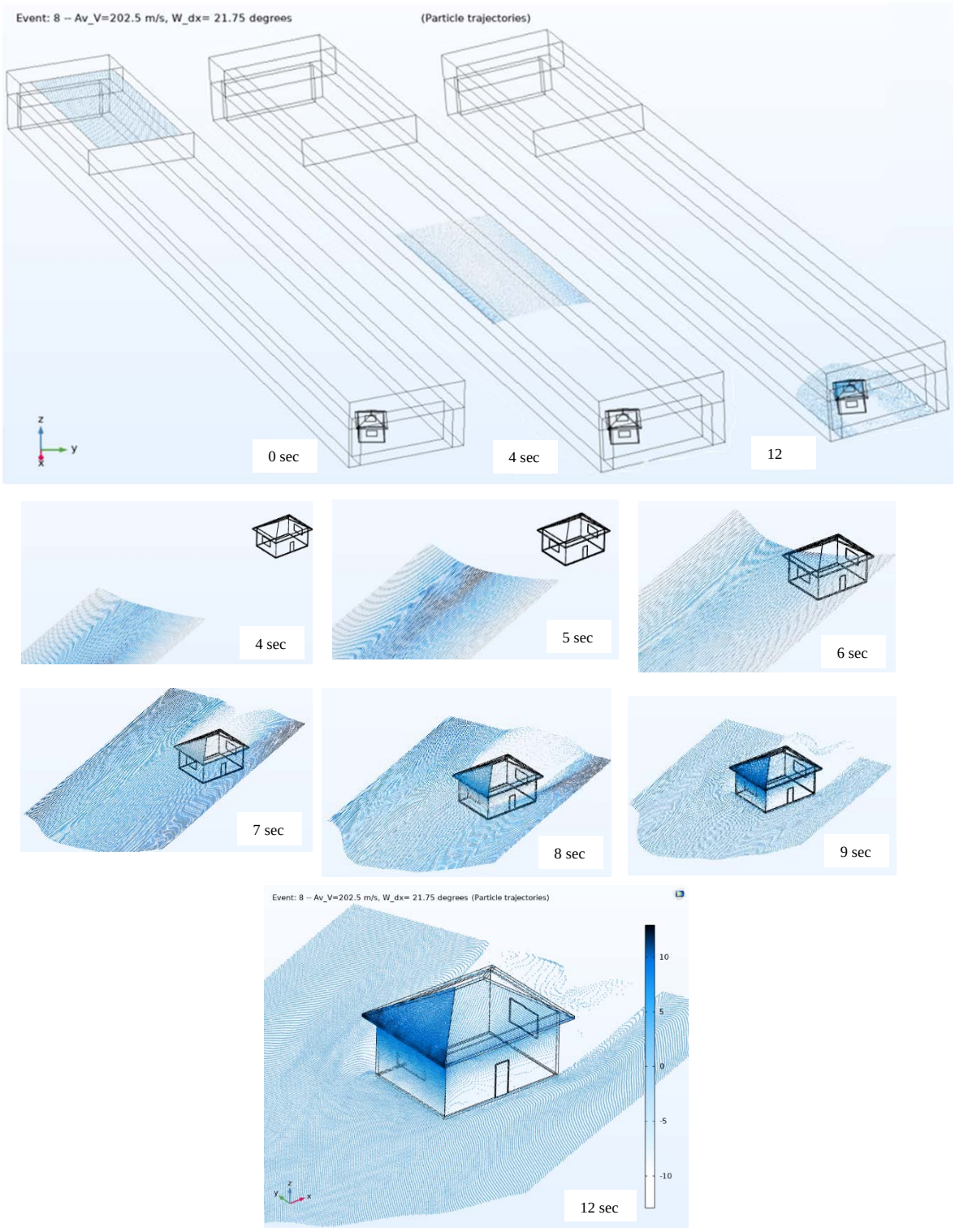

Figure 19: Time step of Wind Drive Rain Simulation

3.2.1 Wind Driven Rain Scenario 1

APPENDIX A presents the wind flow around the building and within the computational domain for WDR scenario 1, performed with a reference wind speed of 11.25 m/s and a reference wind direction of 112.5°. The steady state wind flow was oriented towards the eastern and northern elevations of the building geometry as can be seen in APPENDIX A. It was also found that the rain trajectories for WDR scenario 1 are more inclined to the eastern and northing faces of the building geometry what is following the wind flow pattern. The distinct wetting pattern as presented in APPENDIX B is directly related to the results of the wind-flow pattern around the building geometry for WDR scenario 1. The wetting pattern was found to be pronounced at the east elevation of the building. It can also be observed that there are non-wet areas at the top stretch of the facade's surfaces (prevalent on the east elevations). These non-wet areas can be attributed to the protective effect of the overhangs. Similar results were recorded by Mohaddes Foroushani, et al [24].

3.2.2 Wind Driven Rain Scenario 2, 3 and 4

APPENDIX A presents the wind flow within the computational domain and around the building for WDR scenarios 2, 3 and 4 respectively. Correspondingly, in APPENDIX B represents the wetting patterns recorded for WDR scenario 2, 3 and 4 respectively. These WDR scenarios have a common wind direction of 157.5° clockwise from North. The wind flow pattern around the building was prevalent towards the Northern and Eastern elevations, with the dominance on the Northern face of the building facades. The results for WDR scenarios 2, 3 and 4 are relatively similar to the wind flow pattern as recorded in the WDR scenario 1.

The results recorded after the particle tracing simulation as presented in APPENDIX B indicates wetting patterns prevalent on the eastern and northern faces of the building facade. The wetted faces of the building geometries had a strip of dry areas clearly noticeable right beneath the roof overhangs. This indicates the rain shadowing influence of the roof overhangs protecting the upper zones of the building walls.

It is important to mention that the amount for wetting recorded on the building facade (apparent number of raindrops appearing on the wall) increases with an increase in the wind velocity. This trend is most noticeable on the Eastern elevation at the back of the building. The highest wetting was recorded for WDR scenario 4 (18.75 m/s), followed by scenario 3 (13.75 m/s). Conversely, no wetting of this wall was detected for WDR scenario 2 (11.25 m/s). These findings are in consistence to research finding as reported by Karagiozis et al [22].

3.2.3 Wind Driven Rain Scenario 5, 6, 7 and 8

WDR scenarios 5, 6, 7 and 8 share the same wind direction of 202.5°. The wind flows in these simulations were perpendicular to the western and northern facade surfaces of the building. The wind flow pattern for WDR scenarios 5, 6, 7 and 8 are presented in APPENDIX A. The results for the raindrop trajectories recorded in this study followed the wind flow pattern of the corresponding WDR scenario. The resulting wetting patterns are presented in APPENDIX B , respectively. It is evident from the results that the wetting pattern recorded for WDR scenarios 5, 6, 7 and 8 are oriented to the western (front) elevation and the northern elevation of the building. Evidence of non-wetted strips right beneath the roof hangings are clearly noticeable, that is in analogy to other WDR scenarios investigated. In addition, the wetting areas over the facade increased with an increase in the wind velocity. This drift is most evident for the wetting pattern on the west (front) elevation of the building. It is apparent that the WDR scenario 8 (21.75 m/s) possessed the most wetted areas, followed by scenario 7 (18.75 m/s) and 6 (13.75 m/s). Almost no wetting was noticed on the west elevation of the building in WDR scenario 5 that had the lowest wind velocity. These observations are consistent with findings by Karagiozis et al [22].

3.3 DOSE MAP GENERATION

Based on the wetting patterns as discussed in section 3.2, the rain drops co-ordinates as well as the rain drop density maps were generated. These were used as a basis for computing the weathering dose maps representing the wetting form as observed on each of the model building facade face and all relevant WDR scenarios. Figure 20 presents an exemplar rain drop coordinates generated with COMSOL Multiphysics simulation software. Each identified drop was used in the next step to as a contributor for creating the so called “drop density map. In that case the facade surface was divided for a matrix of rectangles covering unit areas of 20 cm x 20 cm. The rain density corresponded therefore to the number of drops per m^2 of the unit façade. From definition, its minimal value was 0 drops/m^2 that corresponded to surface area not wetted by the WDR. Figure 21 represents and exemplar 2D distribution of the Wind Driven Rain drops density assessed for the facade with a window.
In addition, the WDR density maps were corrected to account the drop dripping effects. This is a compensation for the facade surface wetting not directly by the water drops driven by rain, but rather to the gravity force and natural dripping effect of the rain drops after they hit the surface of the building facade. The approach used here was to sum the total number of drops above the given unit surface area. Figure 22 presents a graph illustrating the corrected dripping effect computation. The native resolution of the WDR density maps was relatively low (31 x 20 pixels for the wall presented in Figure 22). For that reason, the results were interpolated to the size of the texture map used for the appearance visualization, as described

in the following chapter. Moreover, the numerical data were converted to the image form that was easier to handle by the visualization software. Figure 23 presents an exemplar of native and interpolated dose map images.

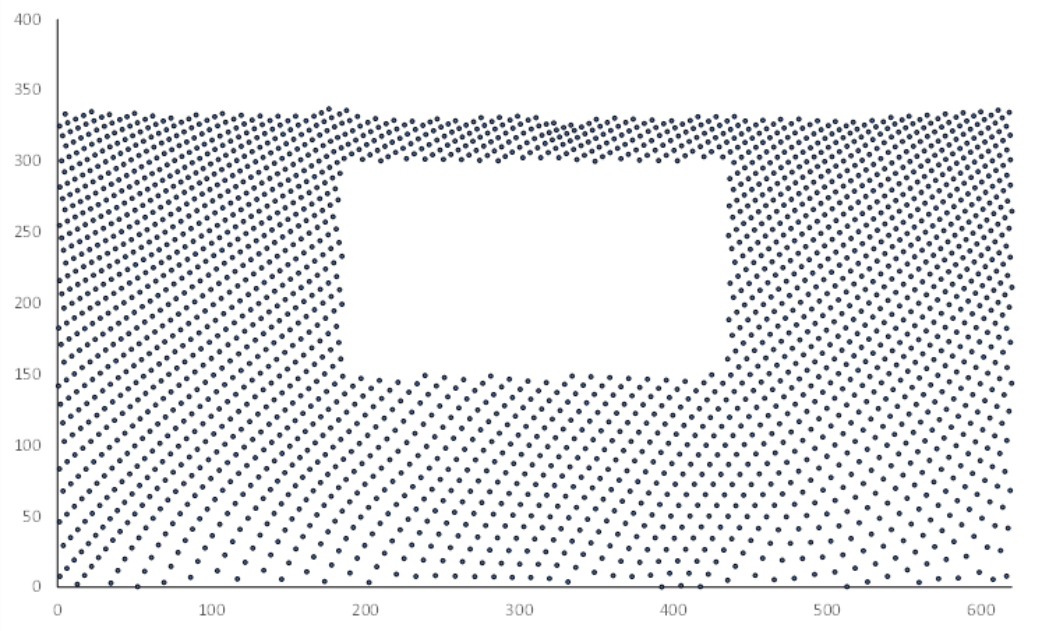

Figure 20: Rain Drop Co-ordinates

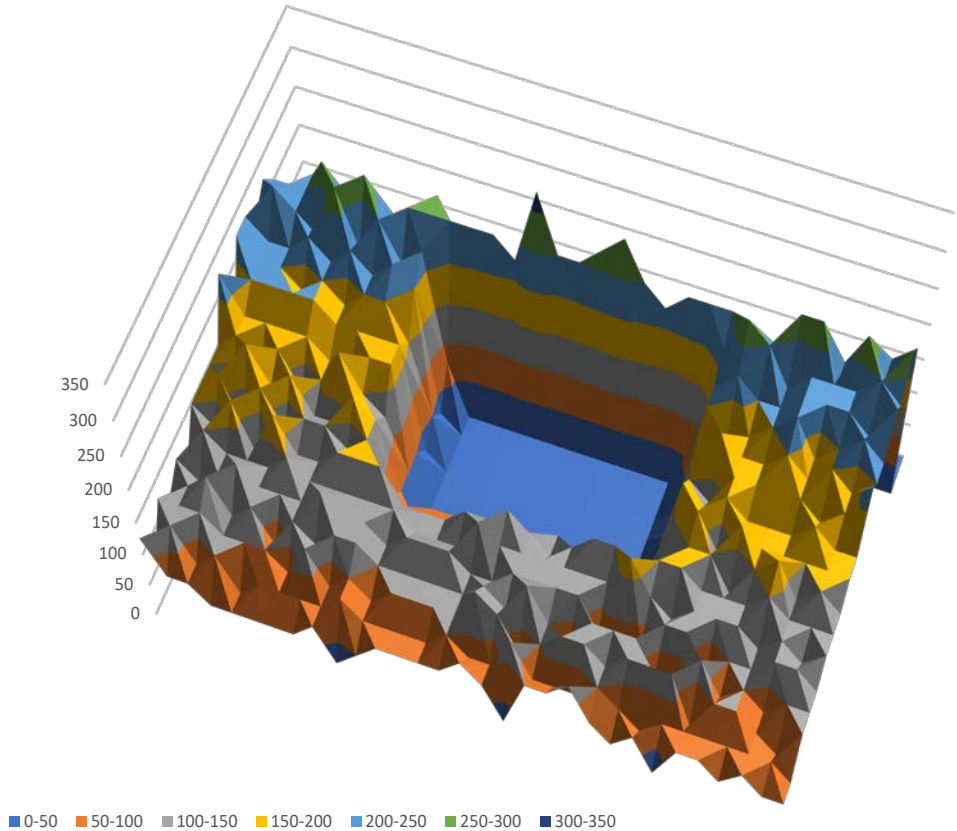

Figure 21: Raindrop density (drops/m^2)

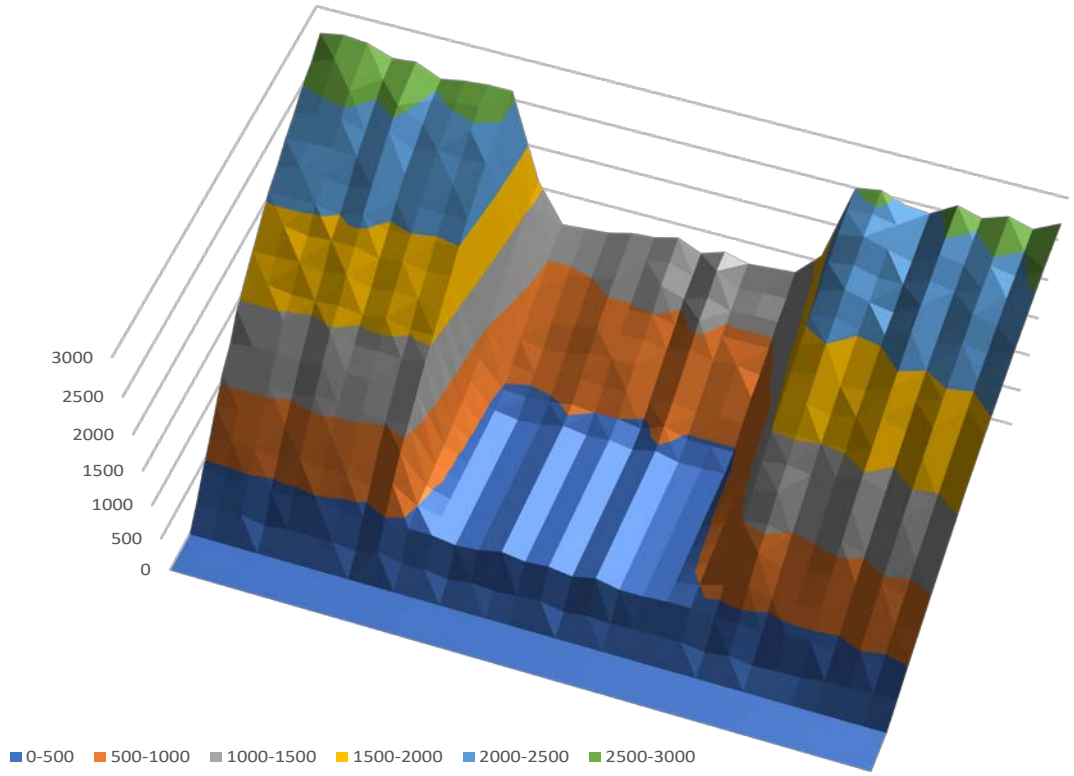

Figure 22: Graph for Corrected Dripping Effect of Drops

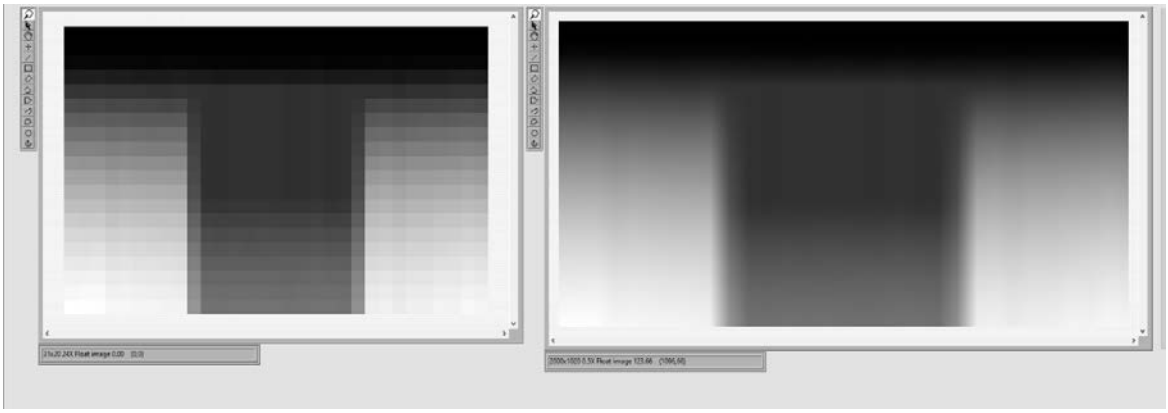

Figure 23: Native Dose Map Image Generated (left) and Interpolated (right)

3.4WEATHERED WOOD TEXTURE GENERATION

The WDR dose maps for each of the relevant rain scenarios were used as the input for the custom software developed withing the CLICKdesign project framework. The algorithm implemented is not described here in detail as was developed as a separate research initiative. It bases, however, on implementation of the dose-response models for wood samples exposed to natural weathering. The change of colour was mapped over the artificially generated wood texture, assuming extreme colour differences corresponding to the early and late woods. The textures for each of the faces of the building facade were generated based

on the accumulated dose maps and the previously determined respond of spruce wood. Figure 24 presents an example of the texture generated. The print screen of the proprietary LabView software user interface and implemented script are presented for reference in APPENDIX G**.**

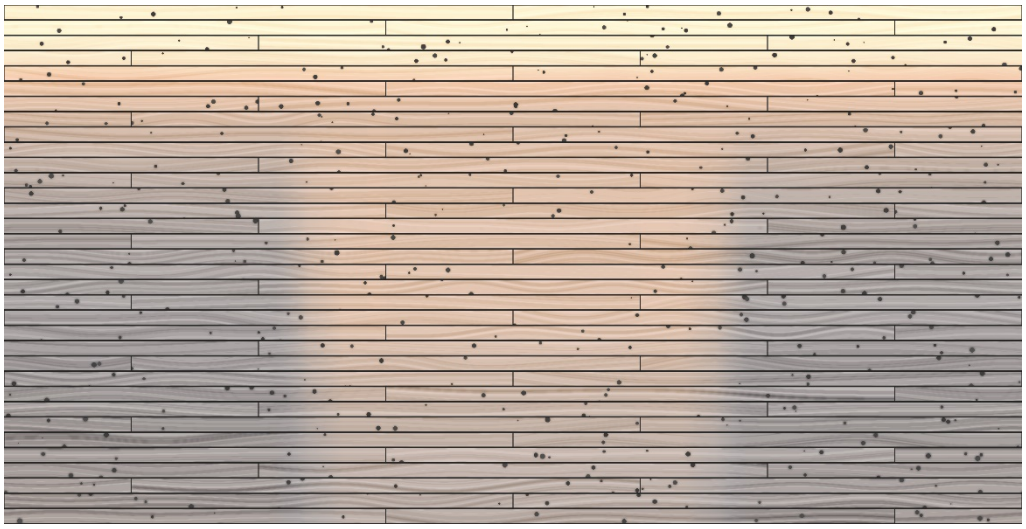

Figure 24: Colour texture of the weathered model building facade generated by the custom software tool.

3.5 VISUALISATION OF RESULTS IN BIM

The final visualization was performed implementing the Dynamo for Revit script developed for the needs of this research. It used the colour textures generated from all the above-described data processing stages. An example of the final results after re-integration to the BIM software (Revit) are presented in Figure 25 and Figure 26 The series of images illustrates the progress of the aesthetical appearance deterioration of the building facade from the original stage (top image), through 3 (middle image), and 12 (bottom right image) months of the exposure to the natural weathering conditions. A more detailed set of the visualisation results is summarized in APPENDIX H.

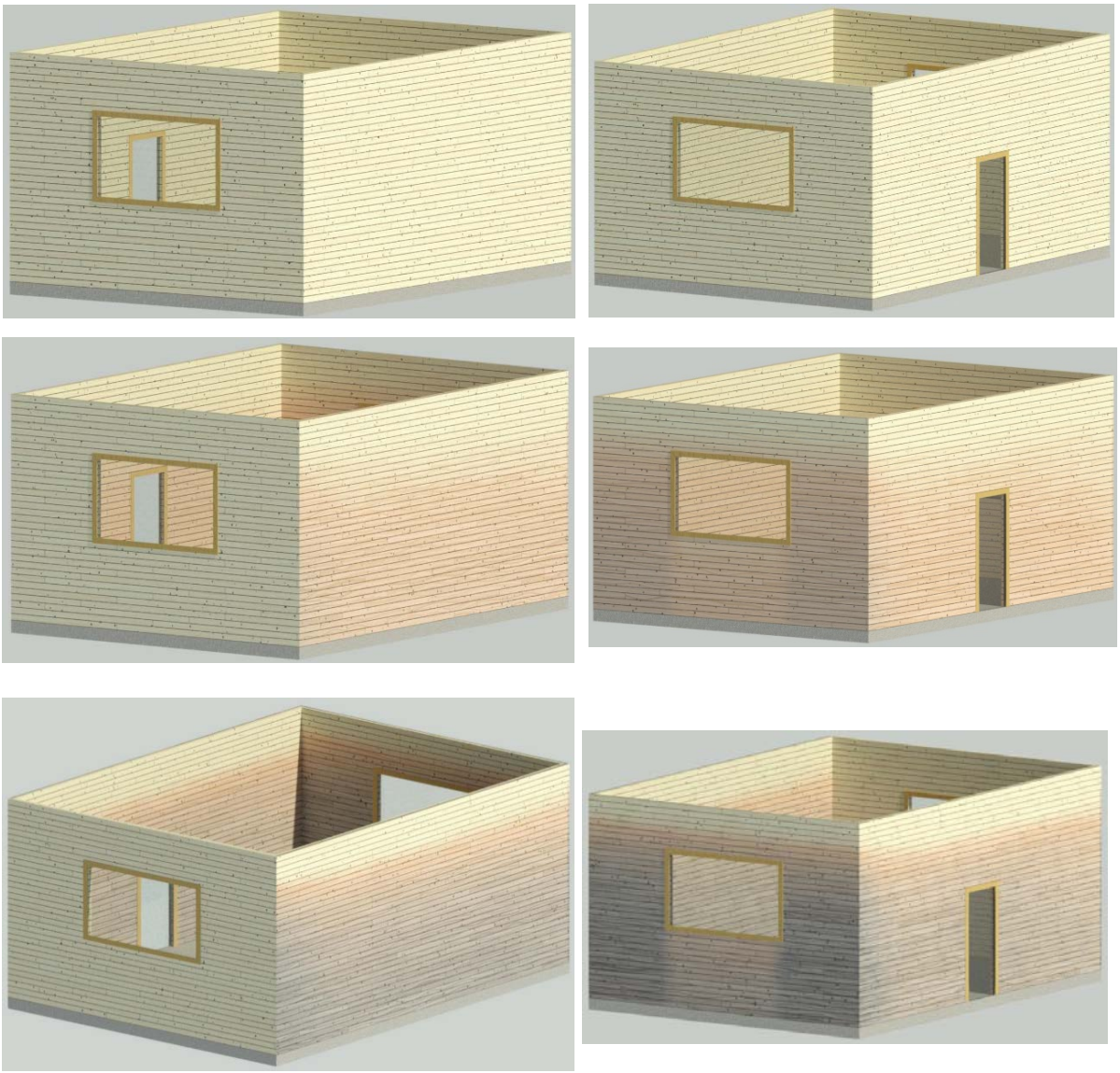

Figure 25: Time - Step Visualization of Wooden Facade Appearance Changes in Revit

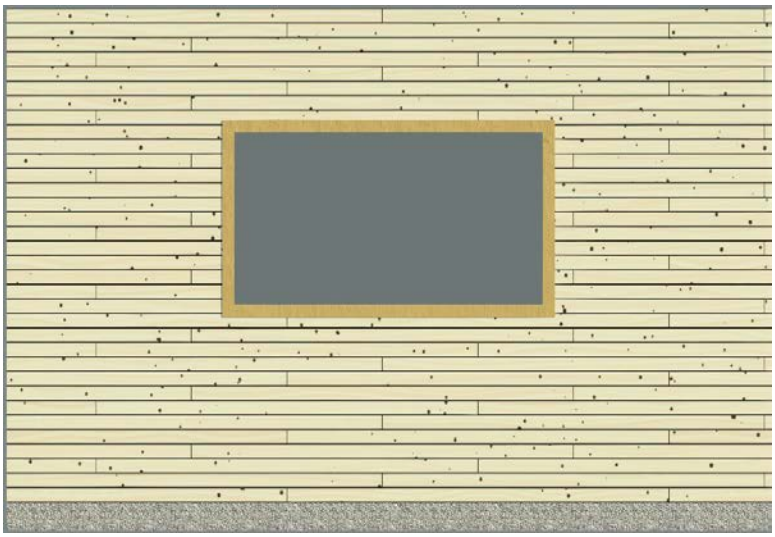

(a) Appearance of Unexposed Wood Facade

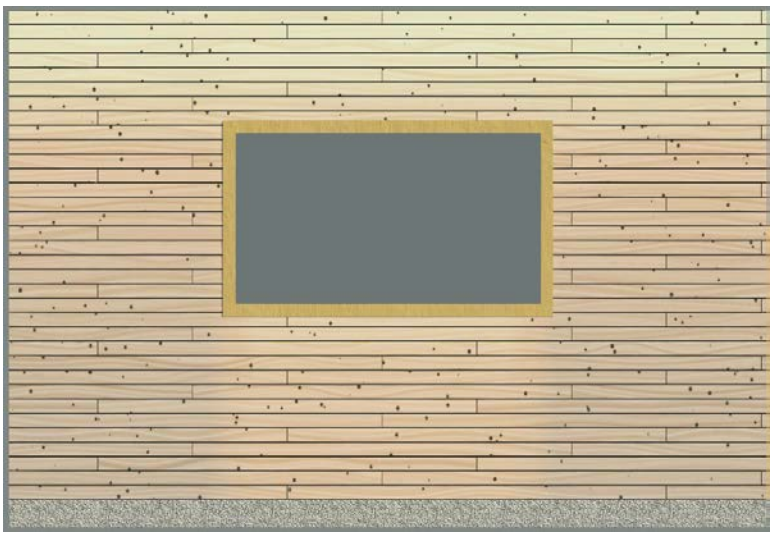

(b) Appearance After 3 months Exposure

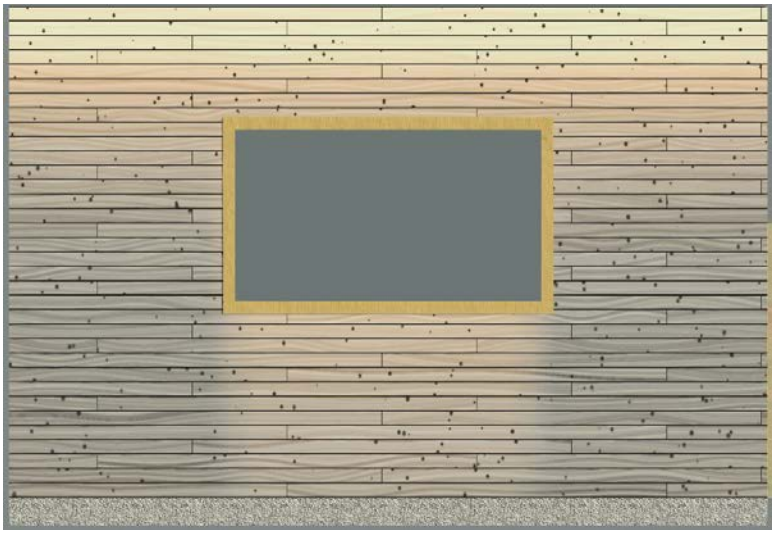

(c) Appearance After 12 months Exposure

Figure 26: Time - Step Visualization of Wooden Facade Appearance Changes in Revit

4 CONCLUSION

As discussed in the introductory chapter of this Thesis, numerical simulation of the wind driven rain on building facade have not yet received enough attention in the scientific research. To the best knowledge of the author, there is no study on numerical simulation of the wind driven rain effect on the appearance of wood or other materials. Similarly, the integration of CDF tools and BIM tools for aesthetical modelling of building facades is not reported in the available literature. This study has succeeded to simulate wind driven rain by using (for the first time) combined CFD and BIM tools. The doses of wind driven rain on the wooded facade were successfully quantified on the example of the model building "located" in Ljubljana region. Finally, an estimation of the appearance alterations of the wooden facade based on the wind driven rain doses for a period of one year was successfully implemented. This case study object was intended to be as simple and easy to understand as possible. This is to allow for further discussions and extending the research in the same or similar directions. In this final chapter, the results obtained and discussed are summarized and concluded. In addition, a list of limitations encountered during the entire research process are pointed out. Finally, further research directions and considerations for extension of forthcoming studies are stated.

Although there are some reported studies that uses CFD to estimate wind driven rain interaction with the building facade, to the best knowledge of the author, there is no research that integrates BIM and CFD to simulate the aesthetical performance of buildings. The main motivation for this study was to initiate a discussion on the combining of CFD and BIM tools to estimate the aesthetical appearance of wooden facade when exposed to external climatic conditions. This is expected to help architects, building designers and engineers to predict how the wooden facade may look after a particular period of the service life. Such functionality is very relevant for the decision making at the early stages of the building design process. Even though this study does not entirely solve the abovementioned problem (only wind driven rain was considered at this stage of the model development), it offers a very comprehensive workflow for extensive exploration of this concept.

The main result of this study is demonstration of a promising prospective for integrating CFD with BIM to estimate the aesthetical appearance of building facades made of wood or other biological origin materials.

Although there are some constrains limiting the reliability of the simulation model presented, the guidelines provided in [40], [41] are relevant and helpful in the analysis of the wind driven rain effect on wooden facade.

4.1 RESEARCH LIMITATIONS AND CONSIDERATIONS FOR FURTHER STUDIES

The author of this study acknowledges that there are several factors not integrated with the model at this development stage. The missing factors include for example mould or insect infestations that might determine the overall aesthetical appreciation of the wooden building facade. Moreover, only colour changes are considered as a key factor determining the aesthetical performance diminishing importance of other surface characteristics, such as gloss, roughness, dirt accumulation or wettability. Whilst it must be mentioned that aside wind driven rain, there are also other important elements that contribute to the aesthetical deterioration of the wooden facade. These include factors such as solar radiation, wood moisture content fluctuations or daily changes of the facade surface temperature.
This study presents a first attempt to provide designers and architects with a reliable means of predicting the aesthetical appearance of the wooden facade by integrating CFD and BIM tools. Future studies are indispensable to achieve the entirety of the goal for which this study was motivated. Some of the suggestions that are made in this part of the study for the further research are listed below. It is important to consider other, preferably all, relevant factors that influence the change in appearance of the wooden facade when exposed to the external climatic conditions. There are also several specific processes and “physic” definitions within the present simulation model that can be improved during further studies. These are the main limitations of this study which also serve as a basis for extension of this work to the further research. Particularly, the following aspects are worth considering in further studies.

4.1.1 Other Factors Influencing Change in Appearance

As briefly explained in section 1.5, solar radiation, wood moisture and temperature are the key wood weathering factors that influences the aesthetical performance of the wooden facade. Wind driven rain was the sole factor modelled in this study. Therefore, all the other wood weathering factors can be considered in the follow-up research.

4.1.2 Other Factors Influencing Wetting Pattern

In this study, changes in the aesthetical appearance of the wooden facade due to the effect of liquid water (wetting) originated from the wind driven rain was simulated and visualised. However, not all the possible factors associated with the liquid water were considered so far. Other factors such as splashes and bounding effect at raindrop impact on the facade should be considered within the subsequent simulation model to precisely quantify for the wetting of the wooden facade in service life.

4.1.1 Other prospects with the Integration of BIM and CFD

In this study, the integration of BIM and CFD was performed by the LiveLink for Revit feature in the COMSOL Multiphysics software. This feature is not found in most of the alternative CFD tools. As a recommendation, future studies related to the integration of BIM and CFD for the simulation of wind driven rain can consider approach the integration with open-source BIM and CFD tools. Common open-source BIM tool such us Blender and open CFD tool such as OpenFOAM can be considered in future studies. Moreover, IFC standard should be also considered as an interesting interface solution.

4.1.1 Dose Responds

As a limitation, the author of this research admits the use of an experimental dose-response results related to San Michele All Adige (Italy) instead of that declared as a reference study location (Ljubljana, Slovenia). The dose-response material characteristics were obtained with framework of the BIO4ever and CLICKdesign projects. Estimation of the for the dose-response models for the reference location was not possible due to elongated duration of natural weathering tests. As a recommendation for further studies, a dose response factor should be computed for any location based on the experimental material response results and the climatic doses acquired at the reference location. A dedicated correction factor must be determined for such location compensating the difference in the yearly weather conditions and particular exposure circumstances.

4.2 MAIN CONTRIBUTION

To the best knowledge of the author of this study, there is no research study that simulates the effect of the wind driven rain on the aesthetical performance of wooden facade by integrating BIM and CFD. This makes this work the first to propose an original algorithm and fully integrated solution. This study serves as a conversation opener for research discussions on the integration of BIM and computational simulation techniques, particularly to quantify the aesthetical appearance of the wood when exposed to the external climatic conditions.

5 DALJŠI POVZETEK V SLOVENSKEM JEZIKU

Les kot biološki material se že stoletja uporablja v gradbeništvu. Naraščanje negativnih učinkov emisij ogljikovega dioksida dviguje ozaveščenost o potrebi po ustvarjanju trajnostnega življenjskega okolja. Posledično je vedno več zanimanja za uporabo bioloških materialov, v veliki meri lesa, v gradbeni industriji. Po mnenju strokovnjakov bodo naravni materiali bistveno prispevali k ustvarjanju trajnostne gradbene industrije in tudi življenjskega okolja. Ravno zaradi nizkih stroškov, enostavne obdelave in lahke dostopnosti je les v gradbeništvu postal zaželena izbira [1]. Kot navajajo [1], so [2], ugotovili da je uporaba lesa v fasadah ugodnejša v primerjavi z uporabo cementa, opek ali cinka, saj ima manjši negativni učinek na okolje. Trendi sodobne arhitekture stremijo k zmanjševanju finalne obdelave vidnih površin gradbenih materialov. Vendar kadar se uporablja neobdelan les, le-ta spremeni svojo naravno barvo ob izpostavljenosti zunanjim podnebnim dejavnikom. Ko govorimo o lastnosti fasad, nas zanimata dve glavni učinkovitosti, kako dobro nas fasada zaščiti pred zunanjimi klimatskimi pogoji, tj. tehnična učinkovitost, in kako se bo fasada spreminjala skozi čas oz. kako privlačna bo fasada po določenem obdobju, tj. estetska učinkovitost. Simulacija učinkovitosti stavbe (ang. Building Performance Simulation, BPS) je metoda, ki replicira učinkovitost celotne stavbe ali le določenega dela s pomočjo uporabe informacijskih modelov. Ponuja poenostavljeno evaluacijo učinkovitosti stavb in zaradi tega je v zadnjih letih zelo priljubljena med gradbenimi inženirji. Tehnična zmogljivost lesene fasade je skozi leta pridobila veliko pozornosti pri raziskovanju s tehnologijo BPS, na drugi strani je estetska učinkovitost (lesenih) fasad bila v večji meri zapostavljena.

Inženirji in oblikovalci že v zgodnjih fazah gradbenih projektov hočejo vedeti, kako bo lesena fasada izgledala čez nekaj let izpostavljenosti zunanjim dejavnikom. Zaradi kompleksnosti tega pojava, je natančno predvidevanje izgleda fasade po nekaj letih kompleksen problem, ki ne daje gotovih rezultatov v času analize. Vendar tehnologije, kot so računska dinamika fluidov (ang. Computational Fluid Dynamics, CFD) in informacijsko modeliranje gradenj (ang. Building Information Modelling, BIM), ki vse bolj pridobivajo na priljubljenosti, nudijo pomoč pri reševanju tega problema.

V raziskavi predlagamo uporabo CFD in BIM tehnologij za predvidevanje videza lesene fasade po izpostavljenosti zunanjim dejavnikom za določeno obdobje.

Glavni namen te študije je predlagati in preizkusiti potek dela za predvidevanje videza oziroma estetske učinkovitosti lesenih fasad skozi čas uporabe. Potek dela vključuje uporabo CFD in BIM tehnologij.

Za dosego glavnega namena so bili postavljeni trije cilji:

- z uporabo BIM in CFD določiti obtežbo horizontalnega deževja na leseno fasado, ki ga povzroča veter,

- natančno oceniti količino horizontalnega deževja na leseni fasadi, ki ga povzroča veter,
- na podlagi ocenjene količine deževja, izvesti vizualizacijo sprememb videza lesene fasade skozi čas.

CFD spada v skupino znanosti, ki se ukvarjajo z mehaniko tekočin. Uporablja se za analizo pretoka tekočin, toplotnega toka in drugih sorodnih pojavov s pomočjo numeričnih metod in algoritmov. Osnovana je na kombinaciji fizike, mehanike, tehnologije pretoka, matematike in informacijskih tehnologij [31]. CFD se je izkazal kot močno orodje, ki je lahko uporabno v fazi oblikovanja, saj prihrani čas in omogoča hitrejše spremembe geometrije stavb v zgodnjih fazah načrtovanja.
V arhitekturi in gradbeni industriji se CFD uporablja za predvidevanje in analizo toplotnega toka, ravni vlažnosti in zračnega toka. Služi pri analizi učinkovitosti zasnov stavbe in posameznih delov stavb, kot tudi pri primerjavi različnih projektantskih opcij. Podobno kot druge simulacijske tehnike je CFD orodje, s katerim lahko dopolnimo ali pa v celoti zamenjamo že obstoječe analize, ko je potrebna primerjava večjih alternativnih opcij oz. ko je fizično testiranje onemogočeno [31].
V tej študiji smo uporabili tudi orodje COMSOL Multiphysics, zaradi njegove razpoložljivosti in priročnosti. Opravljene CFD simulacije lahko razdelimo na tri procese in sicer pred-obdelava, reševanje in dodatna obdelava.

Pred-obdelava je prvi korak procesa simulacije CFD. Pred-obdelava vključuje definiranje geometrije referenčne stavbe, izdelavo računske mreže, definiranje lastnosti materialov in robnih pogojev.

Prvi korak pri kateri koli CFD simulaciji je ustvarjanje računske domene ter geometrije stavbe, ki služita kot podlaga. V tej študiji smo geometrijo zgradbe naredili z orodjem Autodesk Revit, kot je pojasnjeno v poglavju 2.4. Model smo pripravili za CFD simulacijo z uporabo funkcije LiveLink v orodju COMSOL. Referenčna stavba ima preprosto pravokotno geometrijo v velikosti 8,2 m x 6,2 m, s poševno streho in 60 cm napušča. Slika 1 prikazuje geometrijo stavbe.

Okoli geometrije stavbe smo ustvarili omejevalno pravokotno škatlo, ki služi kot računska domena pretoka tekočin. Definirana računska domena ima dimenzije 225 m x 30 m x 17 m (L x B x H). Dimenzije računske domene so bile določene v skladu s smernicami [42], [43]. Izvleček slednje študije vključuje tudi priporočilo, da naj maksimalno razmerje blokad ne bo več kot 3%, v naši študiji je to razmerje znašalo 0.74 %. Tominaga et al [42] je predlagal, da bi bila bočna razdalja (L) vsaj 5-kratnik višine (H), čemur smo zadostili. Mreža računske domene je predstavljena na sliki 5.

Tretji korak je ustvarjanje mreže. Definiranje mreže je pomemben korak pri CFD simulaciji, ker poenostavlja izračune in prispeva k bolj točnim rezultatom. V orodju COMSOL Multiphysics obstajajo štiri različne vrste elementov [37]. V tej študiji smo uporabili nestrukturirane (proste) tetraedrske mreže za definiranje geometrije stavbe ter računske domene.

V postopku reševanja se je izvedlo vse izračune na podlagi enačb ter robnih pogojev determiniranih v prejšni fazi pred-obdelave. V tej študiji smo modul laminarnega pretoka uporabili skupaj z modulom za sledenje delcev, za potrebe analize horizontalnega dežja, ki ga povzroča veter. Najprej smo izračunali polje pretoka tekočin skupaj z modulom laminarnega pretoka, nato pa so ti pridobljeni rezultati bili uporabljeni kot podlaga za računanje gibanja delcev (dežne kapljice) in padanja na površino referenčne stavbe.

Po pridobivanju rezultatov sledi zadnji korak v procesu, dodatna obdelava. Ta faza CFD simulacije v svojem bistvu predstavlja analizo pridobljenih rezultatov iz prejšnje faze. Glavni namen je vizualizacija rezultatov s pomočjo različnih grafikonov in poročil.

Izbrani potek dela v tej študiji, lahko porazdelimo v štiri glavne korake, kot je prikazano na sliki 3:

- Delo se začne z razvojem modela stavbe v katerem koli orodju BIM. V tej študiji smo uporabili orodje AUTODESK REVIT BIM.
- Drugi korak vključuje izvajanje simulacije dežja, s pomočjo orodja CFD. V tem procesu je bil uporabljen CFD modul v okviru orodja COMSOL Multiphysics. Simulirali smo laminarni tok (simulacija pretoka vetra) ter sledenje delcev (trajektorije dežnih kapljic in vzorci vlaženja). Te dve simulacije sta podrobno opisani v poglavju 2.6 in 2.7
- Tretji korak, pa vključuje dodatno obdelavo podatkov. V orodju LabVIEW smo razvili skripto z namenom obdelave zgodovinskih podnebnih podatkov, da smo pridobili podatke o horizontalnem deževju, ki ga povzroča veter. Obdelavo podatkov, ki smo jih pridobili po simulacijskem postopku, je vključevala tudi količine horizontalnega deževja, povzročenega z vetrom in teksturne mreže, ki predstavljajo spremembe estetike lesene facade. Te smo ustvarili z drugo skripto.
- Končni korak predstavlja vizualizacijo končnih rezultatov v orodju BIM (Revit). Vizualizacijo smo dosegli z vmesnikom Dynamo.

V tej študiji smo uporabili nestisljiv laminarni tok. Pri nestisljivem toku je predpostavljeno, da je temperaturna variacija v toku, ko je tekočino pod normalnimi pogoji in ima nizko hitrost [37]. Za izračune hitrosti ter tlačnega polja enofaznega sistema laminarnega toka smo v orodju CFD uporabili ukazne naloge fizike laminarnega pretoka.

Za vsako izvedeno simulacijo veternega toka so bile izvedene tridimenzionalne trajektorije delcev za kapljice dežja. To smo dosegli s simulacijo injiciranja več tisoč dežnih kapljic pri definiranju robnih pogojev dotoka. Simulacija trajektorije delcev je bila izvedena na podlagi simulacije laminarnega pretoka, kot je pojasnjeno v poglavju 2.6. V tej študiji se je izračun trajektorij delcev opravil z uporabo modula za sledenje delcev orodja CFD. Slednji modul je splošno orodje za računanje poti delcev, ko se le-te premikajo skozi računsko domeno in so podvržene različnim silam.

V tej raziskavi smo uporabili osem samostojnih deževji, ki so bile osnovane na zgodovinskih podnebnih podatkih. Simulaciji laminarnega toka in sledenja delcev sta bili uspešni, kot tudi določitev vzorcev vlaženja in odmerkov vlage. Na podlagi mape vzorcev je bila opravljena tudi simulacija teksture lesa ter videza smreke. Vizualizacija končnega videza lesa smo uspešno naredili s pomočjo orodja Revit. V študiji smo ugotovili, da je predlagani potek dela učinkovit in prinaša ustrezne rezultate. Namen raziskave je, da lahko služi tudi kot podlaga za prihodnje znanstvene razprave o uporabi orodja BIM ter ostale računalniške tehnologije za simulacije predvidevanja videza lesenih fasad, pri izpostavljanju lesa zunanjim klimatskim pogojem.

6 REFERENCES

[1] P. Rüther and B. Time, "External wood claddings–performance criteria, driving rain and large-scale water penetration methods," *Wood Material Science & Engineering*, vol. 10, no. 3, pp. 287–299, 2015.

[2] T. S. W. Plesser, T. F. Kristjansdottir, L. Tellnes, P. O. Flæte, L. R. Gobakken, and G. Alfredsen, "Miljøanalyse av trefasader," 2013.

[3] R. S. Williams, "Weathering of wood," *Handbook of wood chemistry and wood composites*, vol. 7, pp. 139–185, 2005.

[4] R. C. Pettersen, "The Chemical Composition of Wood," 1984. doi: 10.1021/ba-1984-0207.ch002.

[5] C. B. N. Santos, M. R. Gomes, L. J. Colodette, M. T. Resende, G. A. Lino, and V. J. A. Zanuncio, "A Comparison Of Methods For Eucalypt Wood Removal Extractive," *5th International Colloqium on Eucalyptus Pulp*, 2011.

[6] E. Roffael, "Significance of wood extractives for wood bonding," *Applied Microbiology and Biotechnology*, vol. 100, no. 4, pp. 1589–1596, Feb. 2016, doi: 10.1007/S00253-015-7207-8.

[7] P. Nzokou and D. P. Kamdem, "Influence of wood extractives on the photo-discoloration of wood surfaces exposed to artificial weathering," *Color Research & Application: Endorsed by Inter-Society Color Council, The Colour Group (Great Britain), Canadian Society for Color, Color Science Association of Japan, Dutch Society for the Study of Color, The Swedish Colour Centre Foundation*, vol. 31, no. 5, pp. 425–434, 2006.

[8] Y. Yazaki, "Wood colors and their coloring matters: A review," *Natural Product Communications*, vol. 10, no. 3. 2015. doi: 10.1177/1934578x1501000332.

[9] T. C. Chang, H. T. Chang, C. L. Wu, and S. T. Chang, "Influences of extractives on the photodegradation of wood," *Polymer Degradation and Stability*, vol. 95, no. 4, 2010, doi: 10.1016/j.polymdegradstab.2009.12.024.

[10] D. N.-S. Hon and N. Minemura, "Color and discoloration," in *Wood and cellulosic chemistry*, 1991, pp. 395–454.

[11] S. Sandoval-Torres, W. Jomaa, F. Marc, and J.-R. Puiggali, "Causes of color changes in wood during drying," *Forestry Studies in China*, vol. 12, no. 4, 2010, doi: 10.1007/s11632-010-0404-8.

[12] Y. Yazaki, P. J. Collins, and B. McCombe, "Variations in hot water extractives content and density of commercial wood veneers from blackbutt (Eucalyptus pilularis)," 1994.

[13] A. Sandak *et al.*, "Assessment and monitoring of aesthetic appearance of building biomaterials during the service life," 2017.

[14] W. C. Feist, "Outdoor wood weathering and protection," *Archaeological wood, properties, chemistry, and preservation. Advanced in Chemistry Series*, no. 225, pp. 263–298, 1990.

[15] M. Lee, G. Park, H. Jang, and C. Kim, "Development of building cfd model design process based on bim," *Applied Sciences (Switzerland)*, vol. 11, no. 3, 2021, doi: 10.3390/app11031252.

[16] A. Kubilay, "Numerical simulations and field experiments of wetting of building facades due to wind-driven rain in urban areas," 2014.

[17] B. Blocken and J. Carmeliet, "A review of wind-driven rain research in building science," *Journal of Wind Engineering and Industrial Aerodynamics*, vol. 92, no. 13, 2004, doi: 10.1016/j.jweia.2004.06.003.

[18] B. Blocken and J. Carmeliet, "On the accuracy of wind-driven rain measurements on buildings," *Building and Environment*, vol. 41, no. 12, pp. 1798–1810, 2006, doi: https://doi.org/10.1016/j.buildenv.2005.07.022.

[19] B. Blocken and J. Carmeliet, "Validation of CFD simulations of wind-driven rain on a low-rise building facade," *Building and Environment*, vol. 42, no. 7, pp. 2530–2548, 2007.

[20] B. Blocken, G. Dezsö, J. van Beeck, and J. Carmeliet, "Comparison of calculation models for wind-driven rain deposition on building facades," *Atmospheric environment*, vol. 44, no. 14, pp. 1714–1725, 2010.

[21] E. C. C. Choi, "Simulation of wind-driven-rain around a building," *Journal of Wind Engineering and Industrial Aerodynamics*, vol. 46–47, no. C, pp. 721–729, Aug. 1993, doi: 10.1016/0167-6105(93)90342-L.

[22] A. Karagiozis, G. Hadjisophocleous, and S. Cao, "Wind-driven rain distributions on two buildings," *Journal of Wind Engineering and Industrial Aerodynamics*, vol. 67, pp. 559–572, 1997.

[23] U. K. D. Nath, "Field Measurements of Wind-Driven Rain on Mid-and High-Rise Buildings in Two Canadian Regions," Montreal, Quebec, 2015.

[24] S. S. Mohaddes Foroushani, H. Ge, and D. Naylor, "Effects of roof overhangs on wind-driven rain wetting of a low-rise cubic building: A numerical study," *Journal of Wind Engineering and Industrial Aerodynamics*, vol. 125, 2014, doi: 10.1016/j.jweia.2013.10.007.

[25] M. Rychtáriková and A. Vargová, "Bionics and wind-driven rain on building facades," *Slovak Journal of Civil Engineering*, vol. 4, pp. 35–40, 2008.

[26] K. Nore, B. Blocken, B. P. Jelle, J. V. Thue, and J. Carmeliet, "A dataset of wind-driven rain measurements on a low-rise test building in Norway," *Building and Environment*, vol. 42, no. 5, pp. 2150–2165, 2007.

[27] A. N. Karagiozis, M. Salonvaara, A. Holm, and H. Kuenzel, "Influence of wind-driven rain data on hygrothermal performance," in *Proceedings of the Eighth International IBPSA Conference, Eindhoven, the Netherlands*, 2003, pp. 627–634.

[28] J. M. Pérez-Bella, J. Domínguez-Hernández, B. Rodríguez-Soria, J. J. del Coz-Díaz, and E. Cano-Suñén, "Estimation of the exposure of buildings to driving rain in Spain from daily wind and rain data," *Building and Environment*, vol. 57, pp. 259–270, 2012.

[29] J. Wolf and M. Griffith, "Wind-driven rain as a design parameter," in *Structures Congress 2008: Crossing Borders*, 2008, pp. 1–7.

[30] H. Ge, U. K. D. Nath, and V. Chiu, "Field measurements of wind-driven rain on mid- and high-rise buildings in three Canadian regions," 2017, doi: 10.1016/j.buildenv.2017.02.016.

[31] R. K. Raman, Y. Dewang, and J. Raghuwanshi, "A Review on Applications of Computational Fluid Dynamics," *International Journal of LNCT*, vol. 2, no. 6, 2018.

[32] M. S. Thordal, J. C. Bennetsen, and H. H. H. Koss, "Review for practical application of CFD for the determination of wind load on high-rise buildings," *Journal of Wind Engineering and Industrial Aerodynamics*, vol. 186, 2019, doi: 10.1016/j.jweia.2018.12.019.

[33] A. Russell, "Computational fluid dynamics modeling of atmospheric flow applied to wind energy research," 2009.

[34] B. E. Rapp, "Fluids," *Microfluidics: Modelling, Mechanics and Mathematics*, pp. 243–263, Jan. 2017, doi: 10.1016/B978-1-4557-3141-1.50009-5.

[35] COMSOL, "COMSOL Multiphysics release notes for version 5.5," *COMSOL, Inc*, 2020. https://www.comsol.com/cfd-module (accessed Jul. 05, 2021).

[36] J. Tu, G. H. Yeoh, and C. Liu, *Computational fluid dynamics: a practical approach*. Butterworth-Heinemann, 2018.

[37] K. Yokoi, T. Fukuda, N. Yabuki, and A. Motamedi, "Integrating BIM, CFD and AR for thermal assessment of indoor greenery," 2017.

[38] J. Hang, Y. Li, J. Hang, and Y. Li, "Wind Conditions in Idealized Building Clusters: Macroscopic Simulations Using a Porous Turbulence Model," vol. 136, pp. 129–159, 2010, doi: 10.1007/s10546-010-9490-3.

[39] "intro - Meteonorm (en)." https://meteonorm.com/en/ (accessed Aug. 08, 2021).

[40] Y. Tominaga *et al.*, "AIJ guidelines for practical applications of CFD to pedestrian wind environment around buildings," *Journal of Wind Engineering and Industrial Aerodynamics*, vol. 96, pp. 1749–1761, 2008, doi: 10.1016/j.jweia.2008.02.058.

[41] J. Franke, A. Hellsten, K. H. Schlünzen, and B. Carissimo, "The COST 732 Best Practice Guideline for CFD simulation of flows in the urban environment: A summary," *International Journal of Environment and Pollution*, vol. 44, no. 1–4, pp. 419–427, 2011, doi: 10.1504/IJEP.2011.038443.

[42] A. Javidinejad, “FEA practical illustration of mesh-quality-results differences between structured mesh and unstructured mesh,” *International Scholarly Research Notices*, vol. 2012, 2012.

[43] M. Bern and P. Plassmann, “Mesh Generation,” *Handbook of Computational Geometry*, pp. 291–332, Jan. 2000, doi: 10.1016/B978-044482537-7/50007-3.

[44] Fairclough Caty, “Efficiently Mesh Your Model Geometry with Meshing Sequences | COMSOL Blog,” Aug. 18, 2016. https://www.comsol.com/blogs/efficiently-mesh-your-model-geometry-with-meshing-sequences/ (accessed Jul. 18, 2021).

[45] P. Holmlund, “Computational Fluid Dynamic simulations of pulsatile flow in stenotic vessel models.” 2014.

APPENDICES

APPENDIX A *Wind Flow Around Building*

The slides presenting the wind flow velocity following the Y-Z plane of the reference computational domain.

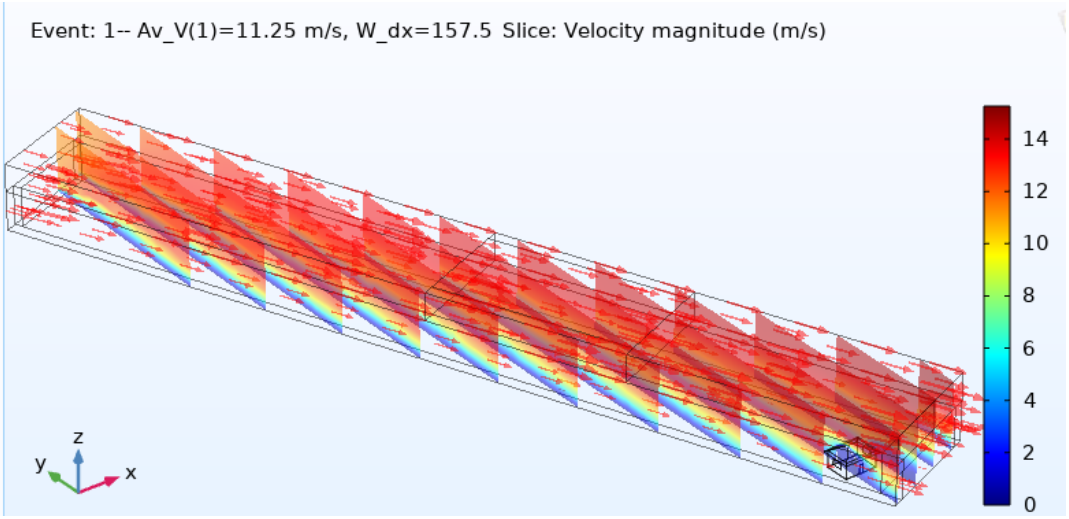

Wind Flow Velocity for WDR Scenario 1

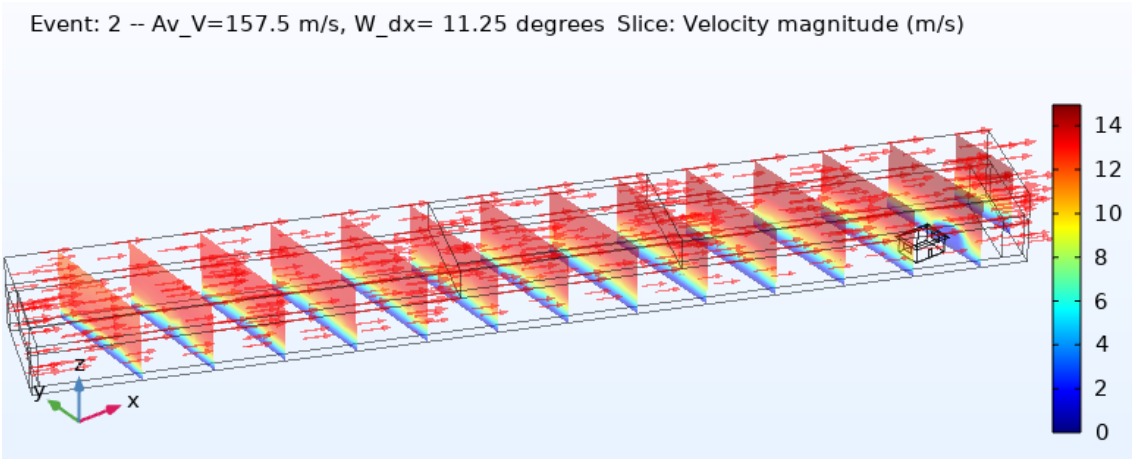

Wind Flow Velocity for WDR Scenario 2

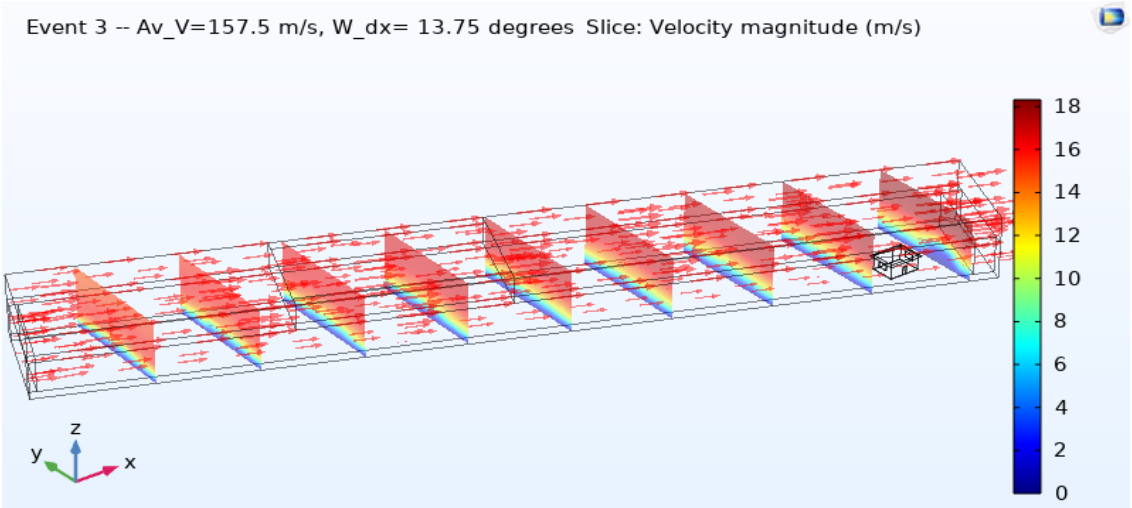

Wind Flow Velocity for WDR Scenario 3

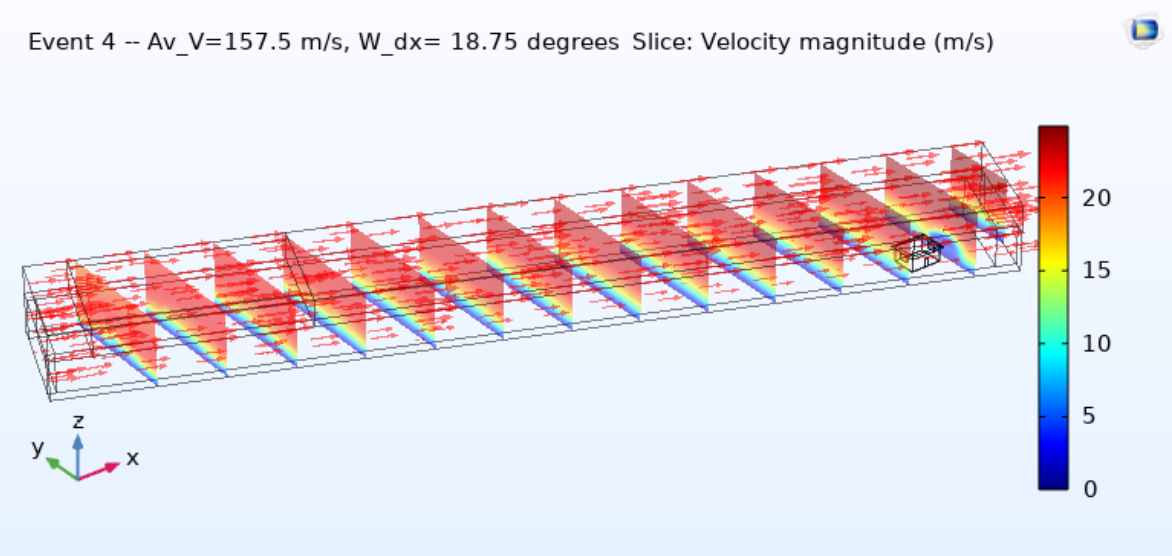

Wind Flow Velocity for WDR Scenario 4

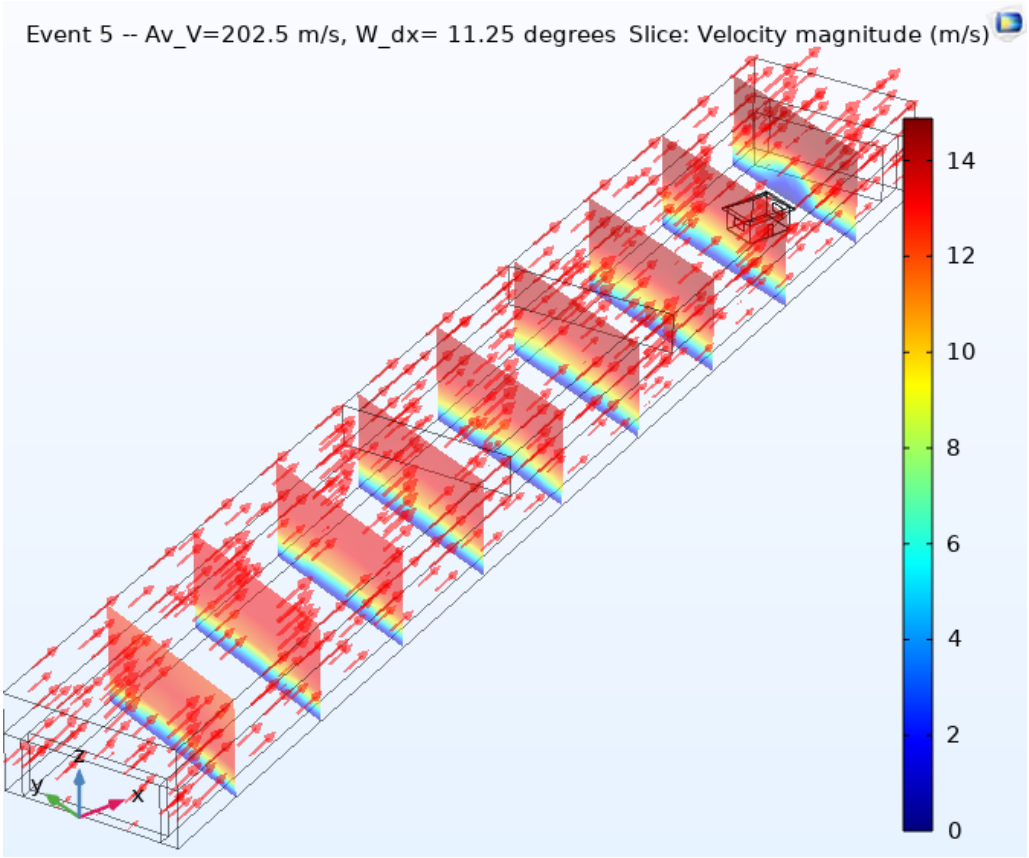

Wind Flow Velocity for WDR Scenario 5

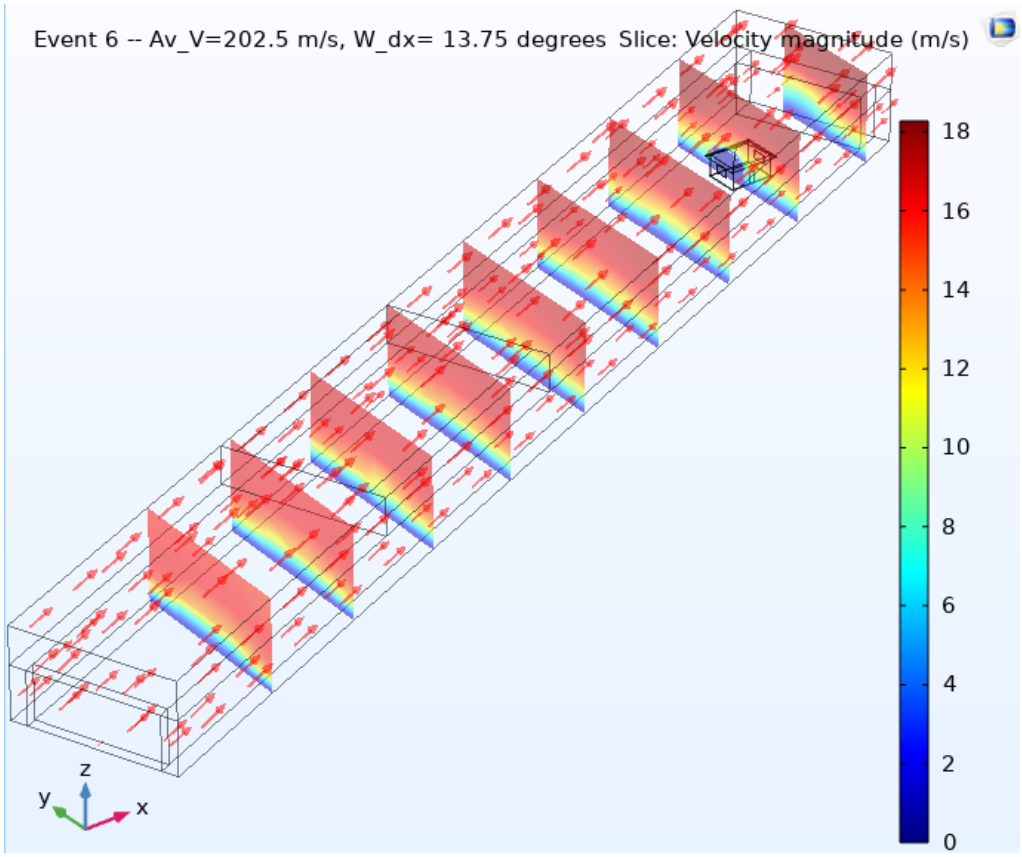

Wind Flow Velocity for WDR Scenario 6

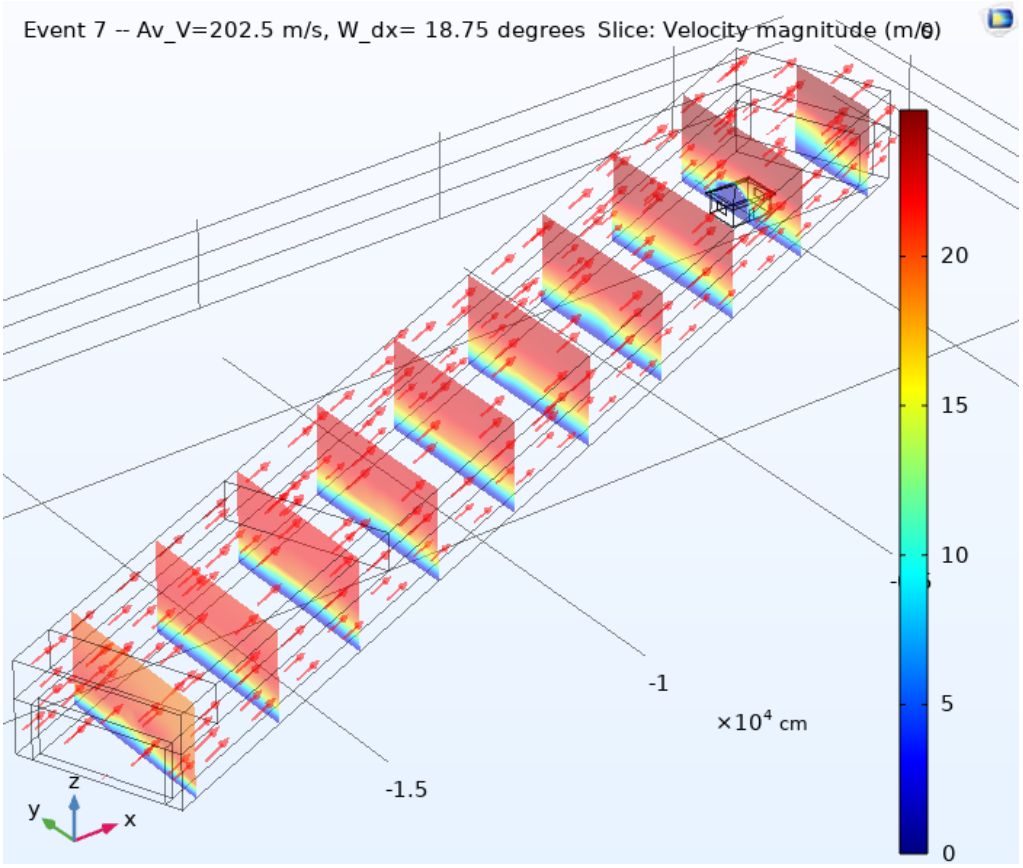

Wind Flow Velocity for WDR Scenario 7

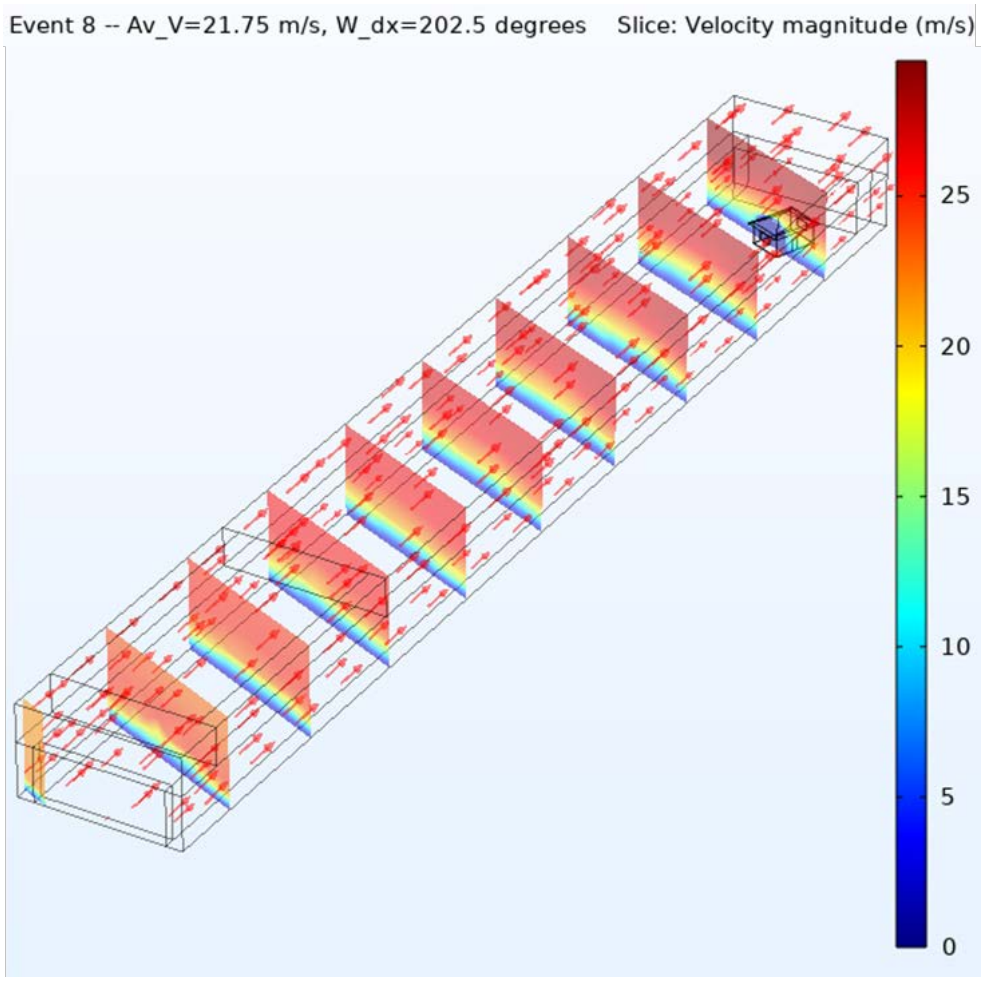

Wind Flow Velocity for WDR Scenario 8

APPENDIX B *Wetting Patterns on Building Facade*

Figures presenting the wetting patterns on the building Facade.

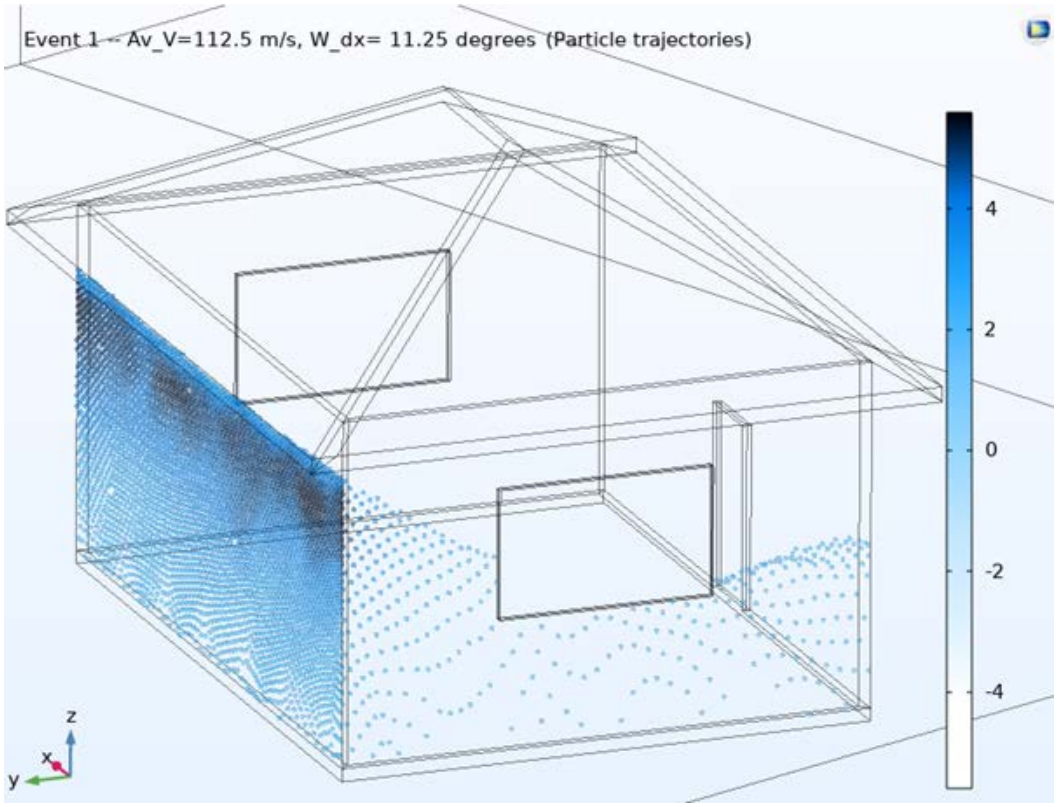

Wetting Pattern of WDR 1

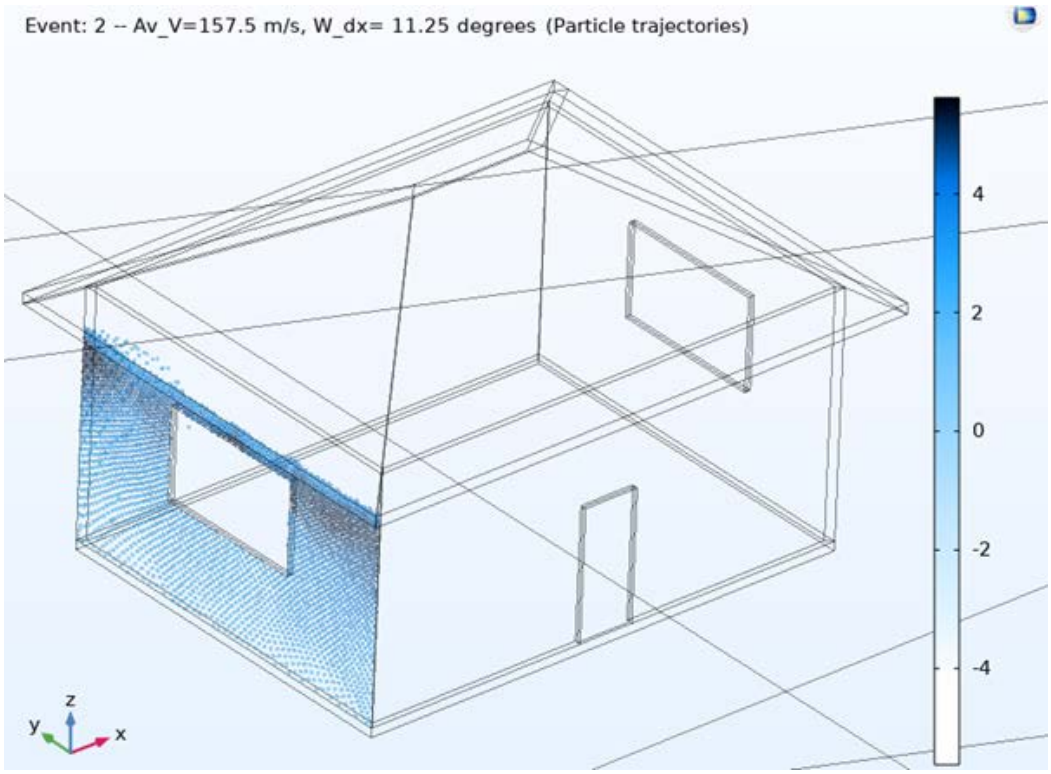

Wetting Pattern of WDR 2

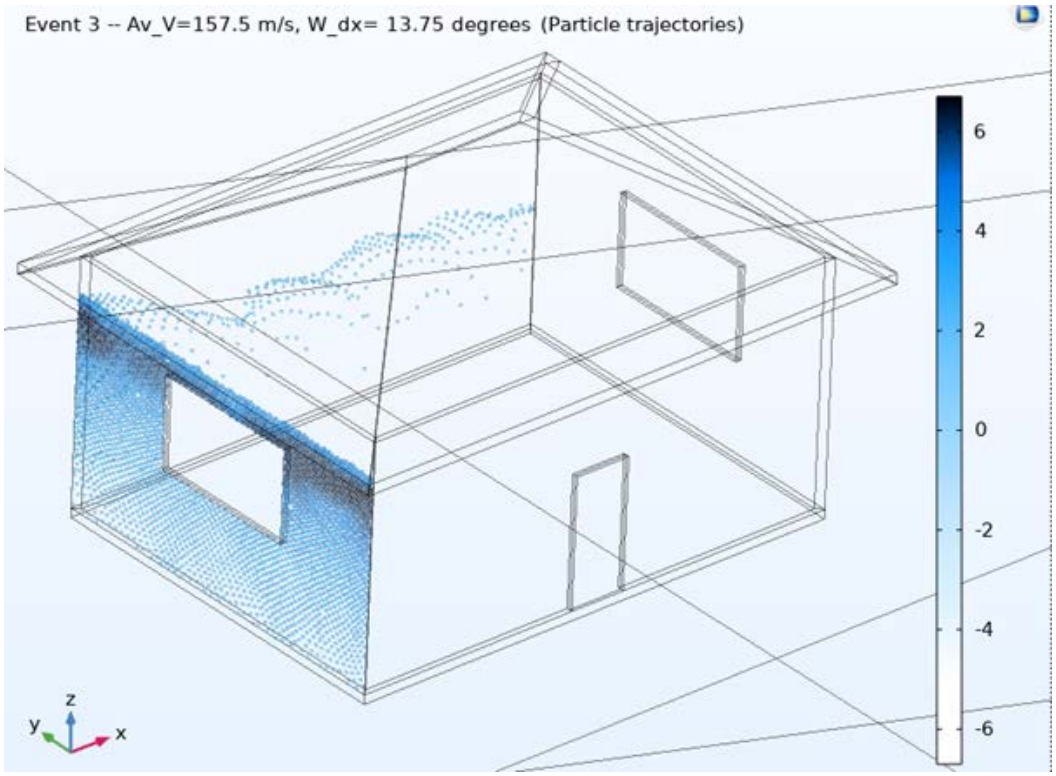

Wetting Pattern of WDR 3

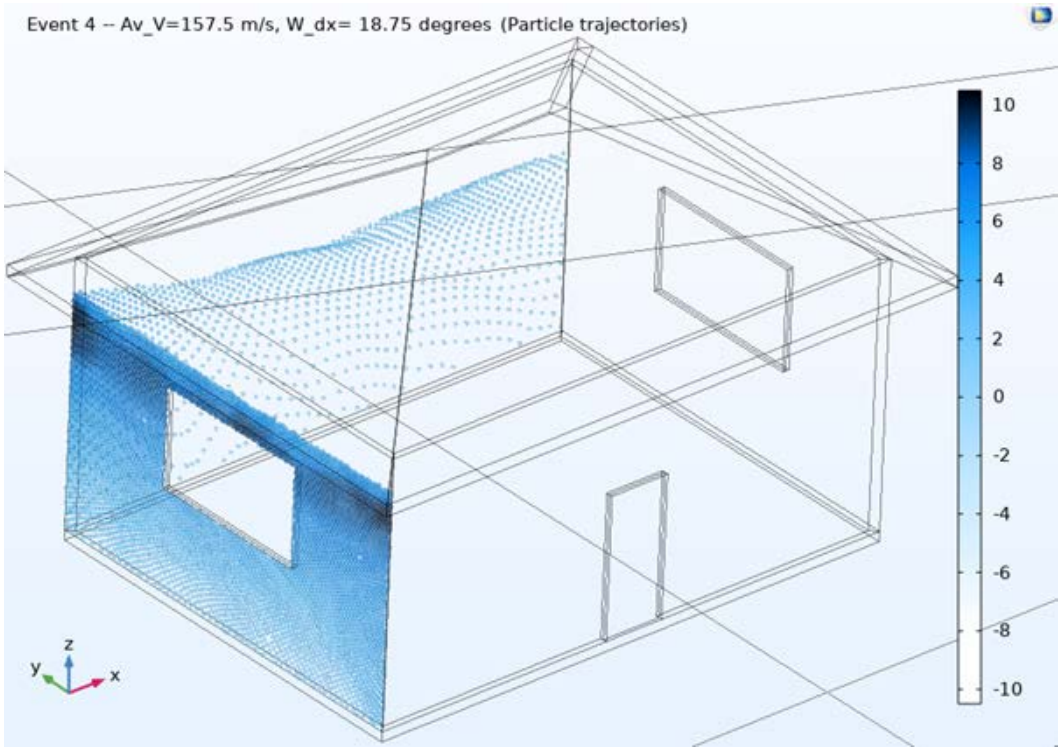

Wetting Pattern of WDR 4

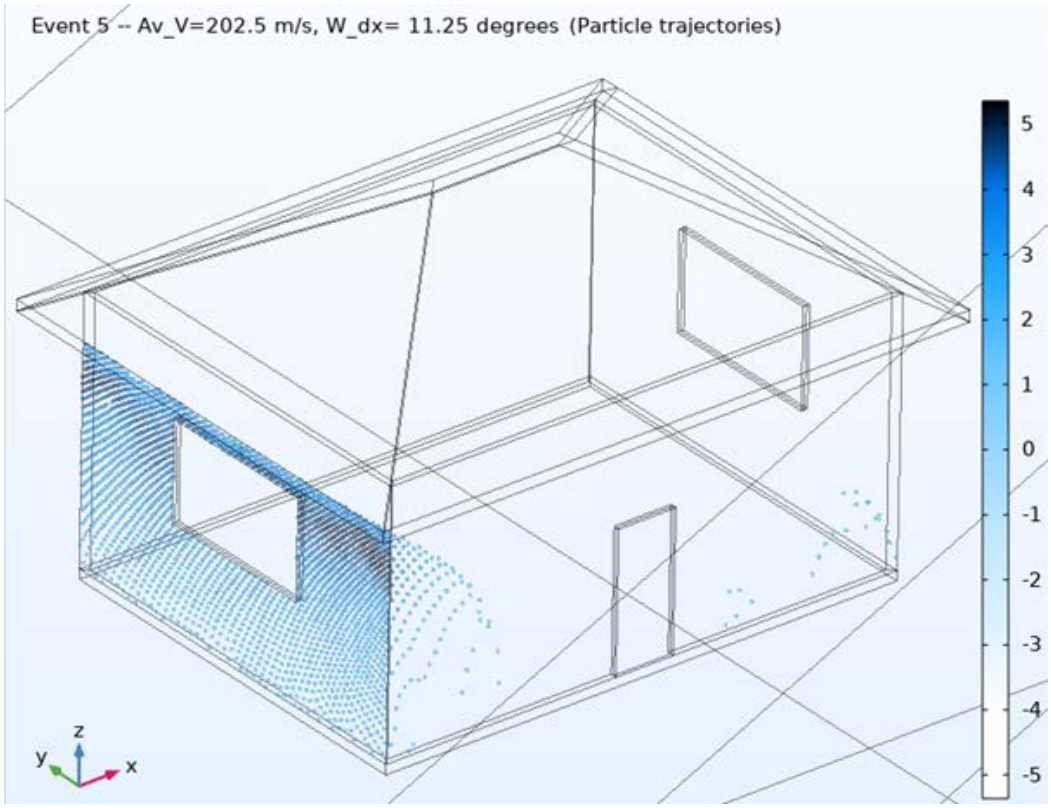

Wetting Pattern of WDR 5

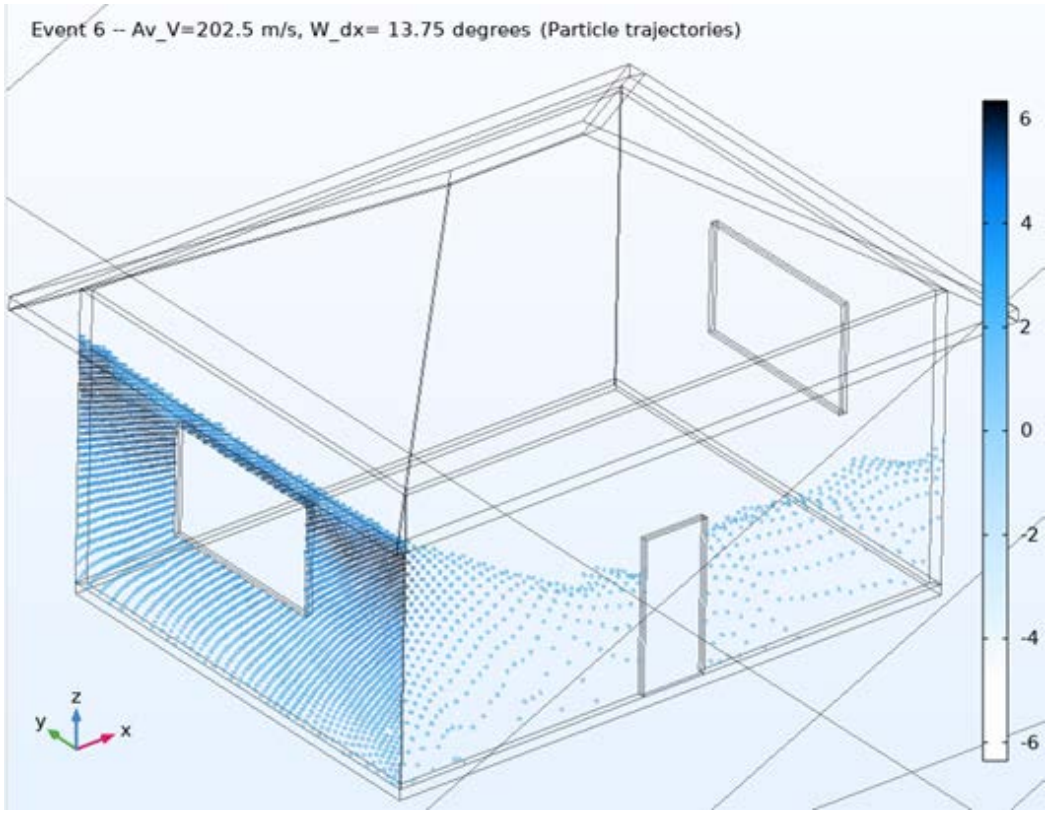

Wetting Pattern of WDR 6

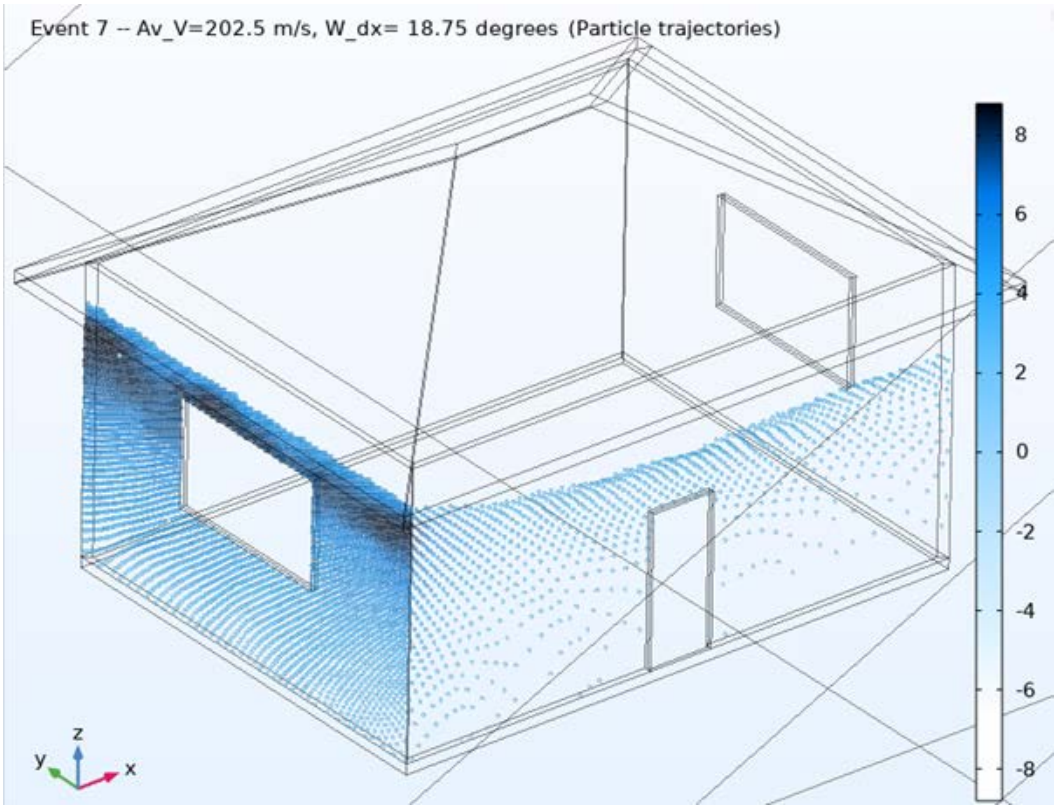

Wetting Pattern of WDR 7

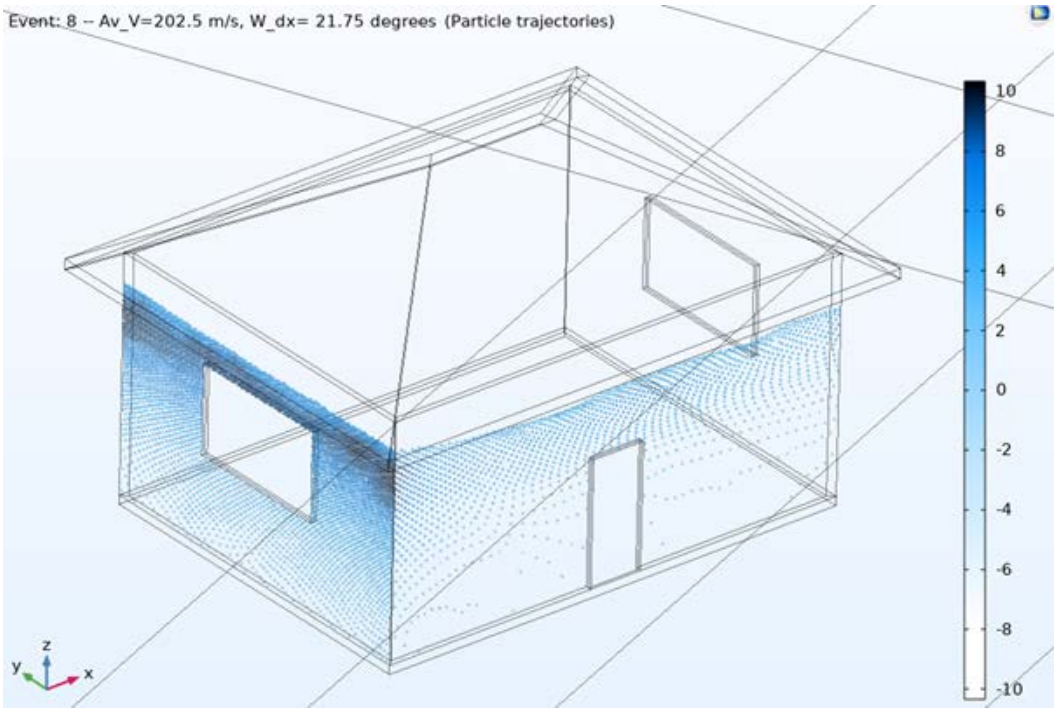

Wetting Pattern of WDR 8

APPENDIX C *Model Settings for The Laminar Flow (Wind Flow) And Particle Tracing (Raindrop Trajectories)*

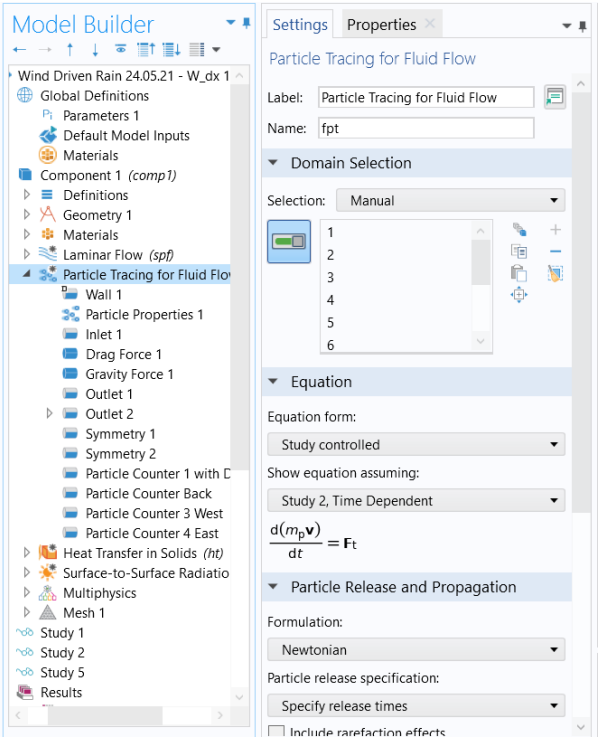

Model Settings (Laminar Flow)

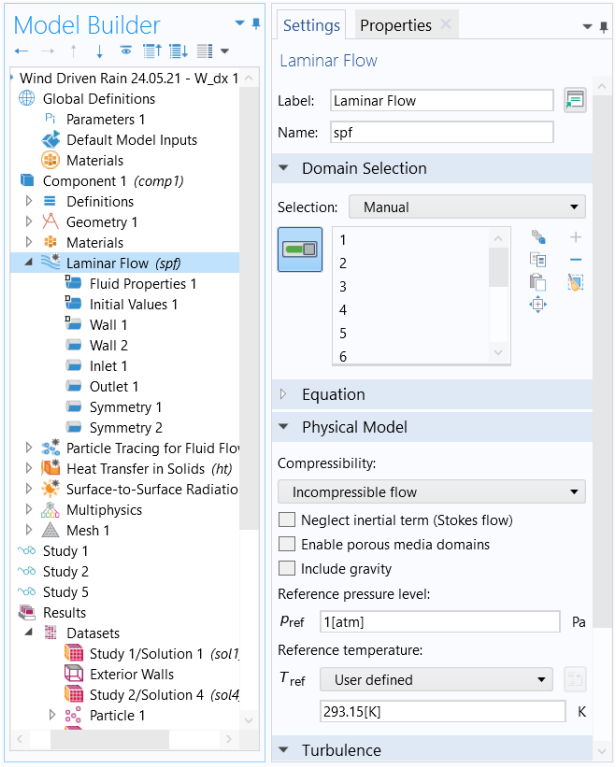

Model Settings (Particle Tracing)

APPENDIX D *First LabVIEW Script and Workflow for Filtering Wind Driven Rain Scenarios*

Front panel of the LabVIEW tool used for the determination of the wind scenarios relevant for numerical simulations.

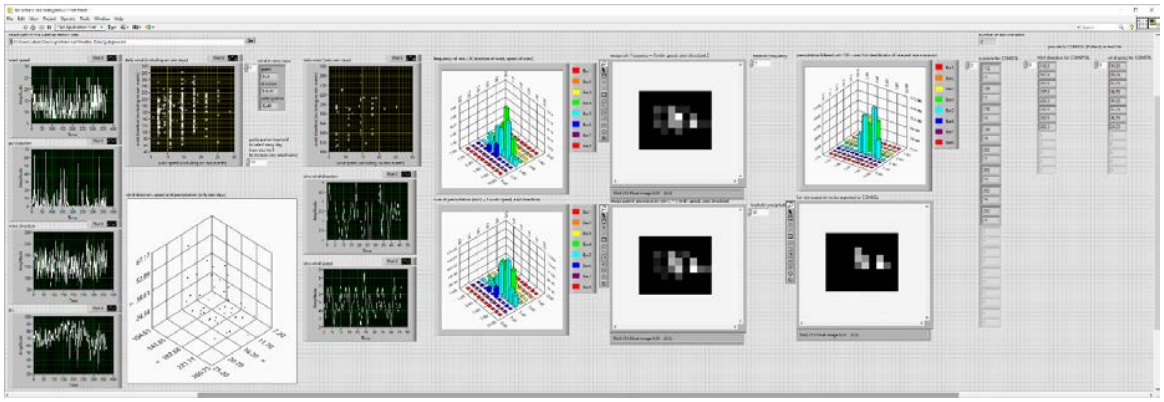

Front Panel of the LabVIEW Script (Filter Scenarios)

Block diagram for determination of the wind scenarios for simulation.

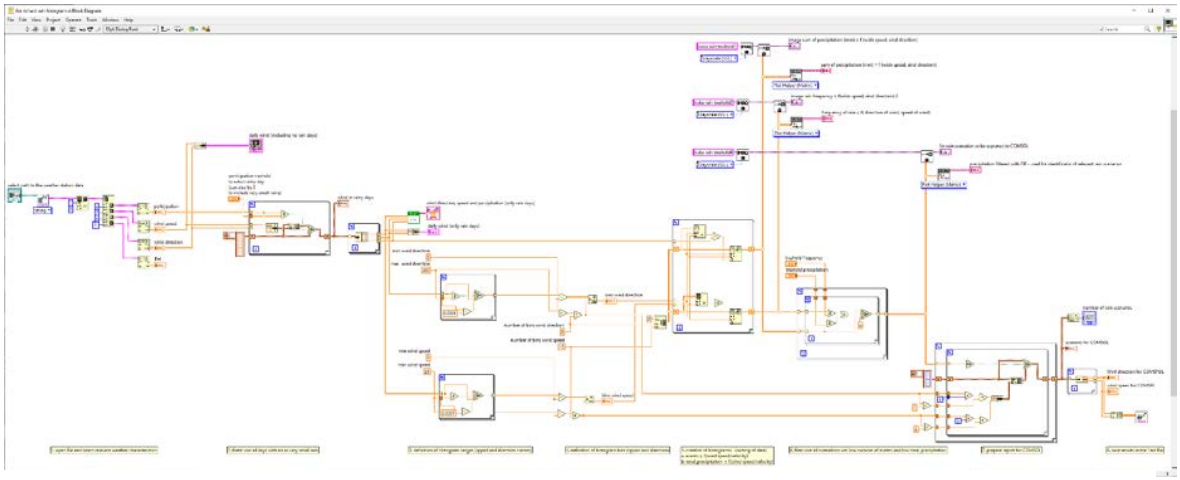

Block Diagram of the LabVIEW Script (Filter Scenarios)

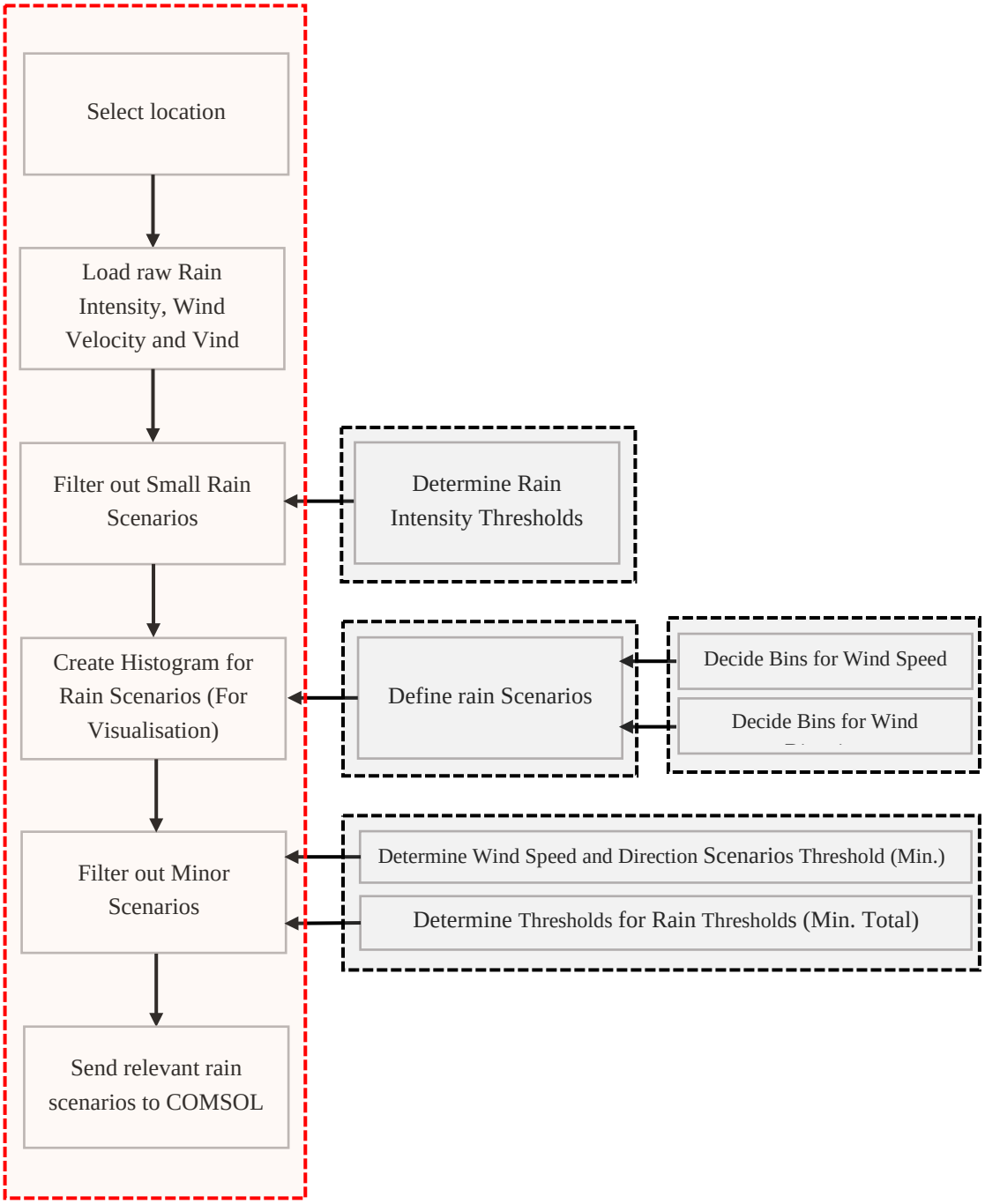

Workflow for Filtering WDR Scenarios (First LabVIEW Script)

APPENDIX E *LabVIEW Script and Workflow diagram for Dose Map Generation*

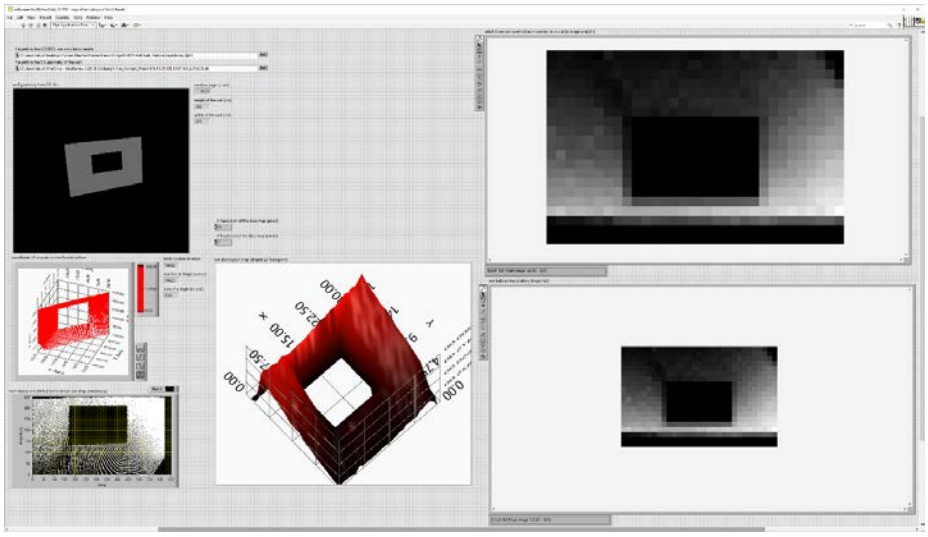

Front panel of the LabVIEW tool used for generation of the wind driven rain dose map

Front Panel of LabVIEW Script (Dose Map)

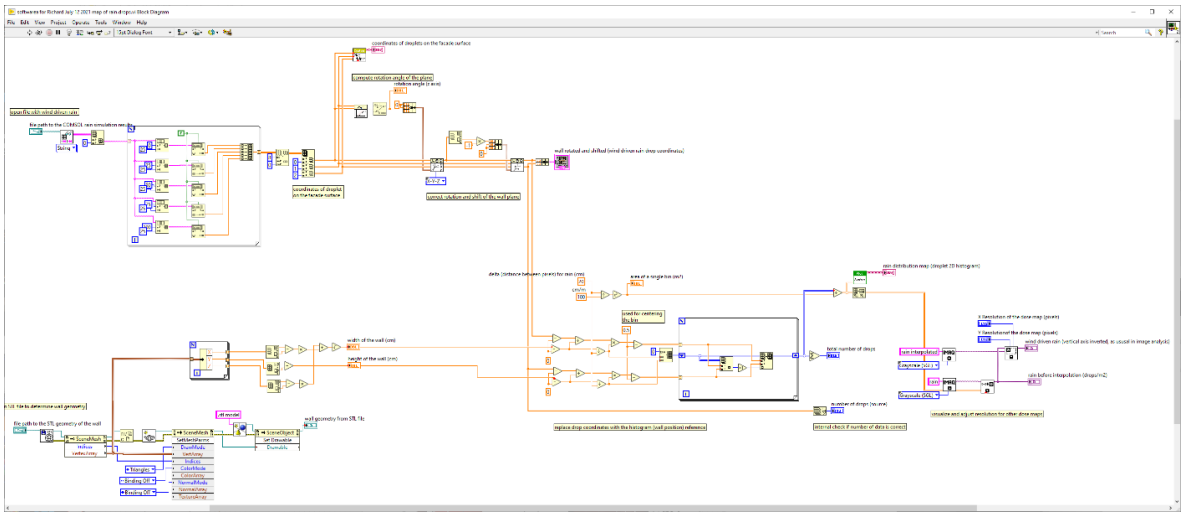

Block Diagram of LabVIEW Script (Dose Map)

Block diagram of the LabVIEW tool used for generation of the wind driven rain dose map

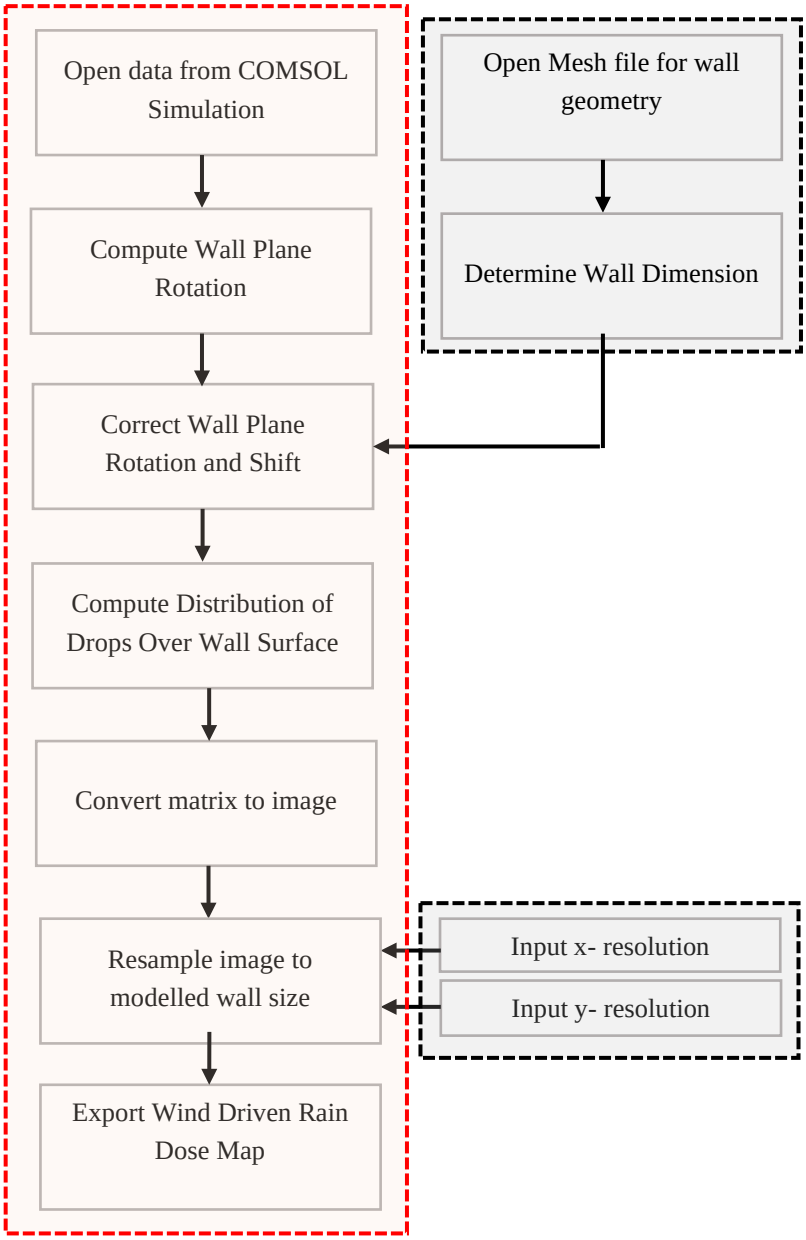

Workflow for Generating Dose Map and Textures (Second LabVIEW Script)

APPENDIX F *LabVIEW Scripts for Computing the Dripping Effect of the Raindrops*

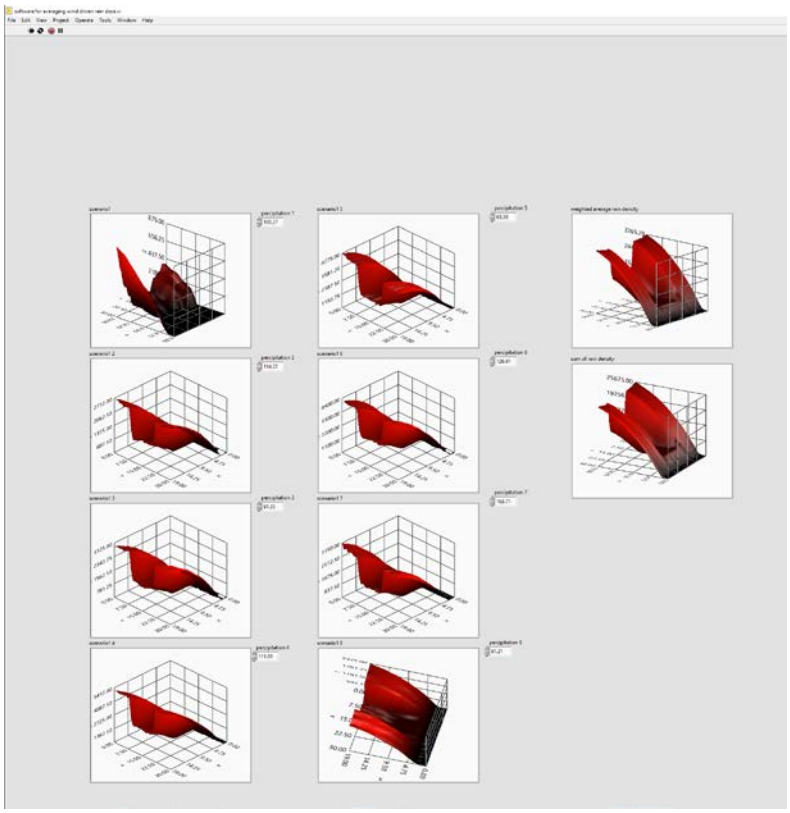

Front panel of the LabVIEW tool used for Computing Dripping Effect

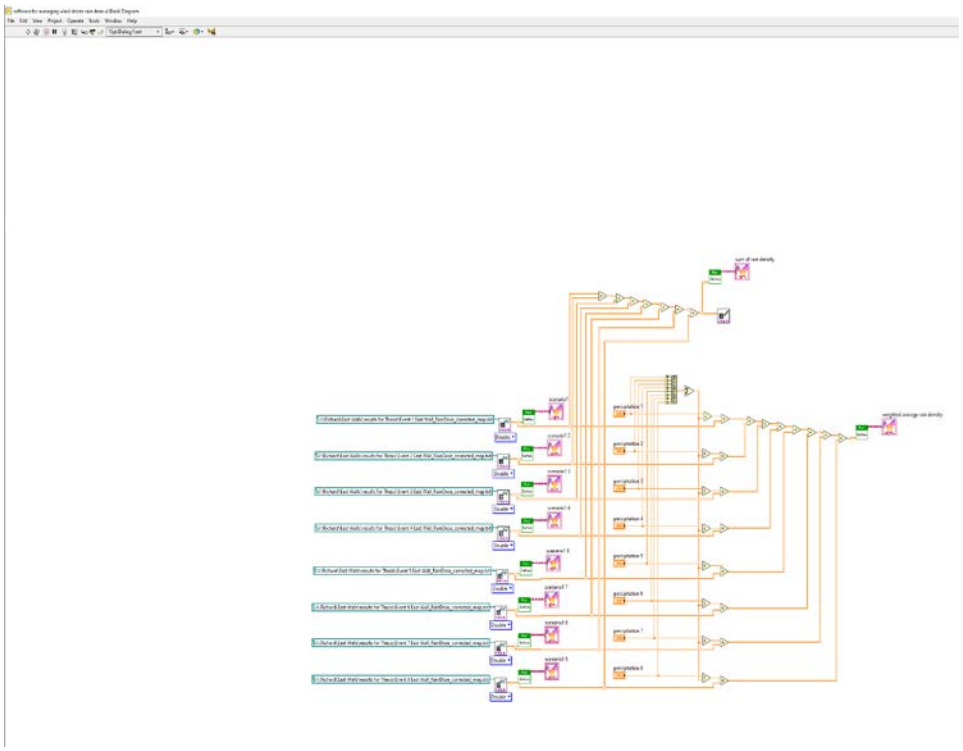

Block Diagram of LabVIEW Script for Computing the Dripping Effect of Raindrops

APPENDIX G *LabVIEW Scripts for Generating Textures*

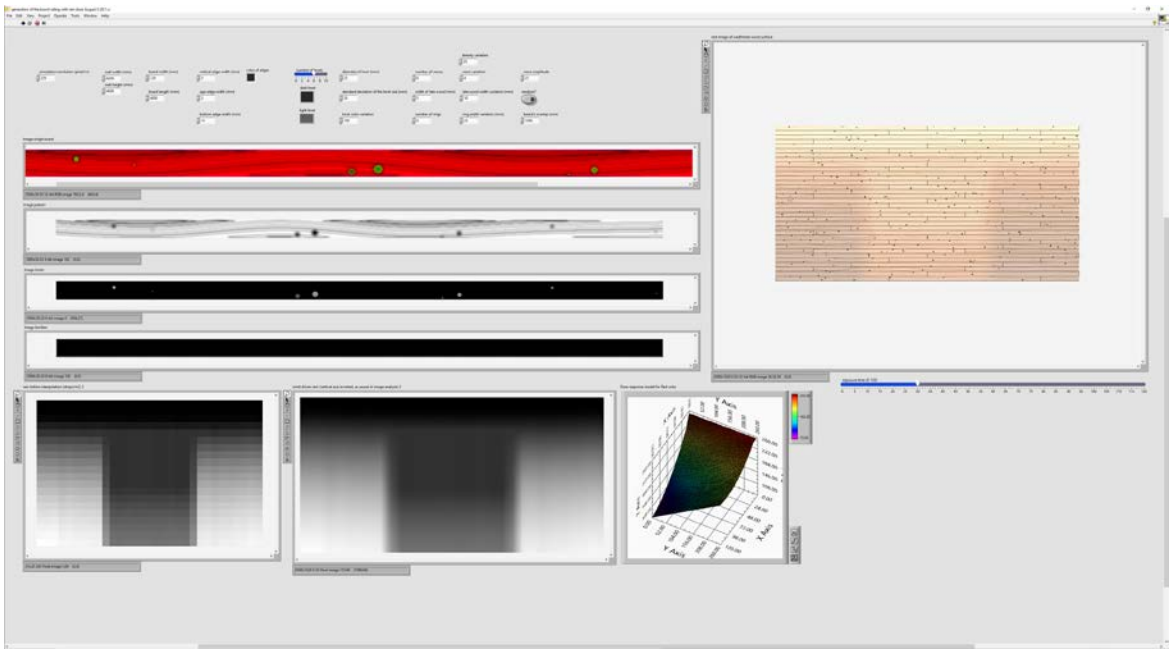

Front Panel for LabVIEW Script for Generating Textures

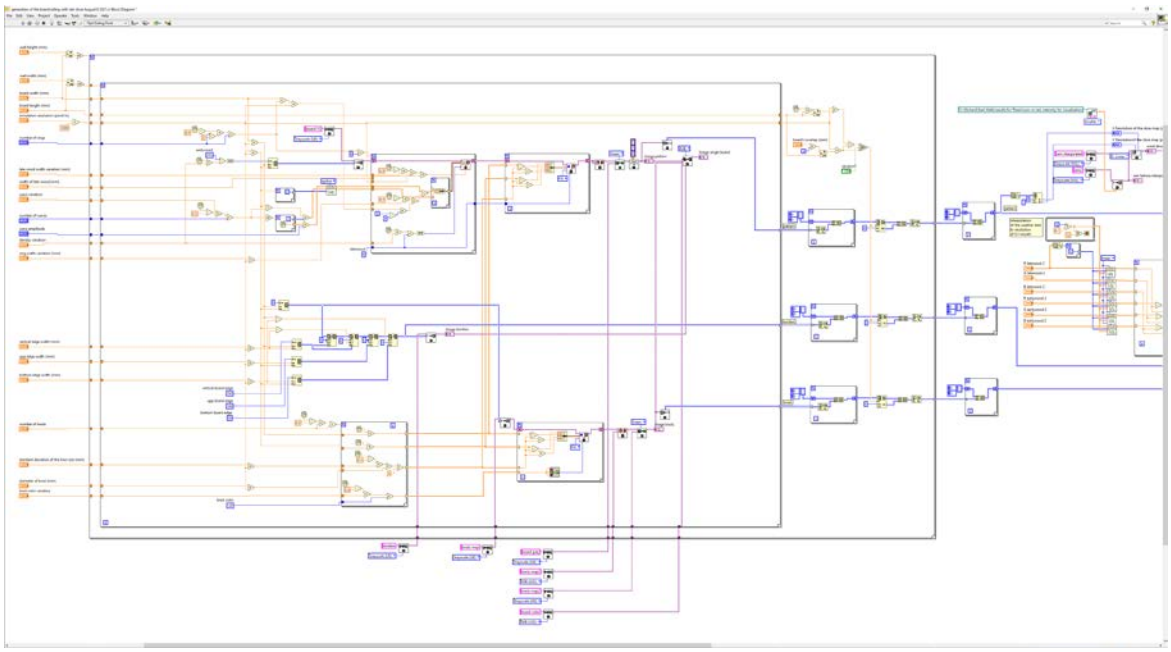

Block Diagram of LabVIEW Script for Generating Textures

APPENDIX H *Dynamo Script and Final Resul Visualisation*

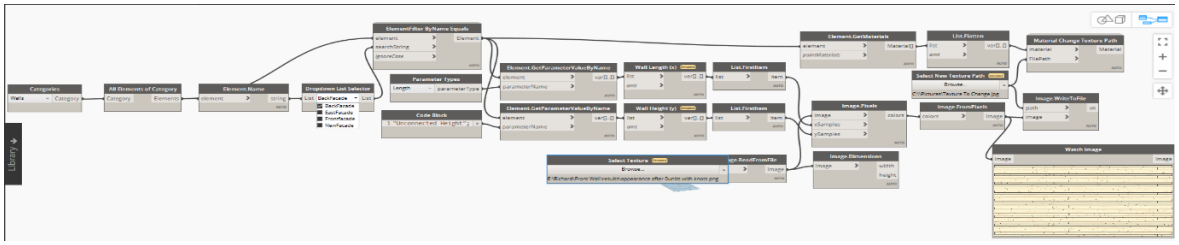

Revit Dynamo Script for Visualization

In this appendix, the Dynamo script developed to visualize appearance (colour) changes is presented. This is presented in below. In addition, the appearance of unexposed wooden facade as well as the final appearance (colour) changes when the wooden facade when exposed to external climatic conditions for a period of 3 months and 12 months are also presented.

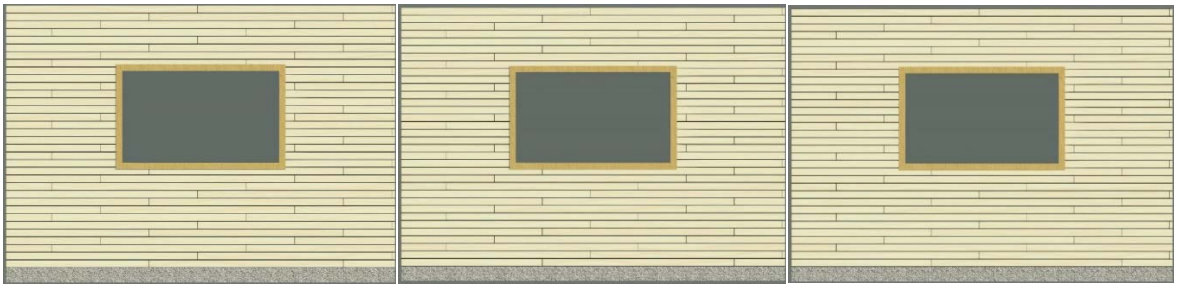

Without Knots - Colour Changes on the Southern face of Facade for 0 months (right), 3 months (middle) and 1 year (left)

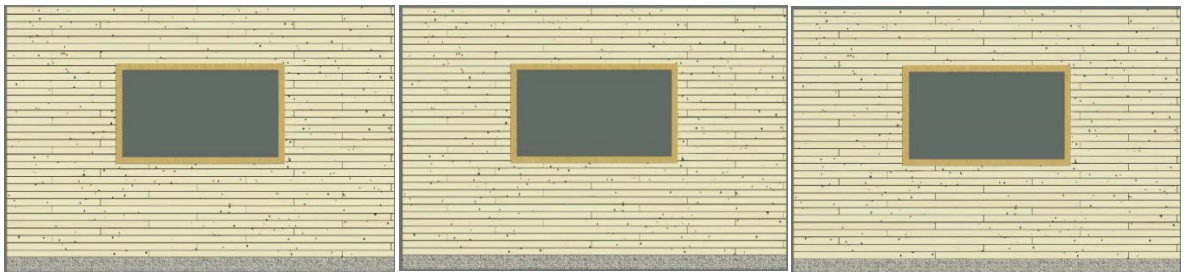

With Knots - Colour Changes on the Southern face of Facade for 0 months (right), 3 months (middle) and 1 y (left)

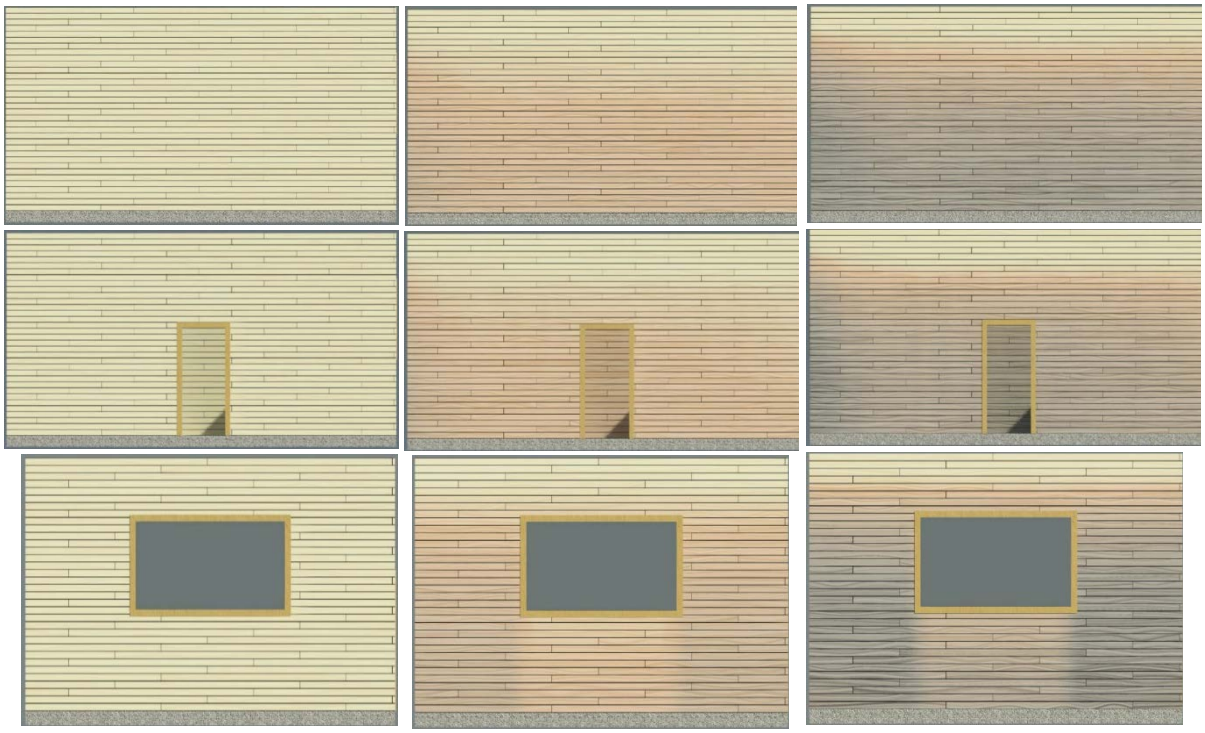

Without Knots - Colour Changes on the East (1st Row), West (2nd Row) and North (3rd Row) faces of Facade for 0 months (right), 3 months (middle) and 1 year (left).

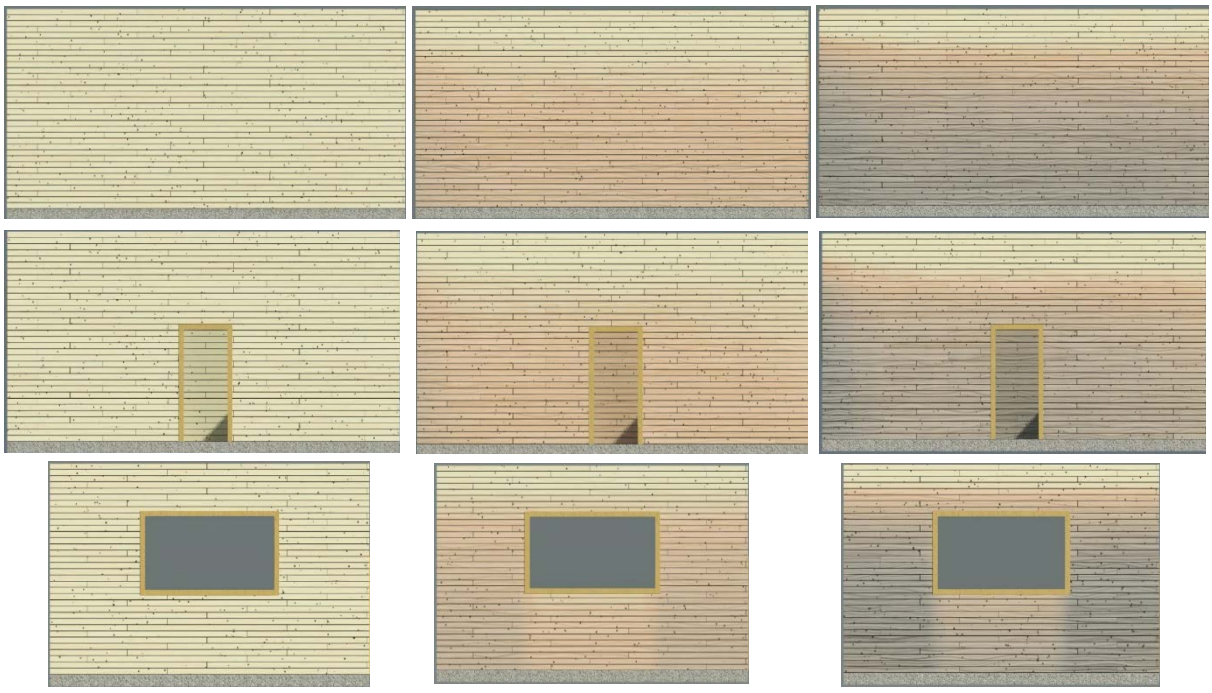

With Knots - Colour Changes on the East (1st Row), West (2nd Row) and North (3rd Row) faces of Facade fo 0 months (right), 3 months (middle) and 1 year (left).